

## Wave overtopping processes for very mild sloping and shallow foreshores

Nguyễn, Hà

**DOI**

[10.4233/uuid206d8f37-4d4c-4af9-9da3-8d57fce769e8](https://doi.org/10.4233/uuid206d8f37-4d4c-4af9-9da3-8d57fce769e8)

**Publication date**

2022

**Document Version**

Final published version

**Citation (APA)**

Nguyễn, H. (2022). *Wave overtopping processes for very mild sloping and shallow foreshores*. [Dissertation (TU Delft), Delft University of Technology]. <https://doi.org/10.4233/uuid206d8f37-4d4c-4af9-9da3-8d57fce769e8>

**Important note**

To cite this publication, please use the final published version (if applicable). Please check the document version above.

**Copyright**

Other than for strictly personal use, it is not permitted to download, forward or distribute the text or part of it, without the consent of the author(s) and/or copyright holder(s), unless the work is under an open content license such as Creative Commons.

**Takedown policy**

Please contact us and provide details if you believe this document breaches copyrights. We will remove access to the work immediately and investigate your claim.

WAVE OVERTOPPING PROCESSES FOR VERY MILD SLOPING AND SHALLOW FORESHORES

WAVE OVERTOPPING PROCESSES  
FOR VERY MILD SLOPING AND SHALLOW  
FORESHORES

HÀ THI THU NGUYỄN



9 789463 665247

**WAVE OVERTOPPING PROCESSES  
FOR VERY MILD SLOPING AND SHALLOW  
FORESHORES**



**WAVE OVERTOPPING PROCESSES  
FOR VERY MILD SLOPING AND SHALLOW  
FORESHORES**

**Proefschrift**

ter verkrijging van de graad van doctor  
aan de Technische Universiteit Delft,  
op gezag van de Rector Magnificus Prof.dr.ir. T.H.J.J. van der Hagen,  
voorzitter van het College voor Promoties,  
in het openbaar te verdedigen op donderdag 31 maart 2022 om 10.00 uur

door

**Hà Thi Thu NGUYÊN**

Master of Marine Engineering,  
Hanoi University of Civil Engineering, Vietnam  
geboren te Thanhhoa, Vietnam.

Dit proefschrift is goedgekeurd door de promotoren

Samenstelling promotiecommissie bestaat uit:

|                          |   |
|--------------------------|---|
| Rector Magnificus        | Voorzitter                                |
| Prof.dr.ir. M.J.F. Stive | Technische Universiteit Delft, Promotor   |
| Dr.ir. B. Hofland        | Technische Universiteit Delft, Copromotor |

Onafhankelijke leden:

|                              |                                   |
|------------------------------|-----------------------------------|
| Prof.dr.ir. A.J.H.M. Reniers | Technische Universiteit Delft     |
| Prof.dr.ir. M.R.A. van Gent  | Deltares                          |
| Dr.ir. T. Suzuki             | Min. Overheid Vlaanderen, Belgium |
| Prof.dr.ir. Tuan Thieu Quang | Thuyloi University, Vietnam       |

Overig lid:

|                     |   |
|---------------------|---|
| Dr.ir. Vu Dan Chinh | Hanoi University of Civil Engineering, Vietnam, Co-author |
|---------------------|---|

The work presented in this thesis was performed at the Department of Hydraulic Engineering of the Faculty of Civil Engineering and Geosciences of Delft University of Technology. This research was funded by the Vietnam International Education Cooperation Department (VIED), the Ministry of Education and Training.



BỘ GIÁO DỤC VÀ ĐÀO TẠO  
**CỤC HỢP TÁC QUỐC TẾ**  
International Cooperation Department

 **TU Delft**

*Keywords:* SWAN, SWASH, wave overtopping discharge, LF waves/ infragravity waves, spectral wave period, (very) shallow foreshore, very gentle foreshore, Weibull parameters, overtopping volume.

*Printed by:* Hà Thi Thu Nguyễn

*Front & Back:* created by Hà Thi Thu Nguyễn

Copyright © 2022 by Hà Thi Thu Nguyễn

All right reserved. No part of this publication may be reproduced, stored in a retrieval system, or transmitted, in any form or by any means, without the written permission of the author.

An electronic version of this dissertation is available at

<http://repository.tudelft.nl/>.

*For my dear departed father*

*For my lovely daughter, my mother and my "special" friend*





# Contents

|   |      |
|---|------|
| Summary.....  | xii  |
| Samenvatting.....   | xiii |
| 1. Introduction.....  | 1    |
| 1.1. Motivation .....   | 2    |
| 1.2. Research objectives .....  | 4    |
| 1.3. Thesis outline.....  | 4    |
| References.....   | 6    |
| 2. Wave overtopping as represented in the current literature .....  | 7    |
| 2.1. Introduction.....  | 7    |
| 2.2. Definition of parameters .....   | 8    |
| 2.3. The choice of numerical models .....   | 10   |
| 2.3.1. SWAN.....  | 10   |
| 2.3.2. SWASH.....   | 11   |
| 2.4. State-of-the-art in wave overtopping processes .....   | 11   |
| 2.4.1. Wave propagation to near-shore.....  | 11   |
| 2.4.2. Research on infragravity waves .....   | 15   |
| 2.4.3. Study on dike-foreshore systems.....   | 16   |
| 2.4.4. Wave run-up.....   | 17   |
| 2.4.5. Wave overtopping discharge .....   | 18   |
| 2.4.6. Probability distribution of individual overtopping volumes .....   | 20   |
| 2.5. Conclusions.....   | 23   |
| References.....   | 24   |
| 3. Wave overtopping as represented in the current literature .....  | 27   |
| 3.1. Introduction.....  | 28   |
| 3.1.1. State-of-the-art in deriving the spectral wave period for different foreshores .....                           | 29   |
| 3.1.2. State-of-the-art in wave overtopping formulae for sea-dikes with steep, mild, and very gentle foreshores ..... | 30   |

|   |    |
|---|----|
| 3.2. Materials and methods .....  | 31 |
| 3.2.1. Site description .....   | 31 |
| 3.2.1.1. Bathymetry .....   | 31 |
| 3.2.1.2. Offshore hydraulic conditions and dike geometries .....                        | 33 |
| 3.2.1.3. Wave dissipation without sea dikes .....                                       | 33 |
| 3.2.2. SWASH setup .....  | 34 |
| 3.2.2.1. Configuration to determine spectral wave period at dike toes .....             | 34 |
| 3.2.2.2. Configuration to determine overtopping of the sea dike .....                   | 35 |
| 3.2.2.3. Mean wave overtopping discharge over the dike crest .....                      | 36 |
| 3.3. Results .....  | 37 |
| 3.3.1. Wind influence on wave transformation .....                                      | 37 |
| 3.3.2. Wave heights and periods at the toes of sea dikes .....                          | 37 |
| 3.3.3. Wave spectra over the shallow foreshore .....                                    | 38 |
| 3.3.4. Spectral wave periods at gentle to very gentle slopes .....                      | 39 |
| 3.3.5. Wave overtopping discharge for a gentle foreshore slope .....                    | 40 |
| 3.3.6. Wave overtopping discharge for Vietnamese conditions with very gentle slopes.... | 41 |
| 3.3.7. Comparison to existing approaches .....  | 42 |
| 3.3.8. Wave overtopping discharge for a high sandy foreshore .....                      | 43 |
| 3.4. Discussion .....   | 43 |
| 3.4.1. Incident spectral wave periods on gently sloping foreshores .....                | 44 |
| 3.4.2. Wave overtopping discharge formulae for very gentle slopes .....                 | 44 |
| 3.5. Conclusions .....  | 45 |
| References .....  | 46 |
| 4. Wave overtopping volume for very mild and shallow foreshores .....                   | 48 |
| 4.1. Introduction .....   | 48 |
| 4.1.1. State-of-the-art in probability of wave overtopping for coastal structures ..... | 49 |
| 4.1.2. State-of-the-art in deriving the maximum individual wave volume .....            | 50 |
| 4.2. Methods .....  | 52 |
| 4.2.1. Description of physical model data .....   | 52 |
| 4.2.2. Numerical modelling setup .....  | 53 |
| 4.2.2.1 Description of numerical model SWASH .....                                      | 53 |
| 4.2.2.2 Use of SWAN model to obtain offshore wave spectral shape .....                  | 53 |

|   |    |
|---|----|
| 4.2.2.3 Test programme.....   | 55 |
| 4.2.3. Data analysis.....   | 56 |
| 4.2.4. Analysis of the a- and b-values from individual wave overtopping volumes .....   | 57 |
| 4.3. Results .....  | 59 |
| 4.3.1. Validation of wave spectra for steep slopes between the experiment and numerical models .....  | 59 |
| 4.3.2. Normally gentle foreshore slope 1:100.....   | 61 |
| 4.3.2.1 In deep water .....   | 61 |
| 4.3.2.2 In shallow water .....  | 62 |
| 4.3.3. Very gentle slopes in shallow water.....   | 63 |
| 4.3.3.1 Wave parameters at the toe .....  | 63 |
| 4.3.3.2 Wave overtopping parameters.....  | 64 |
| 4.3.3.3 Weibull parameters for very gentle slopes in shallow water.....   | 66 |
| 4.3.3.4 The impact of relative crest freeboard, foreshore slope and relative spectral wave period on the shape factor b.....                  | 68 |
| 4.3.4. A new equation of the shape parameter b for very gentle and shallow foreshores.  | 69 |
| 4.3.5. A new equation of the wave overtopping discharge for very gentle bed foreshores  | 70 |
| 4.3.6. The scale parameter and wave overtopping volume for very gentle bed foreshores .....   | 72 |
| 4.4. Discussion .....   | 72 |
| 4.4.1. Accuracy of SWASH in wave overtopping .....  | 72 |
| 4.4.2. New equations of the shape parameter and the average overtopping discharge for sea dikes with shallow and very gentle foreshores ..... | 73 |
| 4.5. Conclusions.....   | 74 |
| Bibliography.....   | 75 |
| 5. Practical implications for dike design in Vietnam .....  | 79 |
| 5.1. Introduction.....  | 78 |
| 5.2. Case study: Sea-dike design in Binhthuan province.....   | 80 |
| 5.2.1. Natural and hydraulic characteristics.....   | 81 |
| 5.2.2. SWAN hydraulic boundary condition .....  | 83 |
| 5.2.3. SWASH model.....   | 84 |
| 5.3. Results .....  | 85 |
| 5.3.1. Wave dissipation over very gentle slope foreshore.....   | 85 |

|   |    |
|---|----|
| 5.3.2. Wave spectra and wave parameters at the toe.....   | 86 |
| 5.3.3. Wave overtopping discharge .....   | 87 |
| 5.3.4. Wave overtopping volume .....  | 89 |
| 5.4. Conclusion .....   | 90 |
| References.....   | 92 |
| 6. Conclusions and recommendations .....  | 94 |
| 6.1. Conclusions.....   | 94 |
| 6.1.1. The evolution of wave parameters at the toe of a sea-dike and the role of IG waves .....           | 94 |
| 6.1.2. Validation of wave spectra and average overtopping discharge for steep slopes ....                 | 94 |
| 6.1.3. Average overtopping discharge for very mild foreshores.....  | 95 |
| 6.1.4. The two-parameter Weibull distribution for very gentle and shallow foreshores...                   | 95 |
| 6.1.5. A case study in Vietnam .....  | 95 |
| 6.2. Recommendations and future research.....   | 96 |
| 6.2.1. Numerical calculations for very gentle and shallow foreshores.....                                 | 96 |
| 6.2.2. New formulae of average discharge and individual volumes for very mild and shallow foreshores..... | 96 |
| References.....   | 97 |
| Acknowledgements .....  | 97 |
| Curriculum vitae .....  | 97 |
| List of publications.....   | 97 |

# Summary

A sea-dike system is of importance for the protection of the hinterland. However, the effect of very gentle and shallow sloping foreshores (in the order up to 1 in 1000) on wave overtopping processes has not yet been quantified enough and, thus, so far is not well understood. This dissertation seeks an answer to the question of whether the existing formulae are suitable for these slopes, and which approach is the most appropriate to quantify the [wave overtopping discharge and volume](#) for these typical (e.g. gentle and shallow) slopes. Along the way, comparative research between the results of numerical analysis and those of existing studies is conducted. Subsequently, new empirical equations are formulated, using a series of test cases in the numerical modeling for this type of slopes, using a [Least Squares method](#).

First, recent state-of-the-art research for wave overtopping behavior and the relevant parameters is investigated. Mechanisms of physical phenomena, such as wind-induced wave transformation from offshore to near-shore, frequency dispersion, shoaling, wave-wave interaction, wave breaking, bottom friction, wave run-up on the slope and the subsequent overtopping process, are briefly described in [Chapter 2](#) with corresponding existing formulae. The literature review demonstrates that the studies of average overtopping rate worldwide focus mainly on slopes, ranging only as gentle as 1 in 250. The phase-averaged [SWAN](#) model is chosen to translate a wave climate from deep water to near-shore waves, and the non-hydrostatic wave model [SWASH](#) is applied to analyse the overtopping process over sea-dikes in coastal areas.

Current empirical formulae of the average overtopping discharge  $q$  all underestimate the values for very gentle foreshores. Subsequently, a more accurate formulation needs to be established for these bed slopes. Therefore, [Chapter 4](#) of this thesis establishing this formulation proposes an extension of the correction of the formulation for gentle slopes, and presents a new equation of the mean overtopping rate for gentle and shallow slopes in the case of low-crested sea-dikes. Moreover, the research reveals that the spectral wave period  $T_{m-1,0}$  at the toe of a sea-dike can reach two times the values in the offshore zone.

However, the average overtopping discharge is not the only crucial factor to design a sea-dike. Under extreme storms, the inner grass-covered dike slopes are often damaged due to overtopping. The grass strength is evaluated through a cumulative overload approach, which can be estimated quantitatively by a two-parameter [Weibull](#) distribution. The shape parameter  $b$  of the Weibull distribution is researched based on a series of test cases for low-crested dikes. Contrasting the previous research of  $b$  created for deep and flat sea beds, the new formula of the shape factor takes the foreshore slope  $\cot(\theta)$  and the relative wave period  $T_{m-1,0,t}/T_{m-1,0,o}$  into account and proves to be valid for shallow water. The remaining scale parameter  $a$  can be easily determined from the Gamma function based on the given shape factor and on the average overtopping discharge.

Finally, a case study in the [Central coast of Vietnam](#) is assessed in terms of wave overtopping behavior using the new formulae. During a heavy storm in this coastal area, one of the dikes has severely eroded and a new dike needs to be designed. Nevertheless, the Vietnamese guidelines, written based on the former standard in the [Netherlands](#), have not yet mentioned the effect of wave overtopping volume in the design of a sea-dike on the coast of [Vietnam](#). The numerical analysis, conducted in this thesis, seems to be satisfactory compared with the new empirical equations as mentioned in [Chapter 5](#) for the very gentle and shallow foreshores.

This dissertation presents the effect of wave overtopping behavior(s) for very mild and shallow foreshores and proposes new formulae of a mean wave overtopping rate and a two-parameter [Weibull](#) distribution for individual overtopping volumes in the specific case of low-crested sea-dikes. Previous knowledge in the field of gentle and shallow slopes had not yet been quantified. As mentioned, in this research it is important that the [Infragravity](#) (IG) waves and the foreshore slope are taken into account in the calculation of the shape factor of the [Weibull](#) distribution. It is recommended to extend the current research of wave overtopping processes over low-crested dikes to very mild and shallow foreshores with high-crested sea-dikes.

# Samenvatting

Een zeedijksysteem is van groot belang voor de bescherming van het achterland. Het effect van zeer mild glooiende en ondiepe, hellende vooroevers (orde van grootte 1 op 1000) op golfoverslagprocessen is echter niet voldoende gekwantificeerd en, derhalve, tot nu toe niet voldoende begrepen. Dit proefschrift zoekt een antwoord op de vraag of de bestaande formules geschikt zijn voor dit type hellingen, en welke benadering het meest geschikt is om de afvoersnelheid en het volume van golfoverslag voor deze (i.e. mild glooiende en ondiepe) hellingen te kwantificeren. Vergelijkend onderzoek tussen de resultaten van numerieke analyse en die van bestaande studies is uitgevoerd. Vervolgens worden nieuwe empirische vergelijkingen geformuleerd, gebruikmakend van een reeks experimenten in de numerieke modellering voor dit type hellingen, gebruikmakend van de “Least Squares” optimalisatiemethode.

Allereerst wordt recent “state-of-the-art” onderzoek naar het gedrag van golfoverslag en de meest relevante parameters onderzocht. De mechanismen van natuurkundige verschijnselen, zoals de door wind geïnduceerde golftransformatie van de offshore naar de near-shore, frequentiespreiding, “shoaling”, golfinteractie, de branding, bodemfrictie, golfoploop op de helling, en het daaropvolgende golfoverslagproces, worden kort beschreven in hoofdstuk 2 met de daarbij behorende, bestaande formules. Het literatuuronderzoek toont aan dat de studies naar de gemiddelde overslagsnelheid wereldwijd vooral gericht zijn op hellingen variërend van slechts 1 op 250. Het “phase-averaged” SWAN-model is gekozen voor de vertaling van een golfklimaat van diep water naar golven dichtbij de kust, en vervolgens wordt het niet-hydrostatisch golfmodel SWASH toegepast om het proces van golfoverslag over zeedijken in kustgebieden te analyseren.

De huidige empirische formules van de gemiddelde overslag afvoersnelheid onderschatten alle de waarden voor zeer mild glooiende vooroevers. Vervolgens is het noodzakelijk om voor deze bodemhellingen een nauwkeurigere formulering vast te stellen. In hoofdstuk 4 van dit proefschrift wordt deze formulering afgeleid en wordt een uitbreiding van de correctie van de formulering voor flauwe hellingen voorgesteld. Een nieuwe vergelijking van de gemiddelde overslagsnelheid voor mild glooiende en ondiepe hellingen in het geval van zeedijken met relatief lage tophoogte wordt gepresenteerd. Bovendien laat het onderzoek zien dat de spectrale golfperiode  $T_{m-1,0}$  aan de voet van een zeedijk twee keer de waarden van die in de offshore zone kan bereiken.

Het gemiddelde overslagdebiet is echter niet de enige cruciale factor bij het ontwerpen van een zeedijk. Bij extreme stormen worden de met gras begroeide dijkhellingen aan de landkant vaak beschadigd door golf overslag. De sterkte van het gras wordt geëvalueerd door middel van een cumulatieve benadering van overbelasting, die op grond van een “twee-parameter” Weibull-verdeling kwantitatief ingeschat kan worden. De vorm-parameter  $b$  van de Weibull-verdeling is onderzocht aan de hand van een reeks experimenten met lage dijken. In tegenstelling tot het eerdere onderzoek van parameter  $b$  voor diepe en vlakhellende zeebodems, neemt de nieuwe formule van de vorm-factor de vooroeverhelling  $\cot(\theta)$  en de relatieve golfperiode  $T_{m-1,0,t}/T_{m-1,0,0}$  in aanmerking en blijkt deze geldig te zijn voor ondiep water. De overblijvende schaal-parameter  $a$  kan eenvoudig worden bepaald uit de Gamma-functie op basis van de gegeven vorm-factor en de gemiddelde golfoverslag afvoer.

Tenslotte wordt een case study in het centrale kustgebied van Vietnam geëvalueerd in termen van golfoverslaggedrag met behulp van de nieuwe formules. Tijdens een zware storm in dit kustgebied is een van de dijken ernstig aangetast en een nieuwe dijk moet worden ontworpen. Desalniettemin hebben de Vietnamese richtlijnen (geschreven op basis van de traditionele norm in Nederland) nog geen melding gemaakt van het effect van golfoverslagvolume in het ontwerpen van een zeedijk voor de kust van Vietnam. De numerieke analyse, die in dit proefschrift is uitgevoerd, lijkt bevredigend te zijn vergeleken met de nieuwe empirische vergelijkingen, zoals genoemd in Hoofdstuk 5, voor de zeer mild glooiende en ondiepe oevers.

Dit proefschrift presenteert het effect van golfoverslaggedrag voor zeer mild glooiende en ondiepe oeverlanden. Het stelt nieuwe formules voor van een gemiddelde golfoverslagsnelheid en

een "twee-parameter" Weibull-verdeling voor individuele overslagvolumes in het specifieke geval van lage zeedijken. Voorkennis op het gebied van mild glooiende en ondiepe hellingen was tot dusver nog niet gekwantificeerd. Zoals vermeld, is het van belang dat in dit onderzoek de "Infragravity" (IG) golven en de vooroeverhelling in aanmerking worden genomen bij de berekening van de factor van de vorm met betrekking tot de Weibull-verdeling. De aanbeveling is om het huidige onderzoek naar golfoverslagprocessen over lagere dijken uit te breiden naar zeer mild glooiende en ondiepe oeverlanden met een hoger top nivo.



# 1

## Introduction

*"Your **time** is **limited**,  
So don't **waste** it living someone **else's** life"*  
- Steve Jobs

All over the world, sea-dikes are used to protect the land and its residents from wave overtopping incidents. Sea dikes, as a type of coastal defence, are investigated and identified in various geological settings and their hydrological response to steep and mild foreshores. This dissertation gains a better insight into the wave overtopping process for very gently sloping foreshores as exist in Vietnam. To begin with, this chapter draws the rationales behind the study and formulates the main objectives.

### 1.1. Motivation

In the past decades, high buildings and resorts have increasingly been constructed close to the seashore. Defense structures, therefore, were built to protect the buildings and residents from floods during storms, typhoons and/or high tides. These structures, in the shape of seawalls or sea-dikes, are designed to diminish the amount of salt water reaching the hinterlands, yet these are not always able to prevent the overtopping of water. In certain cases, it is acceptable that a certain amount of water overtops over the coastal structure as long as the structural integrity of the rear-slope is not violated. The geometric design of a sea-dike can then be based on the tolerable average overtopping discharge or the tolerable mean amount of sea-water that flows over the coastal structure per meter in time (EurOtop, 2018).

To predict the overtopping behavior, the overtopping probability is taken into consideration. The probability of wave-by-wave overtopping volumes, associated with a two-parameter Weibull distribution, is well-described in several recent studies. It is indicated that individual wave overtopping volumes from single overtopping events and, particularly, the maximum volume, become more important in the physical description of overtopping processes and in their role in the failure of the dike's back slope than the use of a mean overtopping discharge. However, these studies focused mainly on deep water - with steeper and moderately mild foreshores.



Figure 1.1. Flooding after the Doksuri typhoon (2017). Source: [financialexpress.com](http://financialexpress.com)



Figure 1.2. Flooding after Goni typhoon in a village of a central province (2020). The upper-right corner image was taken several hours post-storm. The lower images were one day post-storm. The upper-left corner image was several days post-storm (a boy trying to get out of his house).

Source: [tinmoitruong.vn](http://tinmoitruong.vn)

Vietnam has long coastlines with low-lying coastal areas which have always been extremely vulnerable to flooding under extreme weather conditions. Large parts of the coast in Vietnam rely mainly on sea-dikes for their safety. Sea-dikes can be found along many coastal stretches of the country. Thus, these coastal defences protect the hinterlands from hazards originating from the sea. The existing state of the Vietnamese sea-dikes is insufficient to cope with the higher wave attacks and the higher water levels reaching them due to extreme weather events, such as typhoons and associated wave attacks, which are predicted to increase wave overtopping over the present sea-dikes. Accordingly, dike crest levels must also be higher to satisfy the existing regulations in terms of wave overtopping. However, increasing dike crests can cause a major effect on the surrounding areas of a dike. The first consequence is the loss of land since the dike base needs to be widened to ensure the stability of the whole dike. Moreover, the increase of the crest levels of the dikes becomes an enormously costly procedure. Therefore, the guidelines of the wave overtopping process could be extended in cases of existing dikes are still strong enough to be resistant to the stronger wave overtopping.

The existing research and studies on wave overtopping for a sea-dike, including [Van der Meer et al. \(1995\)](#), [Van Gent \(2002\)](#), [Pullen et al. \(2007\)](#), [Van der Meer et al. \(2010\)](#), [Altomare \(2016\)](#), however, are not related to very gentle slopes. Therefore, it is not only important to fully understand the effects of wave overtopping behavior over a sea-dike with very gentle and shallow foreshores, but also new equations need to be proposed for this type of gentle and shallow slopes, as exist in Vietnam.

## 1.2. Research objectives

The main research question addressed in this dissertation is:

*Wave overtopping is very important for the stability of sea-dikes.  
Do existing formulae provide a good agreement for the very gentle and shallow foreshores  
as encountered in Vietnam?*

To provide the answers to this question, the dissertation can be divided into several sub-questions, posed below:

**Question 1:** What is the evolution of the spectral wave period and wave height at the toe of a sea-dike under an extreme condition? What is the impact of infragravity waves on very gently sloping foreshores? (Chapter 3).

**Question 2:** Are the existing formulae of average overtopping discharge appropriate in the case of very mild slopes? (Chapter 3).

**Question 3:** Are the wave spectra and wave overtopping discharge derived from the SWASH model comparable to those in the laboratory experiment for steep slopes? (Chapter 4).

**Question 4:** Can the current equations of the Weibull distribution for the individual overtopping volume be applied to the case of very gentle and shallow foreshores? How to propose new empirical formulae of average discharge and two Weibull parameters for these types of slopes? (Chapter 4).

**Question 5:** Can new formulae of the average discharge and Weibull distribution parameters be used for a case study in Vietnam, where typical very gently sloping foreshores are found? (Chapter 5).

## 1.3. Thesis outline

The basic idea of this dissertation is to gain more insight on the wave overtopping process for very gentle and shallow foreshores in terms of the average discharge and the overtopping probability. The existing formulae are used to evaluate the current values and, subsequently, new equations are given for these types of slopes. The thesis outline used is as follows (figure 1.1):

### *Chapter 1: Introduction*

Presents the problem description of the research, investigates the study purposes and the thesis outline is described.

### *Chapter 2: Wave overtopping as represented in the current literature*

The current knowledge of the wave overtopping process is researched; the major parameters that influence the wave overtopping behavior are further elaborated on. Here, the existing formulae related to wave overtopping discharge and overtopping volume will be presented.

### *Chapter 3: Wave overtopping discharge for very gently sloping foreshores*

The general formula derived from Van Gent (1999) and the recent corrective “equivalent slope” approach proposed by Altomare et al. (2016) were not derived for very mild slopes that are gentler than 1:250. Therefore, the average overtopping rate as predicted by these formulae is compared to a numerical model to determine the applicability of these formulae. Moreover, the relative spectral wave period for this type of slopes is investigated in this chapter.

### *Chapter 4: Wave overtopping volumes at very mild shallow foreshores*

The validation of wave spectra and the average wave overtopping rate for steep slopes (1:35 and 1:50) between physical and numerical models is evaluated. Furthermore, wave attack on the

landward dike slopes caused by wave overtopping is quantified for very gently sloping foreshores. The distribution of individual wave volumes is determined for dikes with shallow and very gentle foreshores based on a dataset of volumes derived by the SWASH model. Eventually, empirical formulae of the scale and shape factors are proposed using a least squared method. An empirical model for the overtopping is established.

*Chapter 5: Practical implications for dike design in Vietnam*

A case study in the Central area of Vietnam is investigated in terms of wave overtopping discharge and overtopping volume under an extreme condition. New empirical equations of average discharge and the shape factor are also used to validate the hypothesis for this typical very gentle slope in Vietnam.

*Chapter 6: Conclusions and Recommendations*

An elaborate conclusion summarizes the previous chapters. Recommendations will be proposed for further studies relating to the wave overtopping behaviors over the sea-dikes for very mild and shallow foreshores.

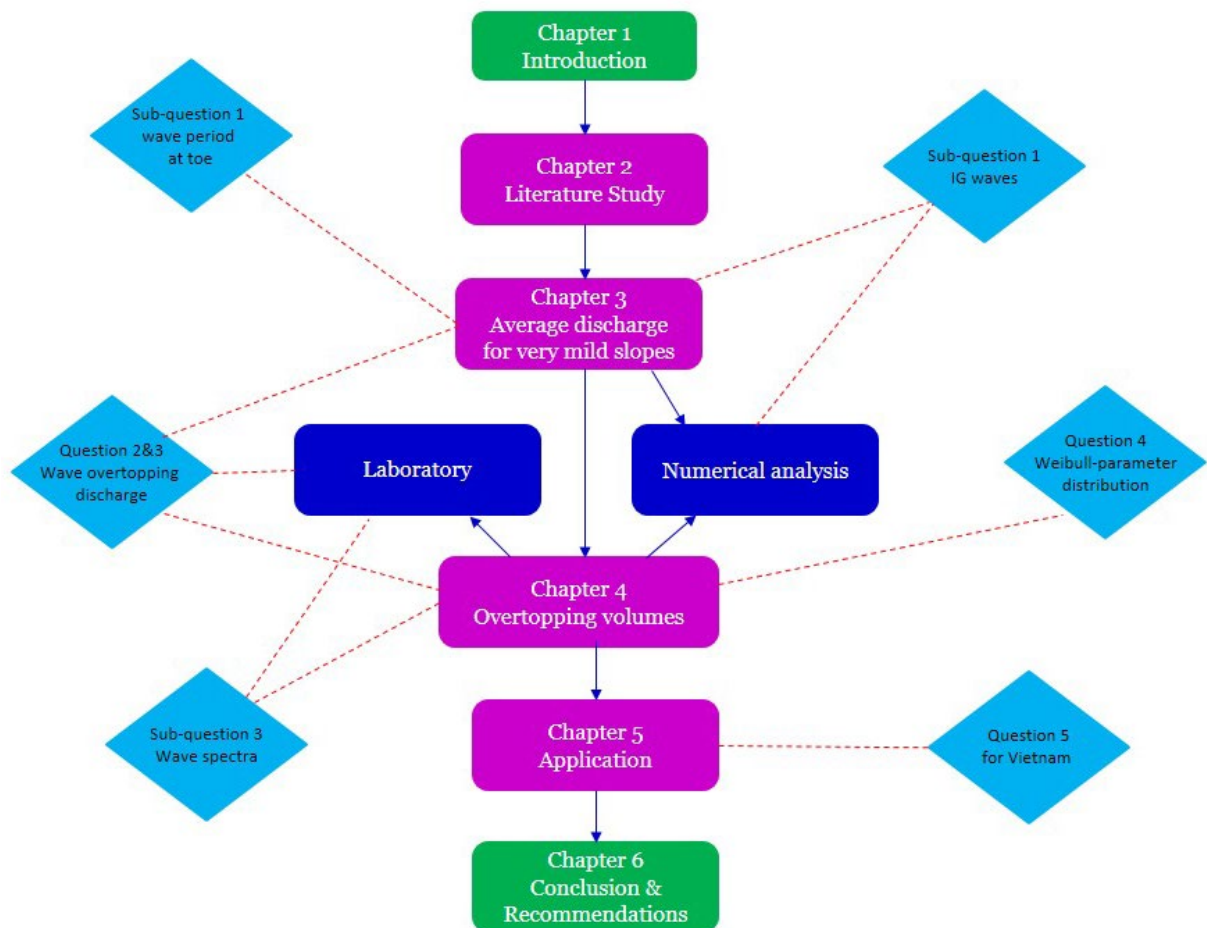


Figure 1.1. Flow chart of this dissertation

## References

Altomare, C., Suzuki, T., Chen, X., Verwaest, T., Kortenhaus, A. (2016). Wave overtopping of sea dikes with very shallow foreshores. *Coast. Eng.* 2016, 116, 236–257, ISSN 0378-3839.

Van der Meer, J., Allsop, N., Burce, T., De Rouck, J., Kortenhaus, A., Pullen, T., Schüttrumpf, H., Troch, P., and Zanuttigh, B. (2016). EurOtop Manual on wave overtopping of sea defences and related structures. An overtopping manual largely based on European research, but for worldwide application. <http://www.overtopping-manual.com/>

Pullen, T., Allsop, N., Bruce, T., Kortenhaus, A., Schüttrumpf, H., and van der Meer, J. (2007). EurOtop Manual on wave overtopping of sea defences and related structures. *Assessment Manual*.

Van Gent, M. R. A. (1999). Physical model investigations on coastal structures with shallow foreshores: 2D model tests with single and double-peaked wave energy spectra. *Technical report, WLI Delft Hydraulics, Delft*.

Van Gent, M. R. A. (2002). Low-exceedance wave overtopping events: Measurements of velocities and the thickness of water-layers on the crest and inner slope of dikes. *Delft Cluster, DC1-322-3*.

## 2

## Wave Overtopping as represented in the current Literature

In this chapter, the background information for this dissertation is provided by describing the wave overtopping processes based on recent physical studies and by comparing these to the empirical existing model in terms of the average overtopping rate and the wave-by-wave overtopping volume. Firstly, in section 2.1 a definition of wave overtopping is given, followed by a description of the terms to explain the crucial parameters used in section 2.2. Next, the choice of numerical models applied in this dissertation is presented in section 2.3, focusing on the SWAN and SWASH models. Subsequently, the recent state-of-the-art studies and the relevant formulae are described, and discussed in section 2.4. Finally, a conclusion is given in section 2.5

### 2.1. Introduction

Overtopping occurs as a result of waves running up the crest of a sea dike. Whenever wave run-up level is exceptionally high, water will exceed and pass over the dike crest. In this case a continuous sheet of water, or the so-called “green water”, passes over the dike crest and overtopping occurs. This type of overtopping is the most dominant occurrence of wave overtopping. Another case of overtopping takes place when waves break on an armoured seaward slope causing significant masses of splash, called “white water”. The less important case, spray, occurs when wind blows water from the seaward carried over the dike crest. Without the impact of strong shoreward wind, this spray will not lead to any significant wave overtopping process.

The following formula can be given: run-up height  $R_u$  is exceeded by incident waves, measured from the still water level (SWL). The distance from the mean water level to the dike crest height is considered as the crest freeboard  $R_c$ . The definition of these terms is shown in figure 2.1

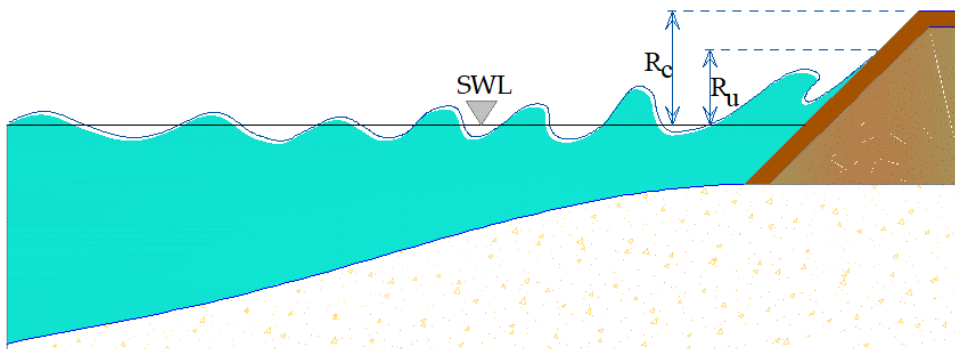


Figure 2.1: Definition sketch of the crest freeboard and wave run-up

## 2.2. Definition of parameters

A critical overview of related parameters is described in this section. The wave height  $H$ , wave length  $L$  and water depth  $h$  are depicted in figure 2.2.

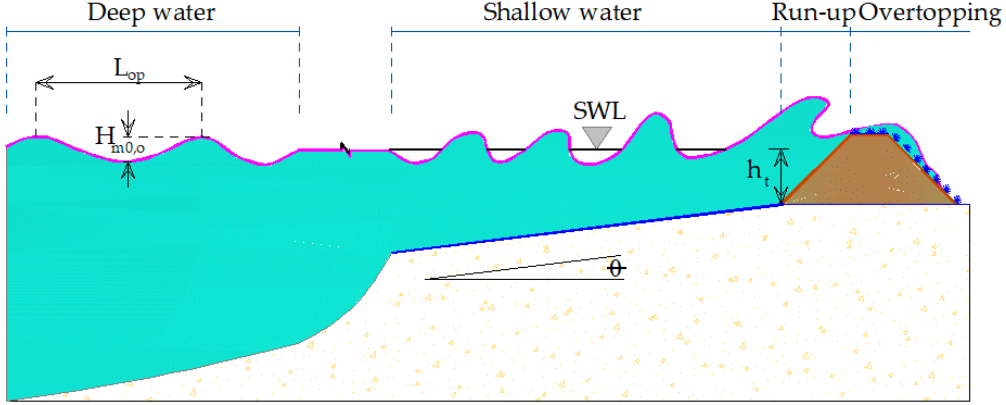


Figure 2.2: Definition sketch of some parameters

### Wave height ( $H$ ) and wave spectrum $E(f)$

An important parameter to characterize a wave, is the height between the crest and the trough of a wave: wave height ( $H$ ). The test data used in this dissertation contain irregular waves that are considered as a superposition of a number of regular waves, however the most important form of a wave, as described here, is the wave spectrum based on random-phase/amplitude model. The shape of the wave spectrum used in this study is the JONSWAP (Joint North Sea Wave Project) that may be applied for arbitrary wind effects in deep water regions. The JONSWAP spectrum (Hasselmann et al., 1973) is defined based on the formula of Pierson-Moskowitz (1964) as below:

$$E(f) = \underbrace{\alpha g^2 (2\pi)^{-4} f^{-5} \exp\left[-\frac{5}{4}\left(\frac{f}{f_m}\right)^{-4}\right]}_{\text{Pierson-Moskowitz}} \gamma^b \quad (2.1)$$

$$b = \exp\left[-\frac{1}{2\sigma^2}\left(\frac{f}{f_m} - 1\right)^2\right] \quad (2.2)$$

$$\sigma = \begin{cases} \sigma_1, & f \leq f_m \\ \sigma_2, & f > f_m \end{cases} \quad (2.3)$$

where  $g$  is gravitational acceleration,  $ms^{-2}$

$\alpha$  is energy scale factor, commonly given as 0.0081,

$f, f_m$  are frequency and frequency scale factor, respectively,  $s^{-1}$

$\gamma$  is peak enhancement factor, commonly given as 3.3

$\sigma$  is peak width factor.

There are two ways to determine a specific wave height. The first approach is based on a time domain in which the wave field can be characterized by significant wave height,  $H_s$ . This parameter is defined as the mean height of the highest one-third waves measured. Another method is to estimate  $H_{m0}$  of the incoming waves at the dike toe from the variance energy spectrum  $E(f)$  based on frequency domain. This is the preferred approach, used in this study, since the wave height at the toe



must be known in order to determine wave transformation and overtopping processes over the sea dike. This type of wave height can be also calculated based on zero spectral moment of waves:

$$H_{m0} = 4\sqrt{m_0} \quad (2.4)$$

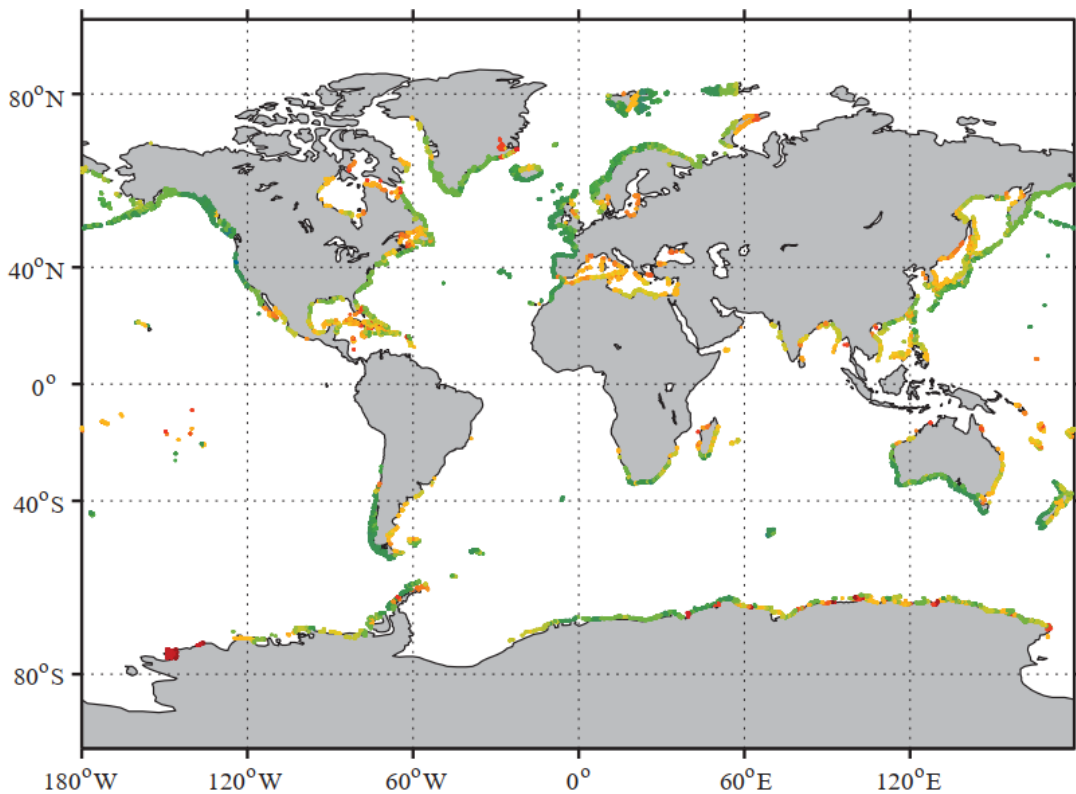
### Wave period (T)

In this dissertation, we use two types of wave period. The first parameter is the peak period  $T_p$ , or the peak incoming wave period at the dike toe. It is often imposed as an input at the offshore boundary condition for the numerical tests, as well as for the physical model. The peak period is also considered as the inverse of the frequency where the frequency spectrum reaches a maximum value. Similar to the wave height, there are several ways to estimate the wave period, such as the average wave period  $T_m$ , and the spectral wave period  $T_{m-1,0}$ . The latter one plays an important role in this study, especially at the toe of sea defense structures since the infragravity wave is considered dominant in this area.

### Wave steepness ( $s_0$ )

Wave steepness is considered as a dimensionless parameter, a ratio between the wave height and wave length. High wave steepness can exert wave breaking. For a typical swell sea  $s_0 = 0.01$ , and for a typical sea wind  $s_0$  is in the range of 0.03 to 0.05.

To investigate locations that are associated with shallow water conditions wave data, collected from the Wavewatch III model by [Tolman et al. \(2009\)](#) and bathymetry data estimated by [Amante and Eakins \(2009\)](#), are applied. The Wavewatch III model includes global data of wave hindcasting in the period from 1979 to 2009 with a time interval of 30 min. The below figure presents the lowest wave steepness obtained from peak wave periods with the ratio  $H_{m0}/h \geq 0.4$  carried out at  $h = 15m$ .



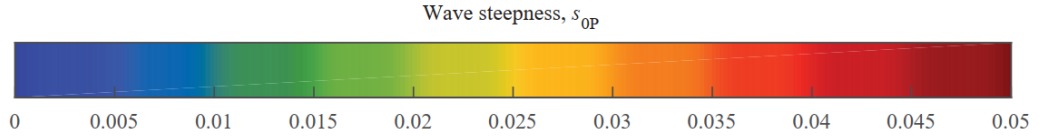


Figure 2.3: Positions where wave breaking occurred at  $h = 15m$  (upper figure). Color presents the lowest wave steepness with  $H_{m0}/h \geq 0.4$  (lower figure).

The figure indicates that the Australian west coast, Western Europe, the west coasts of North and South America and parts of the coast of East Asia exhibit high nonlinear waves.

### Breaker parameter ( $\xi_{m-1,0}$ )

The Iribarren number, or breaker parameter  $\xi$ , is a function of the angle of a dike slope and wave steepness, determined below as:

$$\xi = \frac{\tan\alpha}{\sqrt{s_0}} \quad (2.5)$$

If a wave is irregular, the steepness,  $s_0$ , turns into  $s_{m-1,0}$ , estimated based on the spectral wave period  $T_{m-1,0}$ . The Iribarren number can be considered as an indication of the kind of breaking waves as shown in figure 2.3. There are several types of Iribarren numbers, i.e. when the slope is quite gentle,  $\xi_{m-1,0}$  is less than 0.2, waves are considered spilling. When  $\xi_{m-1,0}$  ranges between 0.2 and 2-3, waves break as plunging types and when  $\xi_{m-1,0}$  lies in a range of 2 to 3, the wave breaking is called collapsing. For steeper slopes, when  $\xi_{m-1,0}$  is bigger than 2 or 3, waves can be seen as surging, which actually results in non-breaking waves.

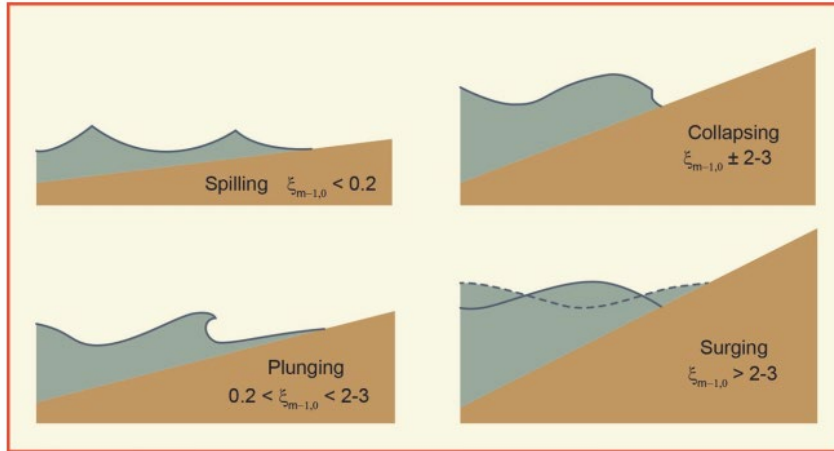


Figure 2.4: Type of wave breaking on a slope (EurOtop 2018 based on Battjes, 1974)

## 2.3. The choice of numerical models

### 2.3.1. SWAN

SWAN (Simulating Waves Near-shore) is introduced by Booij et al. (1999) to estimate short-crested random waves (and ambient currents) in coastal areas with a shallow foreshore. This model is based on a phase-averaged spectral wave calculation and the wave action balance, as described in Garrett (1967) below:

$$\frac{\partial A}{\partial t} + \frac{\partial c_x A}{\partial x} + \frac{\partial c_y A}{\partial y} + \frac{\partial c_\sigma A}{\partial \sigma} + \frac{\partial c_\theta A}{\partial \theta} = \frac{S_{tot}}{\sigma} \quad (2.6)$$

Where  $c_x, c_y, c_\sigma, c_\theta$  are propagation velocities in spatial, spectral and directional space,

---

$A = E/\sigma$  is action density,

$E$  is energy density,  $\sigma$  is relative radian frequency,

$S_{tot}$  contains generation and dissipation sources

With the absence of ambient currents, the above action balance equation can turn into an energy balance formula:

$$\frac{\partial E}{\partial t} + \frac{\partial c_x E}{\partial x} + \frac{\partial c_y E}{\partial y} + \frac{\partial c_\theta E}{\partial \theta} = S_{tot} \quad (2.7)$$

The energy conservation equation can be obtained by integrating frequencies and directions of the above equation, as follows:

$$\frac{\partial E}{\partial t} + \frac{\partial}{\partial x}(E c_g \cos \theta) + \frac{\partial}{\partial y}(E c_g \sin \theta) = S_{tot} \quad (2.8)$$

It is noticeable that the energy balance defines the energy of a travelling wave component.

The dissipation of wave energy is a result of the generation of white-capping, bottom friction, quadruplet wave-wave interaction and depth-induced wave breaking. The dissipation of bottom friction is given by [Bertotti and Cavaleri \(1994\)](#). The generation of white-capping is introduced by [Hasselmann \(1974\)](#). The white capping can be activated in SWAN if taking wind effects into account. The wave breaking mechanism in SWAN is proposed by [Battjes and Janssen \(1978\)](#). Regarding the quadruplet interactions, the equation suggested by [Hasselmann et al. \(1985\)](#) is applied and the triad wave-wave interactions are given by [Eldeberky and Battjes \(1995\)](#).

### 2.3.2. SWASH

A numerical model with non-hydrostatic, free surface, rotational flows is presented by [Zijlema et al., 2011](#) called SWASH. This model uses a non-linear shallow water equation in one and two dimensions, which has been derived from Navier Stokes equations. Moreover, SWASH is a non-hydrostatic wave model, predicting the propagation of a dispersive surface wave from deep water to the foreshore ([the SWASH team, 2015](#)). Additionally, SWASH can be correctly applied for a wide range of relevant physical phenomena such as: wave transformation, frequency dispersion, shoaling, quadruplet and triad wave-wave interactions, wave breaking, bottom friction water run-up and run-down, infragravity waves after breaking. As such, this model is perfect to be used for this study when investigating the wave propagation from the offshore to the dike toe, and the wave overtopping process over coastal structures ([Suzuki et al., 2012a, b](#); [Chen, 2016](#); [Tas, 2016](#); [Lashley et al., 2020](#)). The numerical models applied in this thesis are used not only to judge the performance of existing empirical expressions that were based on data, but also to develop new empirical expressions for applications for dikes in shallow water with a very mild foreshore.

## 2.4. State-of-the-art in wave overtopping processes

### 2.4.1. Wave propagation to near-shore

If waves travel from offshore to near-shore, their parameters, such as wave height, wave length and wave direction, are gradually changed until breaking in the surf zone. Some processes are described, amongst others by [Bosboom and Stive \(2012\)](#) and [Holthuijsen \(2007\)](#).

#### Wind input

When wind blows over the sea water surface, waves are generated. Initially new waves are small and short, over time they are becoming gradually higher and longer. The magnitude of wave parameters relies mainly on wind duration, fetch and water depth. The wind pushes the wave surface down on the windward side of the wave crest and pulls the surface up on the landward side, therefore,

the air pressure at the sea water surface can reach the greatest strength, while at the remaining side of the wave crest, it only has minimum strength. The transfer from wind energy to wave transformation is presented by Phillips (1957) with the concept of resonance mechanism, and Miles (1957) with the feedback mechanism to confirm that wave generation are a result of resonance between water waves and wind-induced pressure waves. The generation of wave-induced wind contains two parts, a linear part and exponential growing one, as formulated below:

$$S_{in}(\sigma, \theta) = A + BE(\sigma, \theta) \quad (2.9)$$

The linear part is proposed by Cavaleri and Rizzoli (1981) and the remaining part is indicated by Snyder et al. (1981) and Plant (1982).

### Shoaling

Shoaling is the change of waves in the propagation direction, as a result of the depth-limited variation of the group celerity in that direction. It leads to the rise of the wave amplitude because the wave propagation slows down when reaching shallow water. Based on linear wave theory, the dispersion relation is given by:

$$\omega = \sqrt{gk \cdot \tanh kh} \quad (2.10)$$

where  $k$  is the wave number,  $rad/s$ ;  $\omega$  is the frequency,  $rad/m$ ,

Using energy balance  $U = Ec_g = Enc$  and the relation  $E = 1/8\rho gH^2$ , we have:

$$\frac{H}{H_0} = \sqrt{\frac{1}{\tanh kh} \frac{1}{2n}} = K_{sh} \quad (2.11)$$

where  $U$  is energy flux per unit wave crest width,  $J/m/s$ ,

$n$  is the ratio of the wave group celerity to wave celerity,

$K_{sh}$  is the shoaling factor, in deep water  $K_{sh} = 1$

### Bottom friction

When the waves come to shallow water or the water depth is decreased, they “feel” the bottom. The friction between seabed and water layer leads to wave dissipation and the reduction of wave height. This phenomenon can be considered as a thin turbulence boundary layer right above the seabed that is caused by wave-induced water particle motion. Moreover, the bottom friction also leads to dissipation over the whole range of frequencies to water energy density.

The dissipation rate of time-averaged energy per unit bottom surface area can be described by:

$$\bar{D}_{bfr} = -\overline{\tau_b u_b} \quad (2.12)$$

in which  $u_b$ ,  $\tau_b$  are magnitude of particle velocity [ $m/s$ ] and shear stress [ $N/m^2$ ], respectively.

The shear stress can be obtained from drag-law models based on quadratic law (Collins, 1972):

$$\tau_b = \rho \cdot c_f \cdot u_b^2 \quad (2.13)$$

Based on the Chézy coefficient  $c_f = g/C^2$  and Manning’s roughness coefficient  $n$ , the dimensionless friction coefficient  $c_f$  can be determined by:

$$c_f = \sqrt{\frac{n^2 g}{h^{1/12}}} \quad (2.14)$$

Substitute this factor to the above equation:  $\bar{D}_{bfr} = -\rho c_f u_{rms,b} |u_{rms,b}|$

in which  $u_{rms,b}$  is the root mean square orbital speed at the sea bottom.

#### Non-linear wave interaction:

Wave-wave interaction is the interaction between waves where water energy is transmitted amongst waves due to resonance. In deep water, two pairs of wave components can interact with each other, leading to energy redistribution over water spectra. This phenomenon is called quadruplet wave-wave interaction. Almost all wave energy is based on transfer from mid-range to lower frequencies, only a small portion shift from mid to higher frequencies. In shallow water, another phenomenon commonly happens, called triad wave-wave interactions, where a diamond pattern of wave components could interact with a third wave component if the appropriate condition can be met. A resonance between freely transformed waves has also occurred. The triad wave-wave interactions transfer energy from the peak to higher frequencies.

#### Wave-induced set-up

Water set-up is the variation of wave amplitudes caused by the transport of wave momentum. The wave momentum transport is equivalent to radiation stress while the gradients in this stress are equal to the wave forces. The wave force can lead to a change of mean water level. The forces exerted on the water body in x- and y- direction can be obtained by:

$$\begin{aligned} F_x &= -\frac{\partial S_{xx}}{\partial x} - \frac{\partial S_{xy}}{\partial y} \\ F_y &= -\frac{\partial S_{yy}}{\partial y} - \frac{\partial S_{yx}}{\partial x} \end{aligned} \quad (2.15)$$

Ignoring horizontal forces and bottom friction, to consider a one-dimensional harmonic wave at normal incidence, a water balance can be determined based on radiation stress and water pressure:

$$\frac{dS_{xx}}{dx} + \rho g(h + \bar{\eta}) \frac{d\bar{\eta}}{dx} = 0 \quad (2.16)$$

According to the above equation, the slope of average water surface is negative for a positive gradient of radiation stress and conversely. The shallow water approximation for set-down can be obtained based on [Longuet-Higgins and Stewart \(1962\)](#):

$$\bar{\eta} = -\frac{1}{16} \frac{H_b^2}{h} \quad (2.17)$$

in which  $H_b$  is wave height at the breaking point,  $m$ .

With the assumption that the depth contour and water depth gradually decrease towards the beach, the maximum wave-induced set-up can be obtained as below:

$$\bar{\eta}_{max} = \frac{5}{16} \gamma \cdot H_b \quad (2.18)$$

#### Wave breaking:

Wave breaking is the phenomenon where a wave crest becomes unstable when the water particle celerity exceeds the wave crest speed. In deep water, wave breaking is called white-capping, which

is caused by the exceedance of wave steepness or wave height becomes bigger compared to its length. The presence of white-capping is not only associated with sea state, but is also closely linked to the wind (Holthuijsen, 2007). Based on Hasselmann (1974), the white capping can be presented by:

$$S_{wc}(f, \theta) = -\mu k E(f, \theta) \quad (2.19)$$

in which  $\mu$  is a coefficient related to a statistical characteristic of the white-capping.

In shallow water, the wave breaking is exerted by depth limitation. The commonly used model for this type of breaking is proposed by Battjes and Janssen, 1978. The mean energy loss per unit time and horizontal bottom area for all waves is determined by:

$$\bar{D}_{surf} = -\frac{1}{4} \alpha_{bj} \cdot Q_b \cdot \bar{f} \cdot H_b^2 \quad (2.20)$$

in which  $\alpha_{bj}$  is a tunable factor,  $H_b$  is the maximum wave height,  $m$ ,

$Q_b$  is the proportion of broken waves passing any one point,

$\bar{f}$  is the mean frequency of a water energy spectrum,  $s^{-1}$ .

A wave starts breaking if the water particle celerity exceeds the wave crest speed, or if a wave crest angle is approximately 120 deg. According to Stokes wave theory, a limitation of wave steepness as below:

$$\left[\frac{H}{L}\right]_{max} = 0.142 \tanh kh \quad (2.21)$$

In shallow water, it becomes:

$$\gamma = \left[\frac{H}{L}\right]_{max} = \frac{H_b}{h_b} \approx 0.88 \quad (2.22)$$

in which  $\gamma$  is the breaker index,  $h_b$  is the water depth at breaking,  $m$ . Using the solitary wave theory, Battjes and Stive (1985) proposed the range of 0.6 to 0.83, the average value is 0.73. Kaminsky and Draus (1993) indicated a range of 0.6 to 1.59 and an average value of 0.78.

### Shallow water wave applications

Shallow foreshore is described as  $1 < h_t/H_{m0} < 4$  where depth-induced wave breaking starts to occur (Hofland et al., 2016) while deep water is indicated as  $h_t/H_{m0} > 4$ . Figure 2.5 presents the diagram of Le Mehaute to apply the linearity of a certain sea state based on the wave theories of Airy, Stokes, Cnoidal and stream function (US Army Corps of Engineers, 1984) for all water regions.

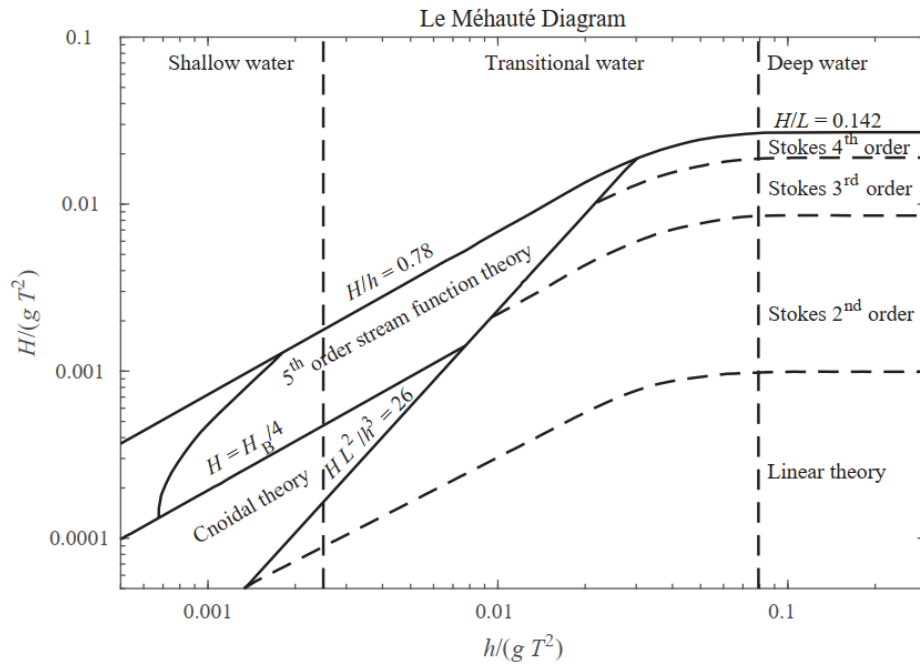


Figure 2.5: Diagram of wave theories validity (adjusted by Le Mehaute, 1969)

#### 2.4.2. Research on infragravity waves

Infragravity waves (IG waves) or surf beat waves were first identified by Munk (1949) and believed to be generated in the surf zone. These waves are commonly called low-frequency waves or long waves. Its generation was supposed due to the change of the mass transport of an incoming wave group in the surf zone. Longuet Higgins and Stewart (1962) and Janssen et al. (2003) also proposed that IG waves are basically generated by the interaction of short-wave groups with different frequencies, which leads to 'groupiness' if superimposed. Additionally, small changes of the average water surface level over wave groups can be seen, having been pushed under the highest short waves, named IG wave trough and pulled up under the lowest short waves, named IG wave crest. These IG waves are imposed to travel together with the same velocity of wave groups, as a result, it is bound to the short-wave groups. When the bound IG waves travel to the surf zone, breaking process occurs; consequently, the bound IG waves are released into free waves and then the groupiness of the short waves entirely disappears. The higher waves of the wave groups start to break first and then the lower waves do. The variation of position of the high-frequency wave breakpoint exerts changes in the groupiness, as a result, more IG waves are generated (Symonds et al., 1982).

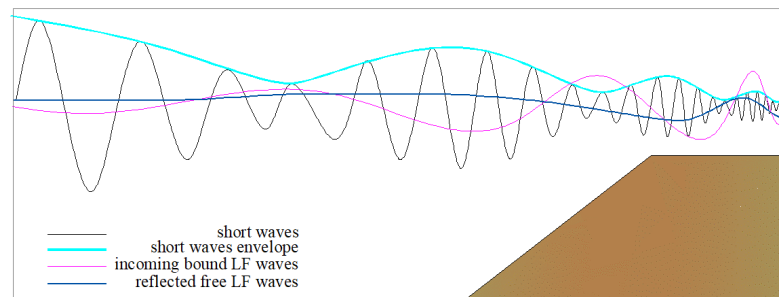


Figure 2.6: A sketch for several types of waves when approaching a sea dike (Ha et al., 2016)

IG waves are able to respond to insignificant effects from breaking short waves in shallow water due to their relatively long wave length and small wave height. Moreover, the IG waves can freely transform and shoal over the nearshore. After that, they are able to break as a bore-like breaking and/or directly approach the beach or the coastal defenses (wave run-up and even wave overtopping) and

---

finally reflect. As a result, the IG waves can become dominant in the nearshore compared with the short waves. The reflected IG waves return seaward as leaky waves or edge waves (where they can become trapped in that nearshore).

According to Battjes et al. (2004), the growth of IG wave energy is obtained by the shift of energy from the short waves to the IG waves. This transferred energy relies mainly on the variation of the groupiness (related to radiation stress gradients) and phase lag between the bound IG waves and the wave groups. Moreover, the foreshore slope is also a crucial factor impacting the growth rate of the IG waves and determines how much the incoming wave can reflect (Van Dongeren et al., 2007).

In gentle wave climates, the influence of IG waves on morphology can be ignored because of relatively small IG wave amplitude. However, during extreme conditions, the hydrodynamics of IG waves is of importance in the nearshore or at the dike toe due to wave transformation, wave run-up and the wave overtopping process, the exact subject of this research.

### 2.4.3. Study on dike-foreshore systems

Over time research has been executed on dike-foreshore systems. An overview of the studies on the various systems is presented here in chronological order.

Van der Meer (1997) investigated that water energy is dissipated on the foreshore due to breaking, a result of a reduction of the magnitude in the wave height compared with the absence of a foreshore. With the presence of a foreshore, the wave height distribution does not follow the Rayleigh distribution anymore. Due to the change in the shape of water energy density spectrum caused by wave breaking in the surf zone, the peak period  $T_p$  is proven not to be useful to estimate wave run-up. Furthermore, wave set-up is considered a key factor on the wave run-up on foreshores at the location where wave breakings happen.

Holterman (1998) indicated that due to wave evolution over a foreshore, a one-peaked frequency is not clearly visible in the wave energy spectra. Furthermore, the Rayleigh distribution is not appropriate to predict the wave run-up. Wave run-up expressions based on various spectral wave periods were examined.

Van Gent (1999) based on validation of a prototype scale between the physical and numerical models, confirms that the wave height distribution and the water energy density significantly change from deep water to the toe of a sea dike. Furthermore, the spectral wave period  $T_{m-1,0}$  is proposed to characterize the influence of the non-standard wave energy spectra on wave run-up and wave overtopping. An empirical formula for wave run-up is derived in the range of deep water from the toe to the shallow foreshores.

Van Gent and Giarrusso (2005) suggested that wave conditions did not depend on the presence of bar and trough, but mostly on the low-tide terrace in front of a dike. Compared with parameters at the offshore, if the wave height decreases to half, the mean period also decreases a half and the rate between the contribution of infragravity wave energy and total energy can reach a 30% at the toe of sea dikes. Therefore, based on offshore boundary conditions and foreshore characteristics, the contribution of the infragravity energy can be determined.

Verheij (2006) calculated the effects of islands, flats and foreshores on wave height distributions in the central Netherlands and revealed that foreshores do not only effectively reduce the wave height but the height of foreshores also strongly reduce this parameter. A formula of 2% run-up level proposed by Van der Meer (2002) is used to calculate the effect of foreshores. He also indicated that the combination of a breakwater and a foreshore caused a remarkable reduction in wave run-up height, compared with only a breakwater. Importantly, the combination of a breakwater and a sloping foreshore led to more reduction in wave height due to more dissipation occurring on the sloping foreshore. Especially, the presence of a swamp foreshore combined with a breakwater is



considered as the most effective way in the dissipation wave energy. The higher and wider the foreshores can get, the more reduction the wave heights achieve.

Suzuki et al. (2012) investigated wave overtopping, taking into account the influence of beach nourishments at shallow foreshores by using SWASH and the research associated with physical laboratory experiments. These indicated that low-frequency waves are released on the surf zone. Moreover, this kind of wave and wave-wave interactions are key factors for wave evolution as well as for wave height at the toe of structures, which are crucial parameters used to predict wave overtopping processes. Authors also indicated that beach nourishments do not always bring more benefits in decreasing the wave overtopping rate. A higher storm wall or an increase of the structural toe were particularly effective in the reduction of the wave overtopping rate. Regarding water energy density, it could be clearly seen that wave energy shifted to a lower-frequency domain, e.g. long wave formation.

Roerber et al. (2015), in observing Typhoon Haiyan in the Philippines, pointed out that low-frequency waves led to severe damage and fatal casualties. Importantly, fringing reefs could prevent the community from mild storms, but could also accumulate more water to cause serious flooding. The characteristic of these reefs is that a high-frequency wave breaks over a steep face of reef, where generates bound long waves combined with less water energy loss. Additionally, these long waves are in resonance due to the reef flat, leading to larger cumulative waves. The proposal of phase-resolving wave modelling, taking long waves into account, is accepted for fringing reefs due to a sudden generation of low-frequency waves.

Altomare et al. (2016), based on various physical data in wave overtopping with a foreshore slope ranging from of 1:35 to 1:250, presented that not only a dike slope, but also a part of foreshore should be included in the case of a water depth at the dike toe being higher than 1.5 times the spectral wave height at that position. Therefore, the concept of "equivalent slope" is introduced to get a more correct overtopping prediction considering the influences of the foreshores to determine the Iribarren number, as in very shallow water the breaking wave does not happen at the dike slope but at the foreshore. This kind of slope is analogous to the average slope proposed in EurOtop (2007) to investigate the influences of berms and composite slopes in relation to the overtopping process.

#### 2.4.4. Wave run-up

The run-up height is often measured from SWL, which is exceeded by 2% of the incoming waves. An initial formula of wave run-up height  $R_{u2\%}$  is derived from Hunt (1959). The relative run-up height  $R_{u2\%}/H_{m0}$  is a function of the breaker parameter  $\xi$ . Based on his study, the dimensionless run-up height is determined as below:

$$\frac{R_{u2\%}}{H_s} = c_1 \xi_p = c_1 \frac{\tan \alpha}{\sqrt{H_s/L_{op}}} \quad (2.23)$$

where:  $c_1 = 1.5$  for wave spectra;  $c_1 = 1.0$  for regular waves.

Some validations between physical experiments and numerical models have been done to develop this empirical formula by Van Gent (2002). It is proven that the run-up relies largely on sea state and the sea dike. The relative wave run-up can be estimated as below:

$$\frac{R_{u2\%}}{H_s} = \begin{cases} c_0 \gamma_f \xi_p, & \xi_p < c_1/2 \cdot c_0 \\ \gamma_f \left( c_1 - \frac{0.025 c_1^2}{c_0 \xi_p} \right), & \xi_p \geq c_1/2 \cdot c_0 \end{cases} \quad (2.24)$$

where:  $\gamma_f = 0.7$ ;  $c_0 = 1.95$ ;  $c_1 = 5.2$ .

Based on his study, the water energy density and wave height distribution at the dike toe depends on the foreshore and the water depth at the dike toe. To develop the wave run-up, several parameters have been included in later studies. If an incoming wave reaches the dike toe under angle  $\beta$ , both the wave run-up and overtopping are decreased, and the reduction factor  $\gamma_\beta$  should be taken into account. These processes are also reduced with the presence of a berm or a roughness of the seaside slope, corresponding to parameters  $\gamma_b$  and  $\gamma_{f'}$  respectively as mentioned by [Van Damme \(2016\)](#):

$$R_{u2\%} = 0.93\varepsilon(-\ln 0.02)^{1/2} \cdot H_s \quad (2.25)$$

$$\varepsilon = \min \left[ \gamma_\beta \cdot \gamma_{f'} \cdot \gamma_b \cdot \xi_m; \frac{\gamma_\beta \cdot \gamma_{f'}}{1.65} \left( 4.0 - \frac{1.5}{\sqrt{\xi_m}} \right) \right] \quad (2.26)$$

The wave run-up formula derived by [Van der Meer et al. \(2016\)](#) coincides with the equation from [Pullen et al. \(2007\)](#). According to their studies, the empirical formula of wave run-up is estimated based on mean values of the stochastic process called “mean value approach,” which can be applied for prediction or comparison. Regarding the design or the assessment of a dike, a more conservative approach needs to be used, equaling to a mean value plus a standard deviation of the stochastic variables. This approach is also applied in [EurOtop \(2018\)](#). The wave run-up derived by [TAW \(2002\)](#) can be given as below:

$$R_{u2\%} = H_{m0} \cdot \min \left[ 1.65\gamma_\beta \cdot \gamma_{f'} \cdot \gamma_b \cdot \xi_m; \gamma_\beta \cdot \gamma_{f'} \left( 4.0 - \frac{1.5}{\sqrt{\xi_m}} \right) \right] \quad (2.27)$$

Based on the above equations, the wave run-up height derived from [Hunt \(1959\)](#) is much larger than in the other formulae. Conversely, the run-up value from [Pullen et al. \(2007\)](#) and [Van der Meer \(2016\)](#) is the smallest compared with other studies. The wave run-up of [Van Damme \(2016\)](#) is comparable to the wave run-up of [Van Gent \(2002\)](#).

#### 2.4.5. Wave overtopping discharge

When waves approach a coastal structure and overtopping happens, water passes over the crest. This can lead to damage and be a disturbance for the activities on the landward side of the dike crest. As a result, a proper coastal structure, like a sea dike, is designed to prevent this overtopping process. An average wave overtopping discharge  $q$  is a useful tool to calculate inundation of a protected area and to calculate the tolerable amount of waves that may overtop a sea dike. This allowable overtopping rate is determined based on the average rate over a time in order to protect the dike crest or landward side from significant damage. One of the first empirical formulae for wave overtopping rate was proposed by [Owen \(1980\)](#) as below:

$$\frac{q}{\sqrt{gH_{m0}^3}} = a_0 \exp \left( -b_0 \frac{R_c}{H_{m0}} \right) \quad (2.28)$$

in which  $a_0, b_0$  are fitted coefficients. However, the above equation overestimates compared with physical experiments performed in the laboratory.

According to a variety of small-scale physical tests for gentle slopes with different geometries and wave parameters, [Van der Meer and Janssen \(1994\)](#) revealed 2 types of overtopping waves: breaking and non-breaking waves (or surge waves). The intersection of 2 these identified types is roughly at  $\xi_{m-1,0} = 2$  while breaking waves happening for  $\xi_{m-1,0} < 2$ . Based on this revelation, two simple regression equations were performed, indicating the mean overtopping discharge as a function of geometry and hydraulic characteristics for both breaking and non-breaking waves. The original formula includes significant wave height ( $H_{1/3}$ ) and peak period ( $T_p$ ). However, the

influences of multiple-peaked waves and flattened spectra shape are taken into account in this study, turning these above parameters into  $H_{m0}$  and  $T_{m-1,0}$ .

Therefore, new formulae suggested by [Van der Meer and Janssen \(1994\)](#) when taking a Weibull-shaped function into account is given as below:

$$\frac{q}{\sqrt{gH_{m0}^3}} = a_v \exp \left[ - \left( b_v \frac{R_c}{H_{m0}} \right)^{c_v} \right] \quad (2.29)$$

The basic difference between the equations (2.28) and (2.29) is an additional coefficient  $c_v$ , also determined based on experimental data, and associated with the mean value approach and applied for  $R_c \geq 0$ . These formulae are also used for vertical structures. The formulae for the mean overtopping discharge in EurOtop 2007, suggested by [Pullen et al. \(2007\)](#) are quite similar to this above equation:

$$\frac{q}{\sqrt{gH_{m0}^3}} = \frac{0.067}{\sqrt{\tan \alpha}} \gamma_b \xi_{m-1,0} \cdot \exp \left( -4.75 \frac{R_c}{\xi_{m-1,0} H_{m0} \gamma_b \gamma_f \gamma_\beta \gamma_v} \right) \quad (2.30a)$$

With a maximum of:

$$\frac{q}{\sqrt{gH_{m0}^3}} = 0.2 \cdot \exp \left( -2.6 \frac{R_c}{H_{m0} \gamma_b \gamma_f \gamma_\beta \gamma_v} \right) \quad (2.30b)$$

The  $\gamma$  - factors have been taken into account as reduction factors, including the influences of slope roughness  $\gamma_f$ , of the presence of a berm  $\gamma_b$ , of oblique wave attack  $\gamma_\beta$ , and of a vertical wall  $\gamma_v$ . The value of  $\xi_{m-1,0}$  at the transition of a breaking and a non-breaking wave is calculated by the intersection point of both equations (2.30a) and (2.30b). This value is approximately  $\xi_{m-1,0} = 2$ , because it relies mainly on the wave steepness and the foreshore slope.

The reliability of equations (2.30a, b) is determined by considering the constant coefficients 4.75 and 2.6 as stochastic variables with a normal distribution, having mean values of 4.75 and 2.6 and a standard deviation  $\sigma$ . It is noticeable that the validity of equation (2.30b) is for high values of the Iribarren number exerted by high slope angle  $\alpha$ . If a high value of the breaker parameter happens, and associated with a small value of the wave steepness caused by extremely heavy breaking in shallow water, the mean discharges will be underestimated.

The empirical formulae of mean overtopping rate mentioned in EurOtop 2018 are also proposed by [Van der Meer et al. \(2016\)](#). This discharge coincides with the formulae of [Van der Meer and Janssen \(1994\)](#) in the range of non-breaking waves, but is considerable bigger in the range of breaking waves ( $\xi_m < 2$ ). The formulae based on [Van der Meer et al. \(2016\)](#) are as follows:

$$\frac{q}{\sqrt{gH_{m0}^3}} = \frac{0.023}{\sqrt{\tan \alpha}} \gamma_b \xi_{m-1,0} \cdot \exp \left[ - \left( 2.7 \frac{R_c}{\xi_{m-1,0} H_{m0} \gamma_b \gamma_f \gamma_\beta \gamma_v} \right)^{1.3} \right] \quad (2.31)$$

With a maximum of:

$$\frac{q}{\sqrt{gH_{m0}^3}} = 0.09 \cdot \exp \left[ - \left( 1.5 \frac{R_c}{H_{m0} \gamma_b \gamma_f \gamma_\beta \gamma_v} \right)^{1.3} \right]$$

In order to accurately predict the average overtopping discharge in (very) shallow water for sea dikes, [Altomare et al. \(2016\)](#) in recent research, proposed the term of "equivalent slope", which is an average slope including a foreshore part while only the dike slope is taken into account in previous equations. However, these new empirical formulae are valid when the water depth at the dike toe is not higher than 1.5 times the incoming wave height ( $h_t \leq 1.5H_{m0}$ ).

The allowable mean overtopping for a design of a grass-covered dike based on [Van der Meer et al. \(2016\)](#) can be described as follows in table 2.1.

Table 2.1. Tolerable wave overtopping applied for a sea dike with grass cover on crest and landward side.

|  | Mean discharge $q$ ,<br>$l/m/s$ | Maximum volume $V_{max}$ ,<br>$m^3/m$ |
|--|---------------------------------|---------------------------------------|
| $H_{m0} = 1 \div 3m$ ; maintained and closed lawn cover                      | 5                               | 2 - 3                                 |
| $H_{m0} = 0.5 \div 3m$ ; not maintained lawn cover, open spots, bare patches | 0.1                             | 0.5                                   |
| $H_{m0} < 1m$  | 5 - 10                          | 0.5                                   |
| $H_{m0} < 0.3m$  | No limitation                   | No limitation                         |

#### 2.4.6. Probability distribution of individual overtopping volumes

Similar to the formulae of mean overtopping discharge summarized in the previous section, the probability distribution of wave per wave overtopping volumes and exceedance overtopping probability are basically derived for sea dike purpose. Several earlier studies related to the probability of wave overtopping volumes, performed by [Van der Meer and Janssen \(1994\)](#) for the purpose of sloped structures, by [Franco et al. \(1994\)](#) for vertical sea walls, and by [Victor \(2012\)](#) for steep slopes were all applied to relatively deep water. The exceedance probability  $P_V$  of a wave-by-wave overtopping volume  $V_i$  to exceed a particular volume  $V$  ( $P_V = P[V_i \geq V]$ ) seems to be perfectly matched by a Weibull distribution compared with physical tests of sea dikes. The values  $\hat{P}_V$  rely mainly on the number of overtopping waves,  $N_{ow}$ , which applied the Weibull plotting location equation ([Goda, 2000](#)) described as:

$$\hat{P}_V = \frac{i}{N_{ow} + 1} \quad (2.32)$$

in which index  $i$  is known as a rank in descending order of the individual volume. The circumflex of  $\hat{P}_V$  indicates a specified estimator of  $P_V$ .

Meanwhile, the exceedance probability  $P_V$  can be determined by the three parameters of Weibull distribution as equation (2.33):

$$P_V = r \cdot \exp \left[ - \left( \frac{V}{a} \right)^b \right] \quad (2.33)$$

where  $r$  is a set-off factor, the coefficient  $a$  is a scale factor whereas  $b$  specifies the shape of the Weibull distribution and thus it is named as a shape parameter. The factor  $r$  is the probability of wave overtopping  $P_{ov}$ , determined by the ratio of the number of overtopping waves  $N_{ow}$  over the number of incident waves  $N_w$ .

If the probability distribution is determined based on  $N_{ow}$ , the set-off factor  $r = 1.0$  and the exceedance probability turn into two parameters of the Weibull distribution, which is equivalent to the exceedance probability of a wave height at a limited water depth. It is noticeable that if  $r = 2.0$ , the Weibull distribution changes into a Rayleigh distribution.

The expression of the individual wave overtopping volume when the exceedance probability is complied with Weibull distribution can be described by:

$$V = a(-\ln(P_v))^{1/b} \quad (2.34)$$

A maximum individual overtopping volume happened,  $V_{max}$ , corresponding to the index  $i = 1$  in the descending order means the volumes are ranked from highest to lowest order. However, considering  $i = 1$  and an assumption with  $V_{max}$  equivalent to the exceedance probability of a value  $\frac{1}{N_{ow}}$ . The maximum volume turns into:

$$V_{max} = a\left(-\ln\left(\frac{1}{N_{ow}}\right)\right)^{1/b} = a(\ln N_{ow})^{1/b} \quad (2.35)$$

It is noticeable that the above equation contains several uncertainty factors because the assumption related to the relation between  $V_{max}$  and  $\frac{1}{N_{ow}}$  is an approximation.

As mentioned above, the wave-by-wave overtopping volume is estimated by a two-coefficient Weibull distribution. The scale coefficient  $a$  in that equation can be determined through the shape factor  $b$  according to research from [Franco and Franco \(1999\)](#). The average wave overtopping volume can be measured by:

$$\bar{V}_{ms} = \frac{V_0}{N_{ow}} = \frac{\sum V_i}{N_{ow}} \quad (2.36)$$

The mean overtopping discharge  $q$  can be described as the ratio between the sum of  $V_i$  over the sum of  $T_i$  of each wave in the wave group. The average overtopping discharge can be measured by:

$$q = \frac{\sum V_i}{\sum T_i} = \frac{\sum V_i}{N_w T_m} \quad (2.37)$$

Instead the equation (2.36) into (2.37):

$$\begin{aligned} q &= \frac{\bar{V}_{ms} N_{ow}}{N_w T_m} = \frac{\bar{V}_{ms} P_{ow}}{T_m} \\ \Leftrightarrow \bar{V}_{ms} &= \frac{q \cdot T_m}{P_{ow}} \end{aligned} \quad (2.38)$$

On the other hand, using the expected value based on the Weibull stochastic variable, the theoretical average wave-by-wave overtopping volume,  $\bar{V}_{th}$  can be obtained from Gamma function and two parameters of the Weibull distribution as below:

$$\bar{V}_{th} = E(V_i) = a\Gamma\left(1 + \frac{1}{b}\right) \quad (2.39)$$

Both equations (2.38) and (2.39) are comparable only if the individual wave overtopping volume follows completely the two-coefficient Weibull distribution. Balance of both sides of the expressions of (2.38) and (2.39), the scale factor can be determined as follows:

$$\frac{q \cdot T_m}{P_{ow}} = a\Gamma\left(1 + \frac{1}{b}\right) \quad (2.40)$$

$$\Leftrightarrow a = \frac{1}{\Gamma\left(1 + \frac{1}{b}\right)} \frac{q \cdot T_m}{P_{ow}}$$

Denoting  $a' = \frac{1}{\Gamma\left(1 + \frac{1}{b}\right)}$ , the equation (2.40) becomes:

$$a = a' \frac{q \cdot T_m}{P_{ow}} = a' \bar{V}_{ms} \quad (2.41)$$

According to equation (2.41), the scale parameter  $a$  is proportional to the average wave overtopping volume which means it also decides the scale of this volume. It explains the name scale factor in the Weibull distribution. The bigger the individual volume can get, the bigger the scale factor can reach.

Based on this theory, the shape parameter  $b$  relies mainly on wave parameters and structural geometry. According to a number of investigations related to wave-by-wave overtopping volume distribution for coastal structures, [Van der Meer and Janssen \(1994\)](#) adopted 0.75 as a shape factor. This value is also obtained based on physical experiments of vertical sea walls in deep water with a normal wave incident due to [Franco et al. \(1994\)](#). This constant value is also mentioned in [TAW, 2002](#) as the shape factor. In [Besly \(1999\)](#) suggested that this value only relies on the impacting waves and its steepness, while [Bruce et al. \(2009\)](#) found this parameter does not depend on the wave steepness.

When  $b = 0.75$  the scale factor becomes:

$$a = 0.84 \frac{q \cdot T_m}{P_{ow}} \quad (2.42)$$

In [Van der Meer et al. \(2010\)](#) and [Bruce et al. \(2010\)](#), the scale factor is also adjusted based on the relation of (2.42):

$$a = \left(0.84 + 1.2N_{ow}^{-0.8}\right) \frac{q \cdot T_m}{P_{ow}} \quad (2.43)$$

Another study by [Victor \(2012\)](#), based on steep sloping structures and associated with low crest freeboards, found that the factor  $b$  is dependent on the dimensionless freeboard and slope angle. The individual overtopping volumes and the exceedance probability are also used to make a Weibull distribution from each test. Finally, [Victor \(2012\)](#) proposed a new equation of the factor  $b$  as given in (2.44), where the wave steepness is independent on this shape factor.

$$b = \exp\left(-2.0 \frac{R_c}{H_{m0}}\right) + 0.56 + 0.15 \cot \alpha \quad (2.44)$$

After that, parameter  $a'$  is shown with the limited data for  $0.6 \leq b \leq 2.0$ , thus the scale factor  $a$  can be obtained by:

$$a = 1.13 \tanh(1.32b) (q T_m / P_{ov}) \quad (2.45)$$

[Hughes et al. \(2012\)](#) got rid of the slope angle relation from the shape parameter  $b$ , leading to the only dimensionless freeboard relation:

$$b = \left[ \exp\left(-0.6 \frac{R_c}{H_{m0}}\right) \right]^{1.8} + 0.64 \quad (2.46)$$

---

By contrast, the rubble mound coastal structures are taken into account in [Zanuttigh et al. \(2013\)](#), resulting in a new formula for the shape parameter  $b$  in a relation with a relative average overtopping rate:

$$b = 0.73 + 55 \left( \frac{q}{gH_{m0}T_{m-1,0}} \right)^{0.8} \quad (2.47)$$

Most of the above studies are carried out in small-scale two-dimensional experiments and long-crested waves in a relatively deep water.

## 2.5. Conclusions

The brief overview of research shows that several previous studies have been done related to wave overtopping. However, the investigation of this field has focused on steep slopes and on gentle slopes, with a foreshore slope up to 1:250. The research related to very mild foreshores, ranging from 1:500 to 1:1000, or even more, with very wide shelves is not yet fully understood. Therefore, in this dissertation, the wave overtopping process for very gentle and shallow foreshores will be investigated with the application to case studies in Vietnam which will be introduced in the following chapters.

---

## References

- Altomare, C.; Suzuki, T.; Chen, X.; Verwaest, T.; Kortenhaus, A (2016). Wave overtopping of sea dikes with very shallow foreshores. *Coast. Eng.* 2016, 116, 236–257, ISSN 0378-3839.
- Amante, C. and Eakins, B. (2009). Etopo1 arc-minute global relief model: procedures, data sources and analysis. <http://www.ngdc.noaa.gov/mgg/global/global.html>
- Battjes, J.A. (1974). Surf similarity. *Proceedings of the 14th international conference on coastal engineering*, pages 466-480.
- Battjes, J.A. and Janssen, J. P. F. M. (1978). Energy loss and set-up due to breaking of random waves. *Proceedings of the 16th international conference on coastal engineering*, 1(1):569–587.
- Battjes, J.A. and Stive, M. J. F. (1985). Calibration and verification of a dissipation model for random breaking waves. *Coastal Engineering*, pages 649–660.
- Battjes, J.A., H.J. Bakkenes, T.T. Janssen, and A.R. van Dongeren, (2004), Shoaling of subharmonic gravity waves, *J. Geophys. Res.*, 109, C02009, doi:10.1029/2003JC001863.
- Bertotti, L. and Cavaleri, L. (1994). Accuracy of wind and wave evaluation in coastal regions. *Coastal Engineering Proceedings*, 1(24).
- Besley, P. (1999). Overtopping of seawalls; design and assessment manual. *Environment Agency, Bristol, UK, technical report w178 edition*.
- Booij, N., Ris, R. C., and Holthuijsen, L. H. (1999). A third-generation wave model for coastal regions: 1. Model description and validation. *Journal of Geophysical Research*, 104:7649.
- Bosboom, J. and Stive, M. J. F. (2012). Coastal Dynamics I: Lectures Notes CIE4305. VSSD
- Bruce, T., van der Meer, J., Franco, L., and Pearson, J. (2009). Overtopping performance of different armour units for rubble mound breakwaters. *Coastal Engineering*, 56:166–179.
- Bruce, T., van der Meer, J., T.Pullen, and Allsop, N. (2010). Wave overtopping at vertical and steep structures. *World Scientific Publishing Co*.
- Cavaleri, L. and Rizzoli, P. M. (1981). Wind wave prediction in shallow water: Theory and applications. *Journal of Geophysical Research: Oceans (1978–2012)*, 86(C11):10961–10973.
- Chen, X. Impacts of Overtopping Waves on Buildings on Coastal Dikes. *Ph.D. Thesis, Delft University of Technology, Delft, the Netherlands, 2016*.
- Collins, J. I. (1972). Prediction of shallow water spectra. *Journal of Geophysical Research*, 77(15):2693–2707.
- Eldeberky, Y. and Battjes, J. A. (1995). Parameterization of triad interactions in wave energy models. *Proc. Coastal Dynamics Conf. 95, Gdansk, Poland*, 140-148.
- Franco, L., de Gerloni, M. and van der Meer, J. (1994). Wave overtopping on vertical and composite breakwaters. *In Proc. 24th International Conference on Coastal Engineering, New York, ASCE*, pp. 1030–1044.
- Franco, C. and Franco, L. (1999). Overtopping formulas for caisson breakwaters with nonbreaking 3D waves. *Journal of Waterway Port Coastal and Ocean Engineering-Asce*, 125(2): pp. 98-108.
- Garrett, C. J. R. (1967). Discussion: the adiabatic invariant for wave propagation in a non-uniform moving medium. *In Proceedings of the Royal Society of London A: Mathematical, Physical and Engineering Sciences*, volume 299, pages 26–27. The Royal Society.



Goda, Y. (2000). Random seas and design of maritime structures. [Volume 15, Singapore. World Scientific Publishing Co.](#)

Ha, T.T.N., Stive, M.J.F., Verhagen, H.J., 2016. A numerical study on the influence of low-frequency wave period on wave overtopping in a very gentle foreshore. [The ECSA 56 Coastal Systems in Transition Conference, 4-7 September 2016, Bremen, Germany.](#)

Hasselmann, K. (1974). On the spectral dissipation of ocean waves due to white capping. [Boundary-Layer Meteorology, 6\(1-2\):107–127.](#)

Hasselmann, S., Hasselmann, K., Allender, J. H., and Barnett, T. P. (1985). Computations and parameterizations of the nonlinear energy transfer in a gravity-wave spectrum. Part II: Parameterizations of the nonlinear energy transfer for application in wave models. [Journal of Physical Oceanography, 15\(11\):1378–1391.](#)

Holthuijsen, L. H. (2007). [Waves in Oceanic and Coastal Waters. Cambridge University Press.](#)

Hofland, B., Chen, X., Altomare, C., Oosterlo, P. (2017). Prediction formula for the spectral wave period  $T_{m-1,0}$  on mildly sloping shallow foreshores. [Coast Eng. 123 \(Suppl. C\), 21–28.](#)

Hughes, S.A., Thornton, C.I., Van der Meer, J.W., and Scholl, B.N. (2012). Improvements in describing wave overtopping processes. [Coastal Engineering Proceedings, 1\(33\):35.](#)

Hunt, I. (1959). Design of sea-walls and breakwaters. [Transactions of the American Society of Civil Engineers, 126\(4\):542–570.](#)

Janssen, T.T., J.A. Battjes, and A.R. van Dongeren, (2003), Long waves induced by short-wave groups over a sloping bottom, [J. Geophys. Res., 108\(C8\), 3252, doi:10.1029/2002JC001515.](#)

Kaminsky, G. M. and Kraus, N. C. (1993). Evaluation of depth-limited wave breaking criteria. [In Ocean Wave Measurement and Analysis \(1993\), pages 180–193. ASCE.](#)

Lashley, C.H; Zanuttigh, B.; Bricker, J.D.; van der Meer, J.; Altomare, C.; Suzuki, T.; Roeber, V.; Oosterlo, P., 2020a. Benchmarking of numerical models for wave overtopping at dikes with shallow mildly sloping foreshores: Accuracy versus speed. [Env. Model. and Software 130 \(2020\) 104740.](#)

Le Méhauté, B. (1969). An introduction to hydrodynamics and water waves, [Volume II: Water wave theories.](#)

Longuet-Higgins, M. S. and Stewart, R. W. (1962). Radiation stress and mass transport in gravity waves, with application to ‘surf beats’. [Journal of Fluid Mechanics, 13\(04\):481–504.](#)

Miles, J. W. (1957). On the generation of surface waves by shear flows. [Journal of Fluid Mechanics, 3\(02\): 185–204.](#)

Munk, W.H., (1949), Surf beats, [Trans. Amer. Geophys. Un., vol. 30: 849-54.](#)

Owen, M. W. (1980). Design of seawalls allowing for wave overtopping. [HR Wallingford, Report EX 924.](#)

Pierson, W.J. and L. Moskowitz, (1964), A proposed spectral form for fully developed wind seas based on the similarity theory of S.A. Kitaigorodskii, [J. Geophys. Res., vol. 69, 24, 5181-5190.](#)

Plant, W. J. (1982). A relationship between wind stress and wave slope. [Journal of Geophysical Research: Oceans \(1978–2012\), 87\(C3\):1961–1967.](#)

Pullen, T., Allsop, N., Bruce, T., Kortenhaus, A., Schüttrumpf, H., and van der Meer, J. (2007). EurOtop Manual on wave overtopping of sea defences and related structures. [Assessment Manual.](#)

Phillips, O. M. (1957). On the generation of waves by turbulent wind. [Journal of fluid mechanics, 2\(05\): 417– 445.](#)

---

Snyder, R. L., Dobson, F. W., Elliott, J. A., and Long, R. B. (1981). Array measurements of atmospheric pressure fluctuations above surface gravity waves. *Journal of Fluid mechanics*, 102:1–59.

Suzuki, T.; Altomare, C.; Veale, W.; Verwaest, T.; Trouw, K.; Troch, P.; Zijlema, M., 2017. Efficient and robust wave overtopping estimation for impermeable coastal structures in shallow foreshores using SWASH. *Coast. Eng.*, 122, 108–123.

Suzuki, T.; Altomare, C.; Yasuda, T.; Verwaest, T., 2020. Characterization of Overtopping Waves on Sea Dikes with Gentle and Shallow Foreshores. *Journal of Marine Science and Engineering*, 2020, 8, 752; doi: 10.3390/jmse8100752.

Suzuki, T.; Verwaest, T.; Hassan, W., Veale, W.; Reyns, J., Trouw, K.; Troch, P. and Zijlema, M., 2012. The applicability of SWASH for modelling wave transformation and wave overtopping: A case study for the Flemish coast. *Proceedings in ACOMEN 2011*.

Suzuki, T.; Verwaest, T.; Veale, W.; Trouw, K.; Zijlema, M., 2012. A numerical study on the effect of beach nourishment on wave overtopping in shallow foreshores. *Coast. Eng. Proceeding 1(33)*.

The SWASH team (2015). SWASH user manual. *Delft, The Netherlands, 2015*.

Van Damme, M. (2016). Distributions for wave overtopping parameters for stress strength analyses on flood embankments. *Coastal Engineering*, 116:195–206.

Van der Meer, J. and Janssen, W. (1994). Wave run-up and wave overtopping at dikes. In: Kabayashi, Demirbilek, Wave forces on inclined and vertical wall structures. *American society of civil engineers*, pages 1-27.

Van der Meer, J. W. (1997). Golfploop en golfoverslag bij dijken. *Technical report, Waterloopkundig laboratorium | WL, Delft*.

Van der Meer, J. W., Hardeman, B., Steendam, G. J., Schüttrumpf, H., and Verheij, H. (2010). Flow depths and velocities at crest and landward slope of a dike, in theory and with the wave overtopping simulator. *Coastal Engineering Proceedings*, 1 (32):10.

Van der Meer, J., Allsop, N., Burce, T., De Rouck, J., Kortenhaus, A., Pullen, T., Schüttrumpf, H., Troch, P., and Zanuttigh, B. (2016). EurOtop Manual on wave overtopping of sea defences and related structures. An overtopping manual largely based on European research, but for worldwide application.

Van Dongeren, A.R., A. Reniers, J. Battjes, and I. Svendsen, (2003), Numerical modeling of infragravity wave response during DELILAH, *J. Geophys. Res.* 108(C9), 3288, doi:10.1029/2002JC001332.

Van Dongeren, A.R., J.A. Battjes, T.T. Janssen, J.C. van Noorloos, K. Steenhauer, G. Steenbergen and A. Reniers, (2007), Shoaling and shoreline dissipation of low-frequency waves, *J. Geophys. Res.*, 112, C02011, doi:10.1029/2006 JC003701.

Van Gent, M. (2002). Low-exceedance wave overtopping events: Measurements of velocities and the thickness of water-layers on the crest and inner slope of dikes. *Delft Cluster, DC1-322-3*.

Van Gent, M. R. A. (1999). Physical model investigations on coastal structures with shallow foreshores: 2D model tests with single and double-peaked wave energy spectra. *Technical report, WL | Delft Hydraulics, Delft*.

Van Gent, M. and Giarrusso, C. (2005). Influence of foreshore mobility on wave boundary conditions. *Proc. Int. Conference on Ocean Waves Measurements and Analysis, Madrid, Spain, 3-7 July 2005*, pages 1–10.

- 
- Verheij, H. J. (2006). IJsselmeer zoekt verdieping. [Technical Report December, WLI Delft Hydraulics, Delft.](#)
- Roerber, V. and Bricker, J. D. (2015). Destructive tsunami-like wave generated by surf beat over a coral reef during Typhoon Haiyan. [Nature Communications, 6.](#)
- Suzuki, T., Verwaest, T., Veale, W., Trouw, K., and Zijlema, M. (2012). A numerical Study on the Effect of Beach Nourishment on Wave Overtopping in Shallow Foreshores. [Coastal Engineering Proceedings.](#)
- Symonds, G., D.A. Huntley and A.J. Bowen, (1982), Two-dimensional surf beat. Long wave generation by a varying breakpoint, [J. Geophys. Res., vol. 80: 492-498.](#)
- Tas, S. Coastal Protection in the Mekong Delta: Wave Load and Overtopping of Sea Dikes as Function of Their Location in the Cross-Section, for Different Foreshore Geometries. [Master's Thesis, Delft University of Technology, Delft, The Netherlands, 2016; pp. 17–18.](#) TAW (2002). Wave run-up and wave overtopping at dikes. [Technical report, Technische Adviescommissie voor de Waterkeringen, Delft.](#)
- Tolman, H. L. et al. (2009). User manual and system documentation of wavewatch III TM version 3.14. [Technical note, MMAB Contribution, 276:220.](#)
- US Army Corps of Engineers (1984). Shore Protection Manual; [US Army Corps of Engineers: Washington, DC, USA; Volume 1.](#)
- Victor, L. (2012). Optimization of the Hydrodynamic Performance of Overtopping Wave Energy Converters: Experimental Study of Optimal Geometry and Probability Distribution of Overtopping Volumes. [Phd, UGent, Zwijnaarde; Belgium.](#)
- Victor, L., van der Meer, J., and Troch, P. (2012). Probability distribution of individual wave overtopping volumes for smooth impermeable steep slopes with low crest freeboards. [Coastal Engineering, 64:87–101.](#)
- Zanuttigh, B., Van der Meer, J.W., Bruce, T. and Hughes, S. (2013). Statistical Characterisation of Extreme Overtopping Wave Volumes. [Proc. ICE, Coasts, Marine Structures and Breakwaters 2013, Edinburge, UK.](#)
- Zijlema, M., Stelling, G., and Smit, P. (2011). SWASH: An operational public domain code for simulating wave fields and rapidly varied flows in coastal waters. [Coastal Engineering, 58\(10\):992–1012.](#)

# 3

## Wave Overtopping Discharge for Very Gently Sloping Foreshores

*“I have not **failed**.  
I’ve successfully **discovered** 10,000 things that **won’t** work”*

- Thomas Edison

The spectral wave period  $T_{m-1,0}$  at the toe of sea-dikes is a crucial parameter to predict wave overtopping discharge over sea-dikes. It is known from literature that this period quickly increases when waves reach shallow foreshores; however, sometimes the assumption is made that the wave period remains constant from offshore to near-shore, leading to an underestimation of the near-shore wave period. Several formulae have been proposed to resolve the underestimation of wave overtopping discharges for very shallow foreshores. These corrective formulations confirm the tendency of underestimating the overtopping discharges over a very gently sloping foreshore but are not validated for foreshore slopes gentler than 1:500. The “equivalent slope” method based on a recent study is inappropriate for these very gently sloping foreshores due to the breaker parameter being much smaller than seven. This study proposes an extension of the correction and finds that spectral wave periods can reach values two times those offshore.

---

This chapter was published in *Water* 12(6): 1696, June 2020. DOI: 10.3390/w12061695. Thu-Ha Nguyen, Bas Hofland, Vu Dan Chinh, Marcel Stive (2020). Wave Overtopping Discharge for very Gently Sloping Foreshores. The published paper had some changes compared with this version based on the instruction of TU Delft’s template.

### 3.1. Introduction

The Vietnamese coastline is very diverse and quite unique in many respects, such as coastal types, coastline orientation and wave and tidal characteristics (Bosboom and Stive, 2015). The wave characteristics in the North and in the South are very much influenced by the very gentle (ranging from 1 in 500 to 1 in 1000—in the Mekong Delta) and shallow foreshores that are a result of the locally very wide shelves. There is a strong tradition at the northern and southern shores to protect the hinterland against flooding by dikes. In the dike design international guidelines on wave overtopping are applied. Based on recent findings, the EurOtop manual (EurOtop II, 2018) indicates that the wave overtopping discharges are not able to properly account for gentle foreshores (order of 1 in 100). This study investigates this issue for even gentler foreshores.

The focus is on two physical parameters, viz., the relevant spectral wave period and the mean overtopping discharge. Since no data exist for these very gentle foreshores, this study relies on a recent state-of-the-art nearshore time domain wave model SWASH (Zijlema et al., 2011).

First, this chapter starts with a literature review focusing on the wave overtopping of dikes at very shallow foreshores. Next, a site description is given of the North Vietnamese coast, which shows the presence of very shallow associated with very gently sloping foreshores. An exploratory calculation is made using the shallow water wave model SWAN to illustrate the wave processes that occur. This model is used to propagate the wave spectra from far offshore to the near shore. In the SWASH setup section, the configurations are described by the numerical calculations that have been performed to determine the spectral wave period and wave overtopping at very gentle foreshores. The results are used as a boundary condition for the non-hydrostatic wave propagation model SWASH. In parallel, the SWASH model is validated by reproducing the results of the Van Gent (1999) and Altomare formulae (2016). Third, the spectral wave period  $T_{m-1,0}$ -for (very) shallow foreshores on both mild and very gentle slopes and the mean overtopping discharge ( $q$ )-for very gently sloping foreshores are calculated. Cases with very shallow foreshores are calculated, in combination with empirical formulae. The last part of the chapter ends with discussions and conclusions given.

#### 3.1.1. State-of-the-art in deriving the spectral wave period for different foreshores

The spectral wave period is defined based on the first negative wave spectral moment:

$$T_{m-1,0} = \frac{m_{-1}}{m_0} \quad (3.1)$$

$$\text{and } m_k = \int_0^\infty f^k S(f) df \quad (3.2)$$

where  $m_k$  is the  $k^{\text{th}}$  moment of the wave spectrum, and  $f$  and  $S$  are the wave frequency [ $s^{-1}$ ] and the energy density [ $m^2s$ ], respectively.

Van Gent (1999, 2001a, 2001b) indicated that the spectral wave period  $T_{m-1,0}$  at the dike toe is one of the most relevant parameters for both wave run-up and overtopping predictions.  $T_{m-1,0}$  weighs the low-frequency (LF) spectral energy more than the high-frequency (HF) spectral energy. The LF waves are generated in the shoaling and surf zone after being released from the high-frequency (HF) wave groups (Munk, 1949; Tucker, 1950). Furthermore, for non-standard spectral shapes, when the response of coastal structures (e.g., overtopping) is described by  $T_{m-1,0}$ , these responses are not dependent on the wave spectral type, even if the spectral shape is flattened in shallow water (EurOtop II, 2018; EurOtop I, 2007).

A prediction formula for the spectral wave period  $T_{m-1,0}$  has been given by Hofland et al. (2017) for shallow to extremely shallow water with a gently sloping bed slope. According to Hofland et al. (2017) the increase of  $T_{m-1,0}$  is:

$$\frac{T_{m-1,0,t}}{T_{m-1,0,o}} - 1 = 6 \exp(-4\tilde{h}) + \exp(-\tilde{h}) \quad (3.3)$$

where

$$\tilde{h} \text{ is relative depth, } \tilde{h} = \frac{h_t}{H_{m0,o}} \left( \frac{\cot\theta}{100} \right)^{0.2} \quad (3.4)$$

$T_{m-1,0}$  quickly increases when waves attack the shallow foreshores and can reach values roughly eight times compared with those offshore. Shallow and very shallow foreshores were defined as  $1 < h_{toe}/H_{m0,o} < 4$  and  $0.3 < h_{toe}/H_{m0,o} < 1$ , respectively. Mild sloping foreshores as discussed by [Van Gent \(1999\)](#) are limited to  $\cot\theta < 250$ .

### 3.1.2. State-of-the-art in wave overtopping formulae for sea-dikes with steep, mild, and very gentle foreshores

The formulae suggested by [Van Gent \(1999\)](#) and applied in [TAW \(2002\)](#) and [EurOtop I \(2007\)](#) are expressed as follows:

$$\frac{q}{\sqrt{g \cdot H_{m0}^3}} = 10^c \exp\left(-\frac{R_C}{H_{m0} \cdot \gamma_f \cdot \gamma_\beta \cdot (0.33 + 0.022\xi_{m-1,0})}\right) \quad (3.5)$$

With a maximum of

$$\frac{q}{\sqrt{g \cdot H_{m0}^3}} = 0.21 \cdot \exp\left(-\frac{R_C}{H_{m0} \cdot \gamma_f \cdot \gamma_\beta \cdot (0.33 + 0.022\xi_{m-1,0})}\right) \quad (3.6)$$

The factor  $c$  is considered as a normally distributed parameter with mean value and standard deviation of  $-0.92$  and  $0.24$ , respectively. These two equations are recommended by [EurOtop I \(2007\)](#) for  $\xi_{m-1,0} \geq 7$ . In case  $\xi_{m-1,0} \leq 5$ , two equations are valid as below:

$$\frac{q}{\sqrt{g \cdot H_{m0}^3}} = \frac{0.067}{\sqrt{\tan\alpha}} \gamma_b \xi_{m-1,0} \exp\left(-4.75 \frac{R_C}{H_{m0} \cdot \gamma_f \cdot \gamma_\beta \cdot \gamma_v \cdot \gamma_b \cdot \xi_{m-1,0}}\right) \quad (3.7)$$

With a maximum of

$$\frac{q}{\sqrt{g \cdot H_{m0}^3}} = 0.2 \cdot \exp\left(-2.6 \frac{R_C}{H_{m0} \cdot \gamma_f \cdot \gamma_\beta}\right) \quad (3.8)$$

In case  $5 \leq \xi_{m-1,0} \leq 7$ , a linear interpolation is applied between the two above cases.

These equations have been improved by [Altomare et al. \(2016\)](#) for application to even more shallow water depths, which has been adopted in the second release of the [EurOtop II manual \(2018\)](#). [Altomare et al. \(2016\)](#) indicated that [Van Gent's](#) formulae overestimated the mean overtopping discharge in very shallow water foreshores and recommended a new "equivalent slope" concept for appropriate mean overtopping discharge with shallow and very shallow waters.

Very gentle and shallow coastal shelves are often found in mangrove areas, since fine sediments dominate in these areas. The very gently sloping foreshores can cause a large change of wave spectra at dike toes compared with that at offshore locations. Vietnamese sandy coasts are typically represented by mildly sloping foreshores in the North and even very mild bottom slopes in the South ([Hoan et al., 2010](#); [Phan Khanh, 2019](#); [Tas, 2016](#)). Compared to previous studies, the typical foreshores for Vietnamese coasts are very gentle, and are more gentle than those considered in [EurOtop II \(2018\)](#). Very gentle foreshores in combination with shallow water zone can cause wave breaking far from the shore and a remarkable change of wave spectra from offshore to near shore. The effect of these very gently sloping foreshores on wave overtopping is not yet well quantified.

Therefore, the purpose of this chapter is to derive a suitable method to determine the mean overtopping discharge on very gently sloping foreshores and propose the use of extended wave overtopping discharge formulae for this type of foreshores.

## 3.2. Materials and methods

### 3.2.1. Site description

To illustrate the importance of wave overtopping discharge over a very gentle slope, a gently sloping foreshore in the North of Vietnam is taken as an illustrative case study. A very long cross-shore trajectory of 180 km to the near-shore will be investigated where the maximum water depth in the offshore reaches 70 m due to the fact that northern Vietnamese sea has very wide shelves associated with very gentle sloping foreshores in order to find out the change of spectral wave periods over this long distance.

Here Table 3.1 introduces and defines the parameters that are used in the section below.

**Table 3.1.** Nomenclature used in this chapter.

| d                | wave overtopping thickness [m]   | $R_u$          | wave run-up over a slope [m]  |
|------------------|--|----------------|---|
| $D_f$            | wave energy dissipation [ $\text{cm}^2/\text{s}$ ]   | $T_{m-1,0,o}$  | spectral mean wave energy period in SWASH b.c [s]                       |
| E                | spectral density of the water surface elevation [ $\text{m}^2/\text{Hz}$ ]                 | $T_{m-1,0,t}$  | spectral mean wave energy period at toe [s]                             |
| f                | frequency [ $\text{s}^{-1}$ ]  | $T_p$          | peak wave period in SWAN b.c [s]  |
| h                | water depth [m]  | $U_{10}$       | wind speed at 10 m above SWL [m/s]                                      |
| $h_{\text{toe}}$ | water depth at dike toe [m]  | v              | wave overtopping velocity [m/s]   |
| $H_s$            | spectral significant wave height at SWAN boundary condition (b.c) [m]                      | $U_{10}$       | wind speed at 10 m [m/s]  |
| $H_{m0}$         | spectral significant wave height [m]   | x              | distance [km]   |
| $H_{m0,o}$       | spectral significant wave height at SWASH b.c [m]  | $\theta$       | foreshore slope in SWASH [degree]                                       |
| $H_{m0,t}$       | spectral significant wave height at dike toe [m]   | $\gamma_f$     | reduction coefficient which includes the effects of slope roughness [-] |
| k                | wave number [-]  | $\gamma_\beta$ | reduction coefficient which includes the effects of obliqueness [-]     |
| q                | wave overtopping discharge per meter width of structure [ $\text{m}^3/\text{s}/\text{m}$ ] | $\alpha$       | dike slope in seaward [degree]  |
| $R_c$            | crest freeboard [m]  | $\delta$       | equivalent slope in shallow foreshore [degree]                          |
|                  |  | $\xi_{m-1,0}$  | Iribaren number [-]   |

#### 3.2.1.1. Bathymetry

A part from the very central Vietnamese coast, typical Vietnamese cross-shore bathymetries exhibit very gentle and smooth bed slopes due to the large shelf widths (Figure 3.1). These wide shelves create a relatively long distance for wave energy transformation and dissipation or wind generation. Typical bathymetries show that the depth contours are parallel so 1D models can appropriately be applied. From a water depth of less than 20 m to the nearshore, the foreshore slope is roughly 1:500 (Figure 3.2). To derive characteristic wave conditions a typical storm for this area is simulated.

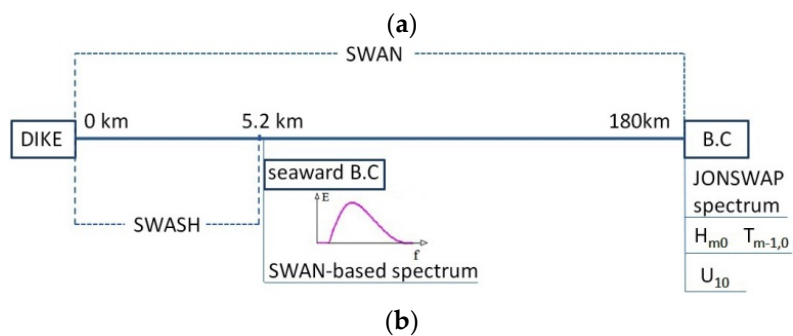
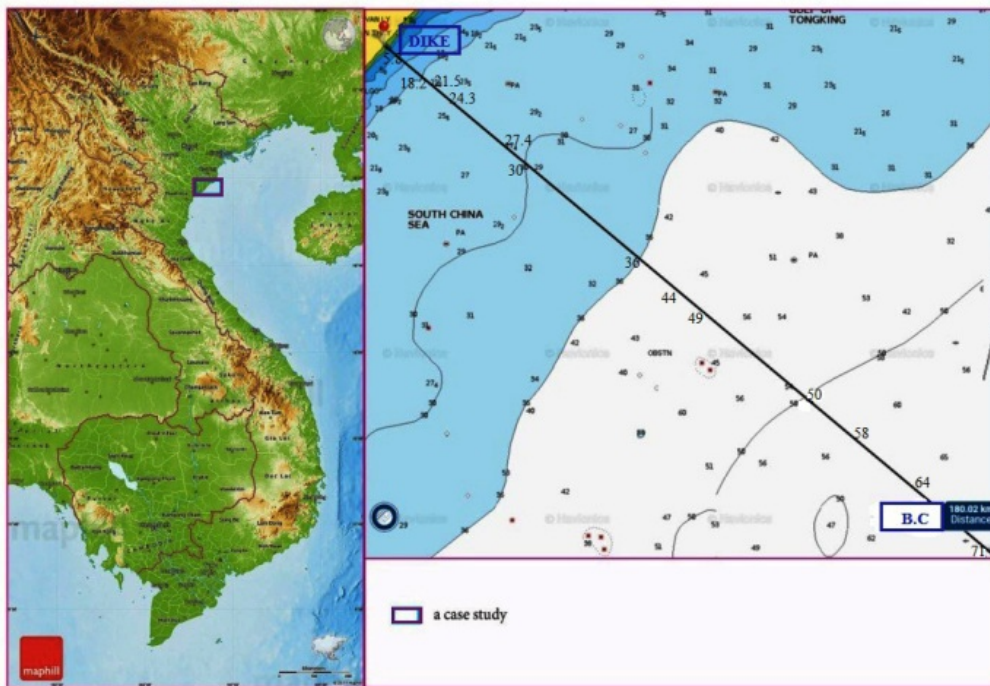


**Figure 3.1.** (a) A case study on the Vietnamese coastlines (top-left figure) and corresponding bathymetry (top-right figure), depths are indicated in meters. (b) Boundary conditions of SWAN and SWASH models (bottom figure).



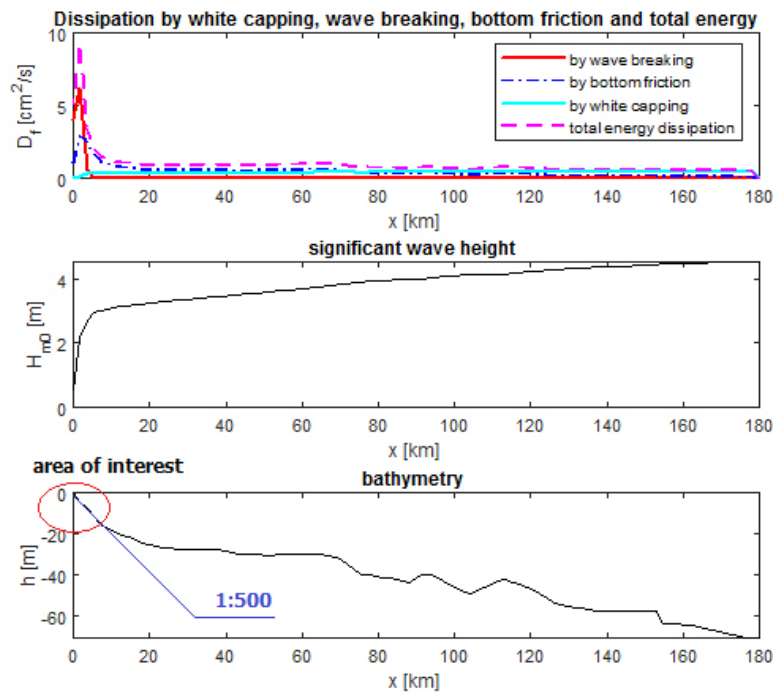


**Figure 3.2.** Wave dissipation, significant wave height calculated by SWAN, and bathymetry of the north site with the interested area.

### 3.2.1.2. Offshore hydraulic conditions and dike geometries

An accurate prediction of the wave transformation from offshore to dike toes is of great importance for coastal areas. The transformation of wave spectra across the cross-shore water areas with wind growth was taken into account. Due to very gently sloping foreshore with a very wide coastal shelf, the wind generation could not be ignored. Moreover, the very wide coastal shelf leads to fully developed sea, so wave parameters will be following the maximum condition according to figures 3–23 in Shore Protection Manual (US Army Corps of Engineers, 1984).

Input offshore wave parameters for the SWAN model used are as follows:  $H_s = 4.5$  m,  $T_p = 11$  s,  $U_{10} = 12$  m/s, for a 10-year return period according to Vietnamese condition (Petronas Carigali Vietnam Limited, 2011). The offshore hydraulic boundary is located at level  $-70$  m whereas landward boundary lies at  $+0$  m. Computational domain has been defined on a regular grid size of  $100$  m in a total length of  $180$  km. At the shoreward boundary a closed boundary is imposed. Wind and wave directions are assumed to be perpendicular to the coastline, as this is the most conservative condition. Extreme water levels, based on a high spring tide and storm surge, are roughly  $3$  m.

Dike crest is  $5$  m with a seaward slope of  $1:4$ . These parameters will be investigated to determine the overtopping discharges for very shallow water later on.

One more case will be considered as follows when a high sandy foreshore is nourished as have being done on the Dutch and Belgian coasts, the water level at the toe is  $1.5$  m.

### 3.2.1.3. Wave dissipation without sea dikes

The purpose of this section is to emphasize that this foreshore is due to a very wide shelf over a long cross-shore trajectory, and therefore the wind effect needs to be included. Moreover, since wind generation is excluded in SWASH, SWAN is an alternative and appropriate model to use over this long distance.

A constant wind is blowing over deep water, developing an internal atmospheric boundary layer starting at the boundary. Initially, the wind growth is equal to wave dissipation, so the wave height more or less stays the same after roughly 50 km seaward before decreasing gradually. When the wave starts to “feel” the bottom, bottom friction increases and significant wave height suddenly decreases until wave breaking, then the wave height rapidly reduces. For mild bottom slopes, the breaking point will lie far from the shore.

### 3.2.2. SWASH setup

It was shown in Section 2.1 that away from the coast wind generation plays an important role. Closer to the coast, infragravity waves and surfzone wave breaking will have a significant role, which is not, or not sufficiently, incorporated in the SWAN model. Hence, for the near shore region the SWASH model is applied in order to obtain the wave period and overtopping at a very gentle sloping coastal profile. The wave spectra from the SWAN calculation results shown above are used as boundary conditions for the SWASH model. The SWASH model is developed based on non-linear shallow water equations with a non-hydrostatic pressure model. It is a time domain model for simulating a non-hydrostatic, free-surface, and rotational flow, including short waves (Stelling and Zijlema, 2003; Zijlema et al., 2011). The smaller the grid dimension gets, the more exact the model becomes; however, it consumes a longer calculation time. The non-hydrostatic pressure is used for Keller-box scheme which will be mainly applied for accurate wave transformation. A JONSWAP wave spectrum with  $\gamma = 3.3$  is used for numerical model. A default Manning’s roughness coefficient of 0.019 is used for all calculations.

#### 3.2.2.1. Configuration to determine spectral wave period at dike toes

The spectral wave period of incident waves at the toes is a crucial parameter to determine the mean overtopping discharge over sea-dikes as mentioned in Section 1.1. In order to determine the spectral wave period and wave height corresponding to the incoming wave signal, the setup as given in Figure 3.3 is applied. In this way the reflection of the waves from the dike is not influencing the signal. Because the sloping bed foreshore is very mild, wave reflection is expected to be insignificant.

In the SWASH calculation the water depth at the offshore boundary condition is taken to be more than 4 times the corresponding significant wave height. Sponge layers are used at the SWASH open boundaries to effectively absorb the wave energy. The sponge layer length is often taken as 3 to 5 times the wavelength at the offshore boundary and schematized by one vertical layer (the SWASH team, 2016). The sponge layer had a length of 1000 m from the dike toe for the foreshore slope of 1:500. For all cases in Sections 3.1 to 3.4 below, the grid size of the bathymetry is adopted as 1 m and time duration is approximately 1 h; however, for the wave overtopping discharge calculations, from Sections 3.5 to 3.8, the grid size is smaller and the time duration is much longer, 0.2 m and 8 h, respectively. Time step of the numerical simulations is changed flexibly due to Courant–Friedrichs–Lewy (CFL) requirement (the SWASH team, 2016).

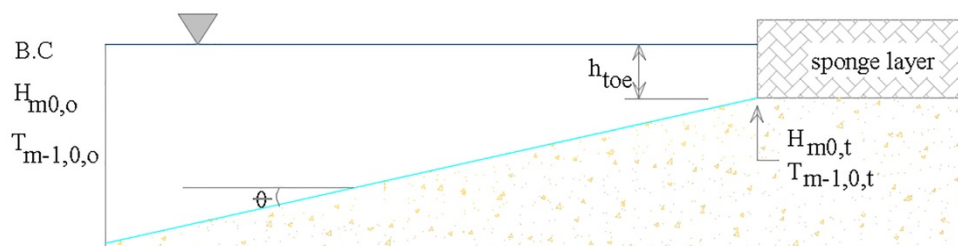


Figure 3.3. Wave parameters at toes in SWASH model for case studies.

In the calculations, the same wave parameters  $H_{m0,0} = 3\text{m}$  and  $T_{m-1,0} = 11\text{s}$  as obtained from the SWAN calculation at the start of the surf zone ( $x = 5.2\text{ km}$  in Figure 3.2) were applied for different foreshore slopes in Table 3.2 as follows:

**Table 3.2.** SWASH input data for different slopes and water depths (no structure).

| Slope | <b>h</b><br>[m] | <b>x</b><br>[km] | <b>h<sub>toe</sub></b><br>[m] |
|-------|-----------------|------------------|-------------------------------|
| 35    | 12.5            | 385              | 1.5                           |
| 100   | 12.5            | 1100             | 1.5                           |
| 250   | 12.5            | 2750             | 1.5                           |
| 500   | 12.5            | 5200             | 1.5                           |
| 700   | 12.5            | 7700             | 1.5                           |
| 800   | 12.5            | 8800             | 1.5                           |
| 900   | 12.5            | 9900             | 1.5                           |
| 1000  | 12.5            | 11,000           | 1.5                           |
| 35    | 13.2            | 385              | 2.2                           |
| 100   | 13.2            | 1100             | 2.2                           |
| 250   | 13.2            | 2750             | 2.2                           |
| 500   | 13.2            | 5200             | 2.2                           |
| 700   | 13.2            | 7700             | 2.2                           |
| 800   | 13.2            | 8800             | 2.2                           |
| 900   | 13.2            | 9900             | 2.2                           |
| 1000  | 13.2            | 11,000           | 2.2                           |
| 35    | 14              | 385              | 3                             |
| 100   | 14              | 1100             | 3                             |
| 250   | 14              | 2750             | 3                             |
| 500   | 14              | 5200             | 3                             |
| 700   | 14              | 7700             | 3                             |
| 800   | 14              | 8800             | 3                             |
| 900   | 14              | 9900             | 3                             |
| 1000  | 14              | 11,000           | 3                             |

### 3.2.2.2. Configuration to determine overtopping of the sea dike

The “virtual” overtopping discharge  $q$ —approximated by using a straight long slope and deriving the discharge exceeding the elevation of  $R_C$  (Figure 3.4)—will be determined efficiently for many  $R_C$  using a straight long slope. To verify the assumption that this yields the correct  $q$ , a realistic dike with fixed  $R_C$  is used. The same boundary conditions are applied for an infinite slope and a realistic sea dike to calculate the wave overtopping discharge based on water velocities and thicknesses for a shallow foreshore. The boundary conditions in the SWASH model are wave height and period from the SWAN model, assuming a JONSWAP spectral shape. The simulation duration for the wave overtopping model is advised to be at least 1000 waves (Suzuki et al., 2017; Chen et al., 2015; Chen, 2016). If LF waves are considered to play an important role at the toe of the dike, wave overtopping durations need 1000 LF waves, or roughly 5000 primary waves. In the calculations, duration is applied equivalent to more than 700 times wave periods. The duration of a calculation on a regular PC is approximately 8 h for one simulation. In SWASH, the bathymetry is calculated every 0.2 m, time steps are 0.05 s, as well and one layer applied. The calculation is based on a linearly sloping and impermeable seabed.

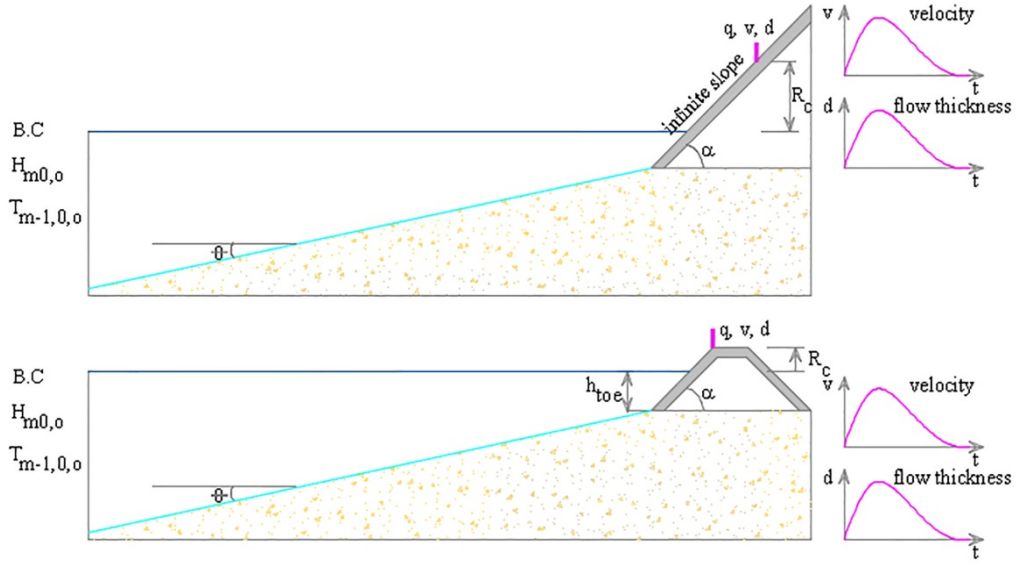


**Figure 3.4.** Virtual wave overtopping discharge (upper figure) and realistic wave overtopping discharge (lower figure).

From the SWASH model a time series obtained of the wave overtopping velocities and thicknesses on the dike are originated at the dike crest (corresponding to lower Figure 3.4). The overtopping discharges are calculated based on wave overtopping velocities  $v$  and layer thicknesses  $d$  at the outer crest line as follows:

$$q(t) = d(t)v(t) \quad (3.9)$$

Mean wave overtopping discharge is determined by integrating  $q(t)$  for  $q(t) > 0$ , over the duration, whereas  $t_{start,i}$  and  $t_{end,i}$  are start and end time of the wave overtopping predictions, respectively.

$$V_i = \frac{\int_{t_{start,i}}^{t_{end,i}} q(t) dt}{t_{end,i} - t_{start,i}} \quad (3.10)$$

For a straight seaward high slope (corresponding to upper Figure 3.4), the instantaneous virtual wave overtopping discharge  $q(t)$  is also similarly predicted as the Equation (3.9) at any elevations of the seaward slope for the high crested freeboards, following Hofland et al. (2015). Hence, this computation is very efficient to obtain the overtopping discharge for many dike freeboards.

### 3.2.2.3. Mean wave overtopping discharge over the dike crest

Simultaneously, similar boundary conditions are applied in the formulae of Van Gent (1999) and Altomare (2016), using Hofland et al. (2017) to compare the relation between the incoming waves overtopping discharge for a very shallow foreshore. Two cases are considered, with the same offshore boundary conditions but different water depths (see Table 3.3). The mean wave overtopping discharges will be calculated with a variety of different crest freeboards, as described in the previous section (or dike crest heights) in numerical models, and these predicted means will be compared with the existing empirical formulae referred to above. According to these formulae,  $q$  will demonstrate in exponential form, which is characterized by incoming wave height and spectral period at the toe of sea-dike, foreshore, and sea-dike geometries.

**Table 3.3.** Two cases of wave overtopping discharge for the Vietnamese slope calculated.

| Slope | SWAN              |              |                   |             | SWASH              |                  |             |
|-------|-------------------|--------------|-------------------|-------------|--------------------|------------------|-------------|
|       | $H_{m0,0}$<br>[m] | $T_p$<br>[s] | $U_{10}$<br>[m/s] | $x$<br>[km] | Boundary condition | $h_{toe}$<br>[m] | $x$<br>[km] |
| 500   | 4.5               | 11           | 12                | 180         | JONSWAP spectra    | 1.5              | 5.2         |
| 500   | 4.5               | 11           | 12                | 180         | JONSWAP spectra    | 3                | 5.2         |

### 3.3. Results

#### 3.3.1. Wind influence on wave transformation

The SWAN calculation in Section 2.1 indicates that the wind impact on very shallow foreshores with wide shelves cannot be ignored. Hereafter, this study will find out an appropriate distance to start the SWASH calculation, on which wind has limited impacts. The effect of wind on wave heights was considered with different speeds in several kilometers. The wind speeds  $U_{10}$  were 0, 12, and 25 m/s, respectively. Calculations were made with 5200 m length between boundary condition and the shoreline, the foreshore slope was roughly 1:500. The results are shown in Figure 3.5, where  $x = 0$  represents the coastline. The difference between wave heights at the coast with, or without, wind input was negligible in case of no, and 12 m/s, wind speeds. The 25 m/s wind showed the different results in wave heights around 2 km away from the shore. Therefore, the wind did not seem to have any influence on wave transformation within several kilometers if the wind speed was 12 m/s, or where the 12 m/s wind was more applicable for this distance. Hereafter, a distance of 5200 m with a wind speed of 12 m/s will be used to calculate wave parameters and wave overtopping in SWASH without wind effect.

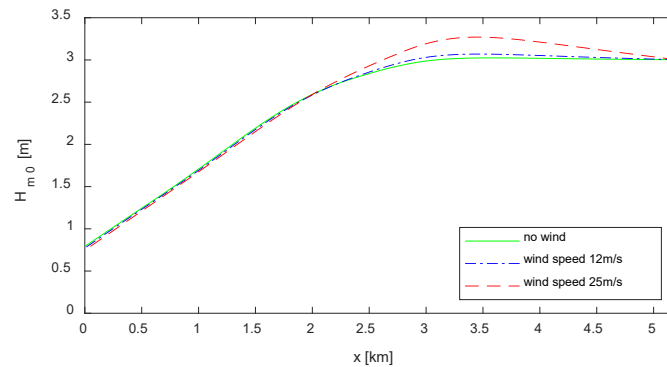


Figure 3.5. Wind effect on wave heights in SWAN for slope 1:500.

#### 3.3.2. Wave heights and periods at the toes of sea dikes

Here, the behavior of wave parameters in the nearshore area for both the SWAN and SWASH calculations is inspected. The same boundary conditions were applied in these models. Wave parameters were both JONSWAP wave spectrum, corresponding to  $H_{m0} = 3\text{m}$ ,  $T_{m-1,0} = 11\text{s}$ . The most important parameters are plotted in Figure 3.6, noticing that high-frequency (HF) and low-frequency (LF) waves were estimated by SWASH. For very gently sloping foreshores, waves seemed to be dissipated over a long distance from offshore to the toes of the dikes, while reflected waves were expected to be minimal over these foreshores.  $H_{m0}$  was somewhat higher for SWAN compared to that of SWASH for distances from shore of  $x = 2$  to 5.2 km. This was possibly caused by the extra wind input in the SWAN calculation.

Both HF and LF waves started breaking when they reached the shallow zone. However, the HF waves started breaking earlier than the LF waves, around the distance of 2 km from nearshore, as the LF waves were mainly generated mainly when the HF waves were breaking. The LF waves broke corresponding to a distance of roughly 1.5 km (see the top of Figure 3.6). After the start of breaking, HF waves decreased linearly, whereas LF waves decreased gradually when reaching the shore.

To investigate further the wave periods  $T_{m-1,0}$ , according to the red line on the spectral wave period curve in Figure 3.6, they stayed more or less unchanged from offshore to surf zone. After wave breaking, LF waves became dominant over the HF waves. Waves with a lower steepness broke closer to the shore and LF waves occurred in SWASH, so waves from SWAN broke further than those in SWASH to the shore.

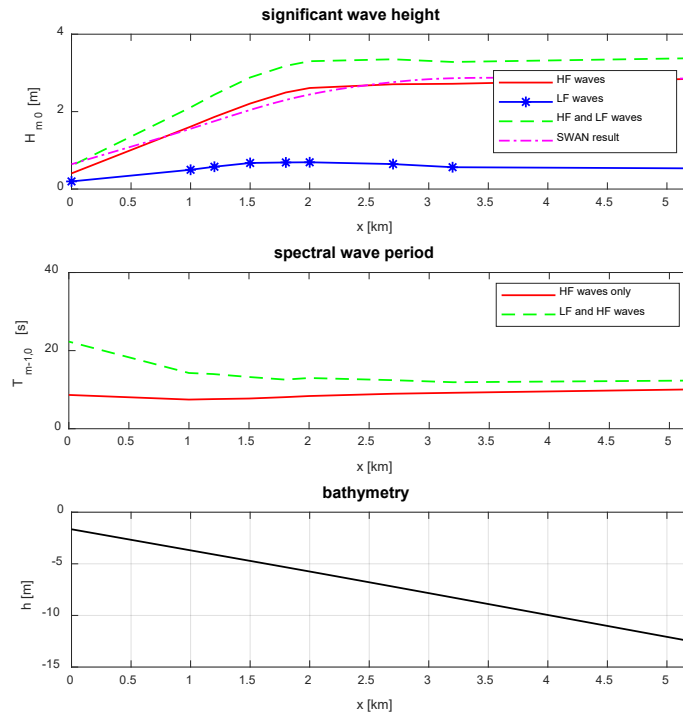


Figure 3.6. SWAN and SWASH results for 1:500 slope.

### 3.3.3. Wave spectra over the shallow foreshore

Here, the near shore spectra as obtained from SWASH for this case are presented. It can be noticed that the wave spectra, shown by red thick lines in Figure 3.7, not only vary their total amount of variance (i.e., wave energy), but also their shape. On a shallow foreshore, due to the process of triad wave–wave interaction, the wave spectral peak constantly migrated towards the lower frequencies; therefore, the wave spectral shape became flattened, completely different from JONSWAP in the offshore. This flattened shape has been investigated based on previous research on shallow foreshore (Van Gent, 2001; Suzuki et al., 2017).

From the offshore boundary conditions in SWASH, the wave energy started to decrease due to increased wave dissipation. Additionally, the energy redistribution occurred because of triad wave–wave interaction, which explains the presence of other peaks around frequencies twice, and four times, the peak frequency. From a certain depth, the energy of HF waves whose frequencies were more than 0.05 Hz dissipated and more energy occurred in low frequencies. The LF wave energy, at frequencies between 0.005 Hz to 0.05 Hz, increased from depths between 10 and 6 m, and subsequently seemed to be more or less constant up to depths of 2.5 m, so the LF waves increased relatively compared to the HF waves.

There is a significant difference when comparing wave spectra between very gentle slope and steeper slope (1:100 as blue thin lines in the Figure 3.7) at the same water depths. The primary waves were more at the gentler slope, as the peak of the primary wave ( $f \approx 0.1$  Hz) decreased faster. This is probably explained by the fact that a change in depth corresponds to a longer distance such that the

waves have more time to break. On the shallow foreshore, both slopes had increased LF energy. The LF energy level between depths of 6 and 2.5 m was higher for the very gentle 1:500 slope.

Additionally, at the original water line ( $h = 0$  m), there was wave energy due to the set-up of the water level that was not included in  $h$ . Here, the 1:100 slope still exhibited much more HF energy.

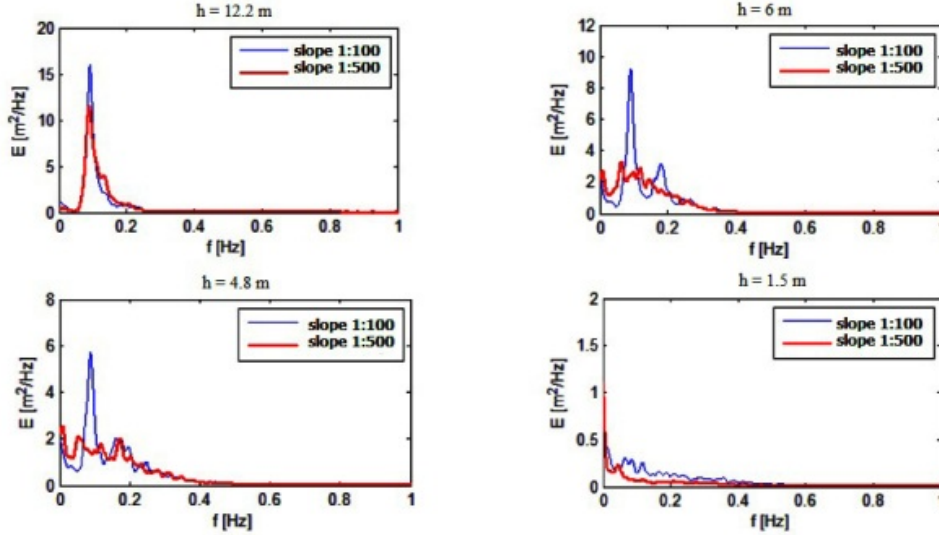


**Figure 3.7.** Wave spectra calculated by SWASH over the distance for a steeper slope 1:100 (blue thin line) and a very gentle slope 1:500 (red thick line), at several equal water depths (note the varying vertical scaling).

### 3.3.4. Spectral wave periods at gentle to very gentle slopes

Here, the evolution of spectral wave periods  $T_{m-1,0,t}$  at the dike toe is investigated, compared with those in offshore, as calculated with SWASH. The spectral wave periods are presented relative to the offshore wave parameters and water depths. In Table 3.4 below, these predictions are compared with those in Hofland (2017), which were derived for this range of slope angles.

**Table 3.4.** A comparison of spectral wave period between Hofland (2017) and SWASH results. These are shallow to very shallow conditions according to the Hofland's classification, where the ratio  $\frac{T_{m-1,0,t}}{T_{m-1,0,o}}$  from the curve indicates the range  $\pm 2\sigma$  for error bands.

| $\cot\theta$ | $H_{m0,o}$<br>[m] | $T_{m-1,0,o}$<br>[s] | SWASH results        |                                   |           |  | Hofland [8]                       |  |
|--------------|-------------------|----------------------|----------------------|-----------------------------------|-----------|--|-----------------------------------|--|
|              |                   |                      | $T_{m-1,0,t}$<br>[s] | $\frac{T_{m-1,0,t}}{T_{m-1,0,o}}$ | $h_{toe}$ | $\frac{h_{toe}}{H_{m0,o}} \left(\frac{\cot\theta}{100}\right)^{0.2}$ | $\frac{T_{m-1,0,t}}{T_{m-1,0,o}}$ |  |
| 35           | 3                 | 11                   | 20.4                 | 1.9                               | 1.5       | 0.4  | $2.7 \pm 0.8$                     |  |
| 100          | 3                 | 11                   | 23.8                 | 2.2                               | 1.5       | 0.5  | $2.5 \pm 0.7$                     |  |
| 250          | 3                 | 11                   | 26                   | 2.4                               | 1.5       | 0.6  | $2.2 \pm 0.6$                     |  |
| 35           | 3                 | 11                   | 21.5                 | 2                                 | 2.2       | 0.6  | $2.2 \pm 0.6$                     |  |
| 100          | 3                 | 11                   | 22.6                 | 2.1                               | 2.2       | 0.7  | $2.0 \pm 0.4$                     |  |
| 250          | 3                 | 11                   | 19.8                 | 1.8                               | 2.2       | 0.9  | $1.6 \pm 0.4$                     |  |
| 35           | 3                 | 11                   | 13.3                 | 1.2                               | 3         | 0.8  | $1.8 \pm 0.4$                     |  |
| 100          | 3                 | 11                   | 14                   | 1.3                               | 3         | 1  | $1.5 \pm 0.4$                     |  |
| 250          | 3                 | 11                   | 13.4                 | 1.2                               | 3         | 1.2  | $1.4 \pm 0.4$                     |  |
| 500          | 3                 | 11                   | 25                   | 2.3                               | 1.5       | 0.7  | $2.0 \pm 0.4$                     |  |
| 700          | 3                 | 11                   | 25.4                 | 2.3                               | 1.5       | 0.7  | $2.0 \pm 0.4$                     |  |
| 800          | 3                 | 11                   | 28.4                 | 2.6                               | 1.5       | 0.8  | $1.8 \pm 0.4$                     |  |
| 900          | 3                 | 11                   | 33.3                 | 3.0                               | 1.5       | 0.8  | $1.8 \pm 0.4$                     |  |

|      |   |    |      |     |     |     |               |
|------|---|----|------|-----|-----|-----|---------------|
| 1000 | 3 | 11 | 39   | 3.5 | 1.5 | 0.8 | $1.8 \pm 0.4$ |
| 500  | 3 | 11 | 22.1 | 2   | 2.2 | 1   | $1.5 \pm 0.4$ |
| 700  | 3 | 11 | 22.3 | 2   | 2.2 | 1.1 | $1.4 \pm 0.3$ |
| 800  | 3 | 11 | 24   | 2.2 | 2.2 | 1.1 | $1.4 \pm 0.3$ |
| 900  | 3 | 11 | 22.6 | 2.1 | 2.2 | 1.1 | $1.4 \pm 0.3$ |
| 1000 | 3 | 11 | 24.5 | 2.2 | 2.2 | 1.2 | $1.4 \pm 0.3$ |
| 500  | 3 | 11 | 20.5 | 1.9 | 3   | 1.4 | $1.3 \pm 0.2$ |
| 700  | 3 | 11 | 18   | 1.6 | 3   | 1.5 | $1.2 \pm 0.2$ |
| 800  | 3 | 11 | 18   | 1.6 | 3   | 1.5 | $1.2 \pm 0.2$ |
| 900  | 3 | 11 | 18.5 | 1.7 | 3   | 1.6 | $1.2 \pm 0.2$ |
| 1000 | 3 | 11 | 20   | 1.8 | 3   | 1.6 | $1.2 \pm 0.2$ |

The calculated evolution of the wave period  $T_{m-1,0,t}$  is plotted in Figure 3.8, as a function of the relative water depth. It is obvious that the spectral wave periods at the dike toe increase when dimensionless depth decreases. It is also seen that compared to slopes up to 1:700, the wave period at low water depth ( $\frac{h_{toe}}{H_{m0,0}} = 0.5$ ), the spectral energy wave period is increased more.

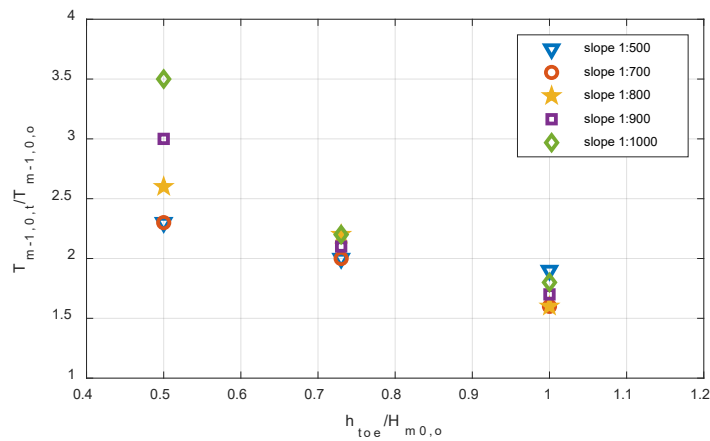


**Figure 3.8.** Calculated evolution of spectral wave period  $T_{m-1,0,t}$  as a function of water depth, offshore wave height and period.

### 3.3.5. Wave overtopping discharge for a gentle foreshore slope

Here, the mean wave overtopping, still the most used design variable for dike heights, is inspected. First of all, the wave overtopping discharge was calculated for a steeper slope of 1:100, which is in the range of previous studies. The offshore boundary condition in SWASH was again  $H_{m0,0} = 3$  m,  $T_{m-1,0,0} = 11$  s, now at the distance 1100 m to the dike toe. The dike slope was 1:4, the crest freeboards applied were 2 m, 3.25 m, and 4.5 m, respectively. Compared with [Altomare's formula \(2016\)](#), the SWASH-based overtopping discharges were very comparable to the formulae (see Figure 3.9).



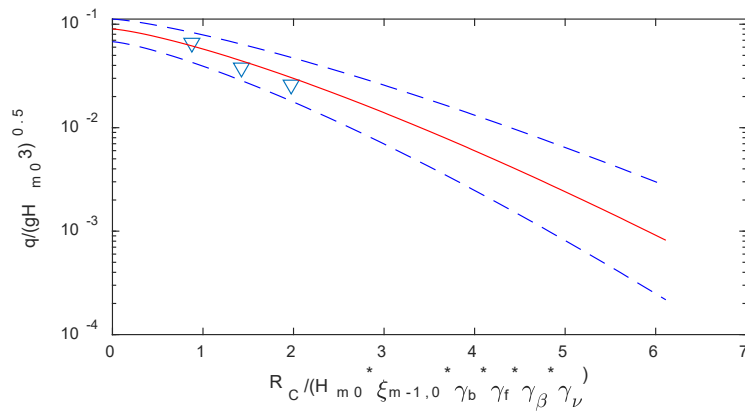


**Figure 3.9.** Comparison to Altomare (2016) (red solid line: prediction using mean value approach of Altomare; dashed line:  $\pm 1.64\sigma$ ; and triangle: SWASH values).

### 3.3.6. Wave overtopping discharge for Vietnamese conditions with very gentle slopes

Now, the typical Vietnamese condition is considered in this section. A SWAN-based JONSWAP wave spectrum was the SWASH boundary, corresponding to  $H_{m0,0} = 3$  m and  $T_{m-1,0} = 11$  s, at a distance of 5.2 km from the dike toe. The foreshore slope was roughly 1:500 whereas the seaward dike slope was  $\tan\alpha = 1:4$  and the crest freeboard was 2 m. The water thicknesses, velocities, and overtopping discharges were considered in short term duration as well. The two different cases were predicted as follows with  $h_{toe}/H_{m0,0} = 0.5$  and 1, respectively, classified from a shallow to a very shallow foreshore.

For the infinite slope the storm duration was 8 h as well, leading to 4660 incident waves and 980 overtopping waves (more than 20% of the waves). The mean overtopping discharge during the event was 400 l/s/m. Figure 3.10 shows the overtopping characteristics (layer thickness depth, velocity, and discharge) for the virtual sea ward crest line of the dike.

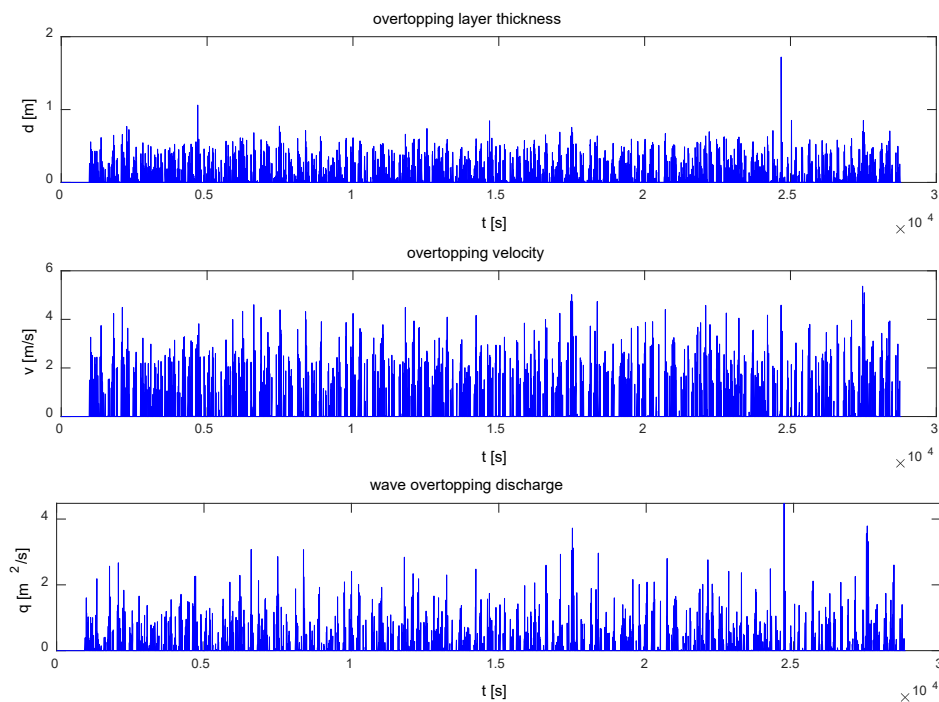


**Figure 3.10.** Water thicknesses, velocities, and discharges for the infinite slope.

For the real dike the same wave characteristics were applied. The mean overtopping discharge during the event was 360 l/s/m.

This overtopping discharge corresponds well to that in the case of the infinite slope. Ten percent difference is not very much for an overtopping discharge. The difference can be explained by the fact that a different realization of the seed values of waves (in SWASH) was used, and that the interaction of reflected and incoming waves was also different in the two cases.

### 3.3.7. Comparison to existing approaches

In this section wave discharges  $q$  are calculated for a variety of crest freeboards at the same wave properties at offshore and the toe of sea dike, foreshore slope of 1:500, and a sea dike slope of 1:4 in SWASH, only the freeboard or virtual dike crest was changed every 0.05 in intervals, in the infinite slope model. These SWASH-based overtopping discharges were compared with the existing empirical formulae according to Van Gent (1999) and Altomare (2016) with 5% under- and upper-exceedance limits, or 90% error interval, using the spectral wave period and wave height at the dike toe as calculated by SWASH (see Figure 3.3) as the input.

The comparison is demonstrated in Figures 3.11 and 3.12 by dimensionless overtopping discharge versus relative freeboard. The relative overtopping discharges were plotted using a logarithmic y-axis. It is obvious that the logarithm of relative overtopping rate decreases with the rising relative freeboard.

The red solid line corresponds to the mean value approach of Altomare and Van Gent. The two dashed lines are 90 percent confidence interval of this approach, and the triangles are the SWASH-computed values of the (virtual) overtopping discharge for the infinite slope.

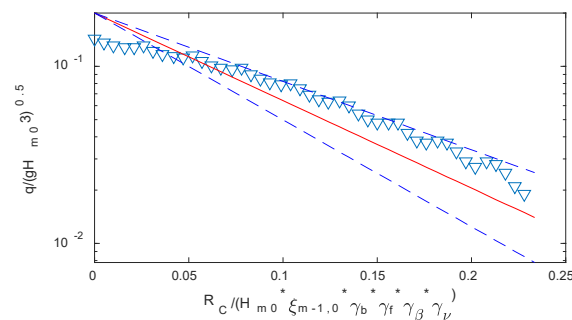


**Figure 3.11.** Comparison to Van Gent (1999) (red solid line: prediction using mean value approach of Van Gent; dashed line:  $\pm 1.64\sigma$ ; and triangle: SWASH values).

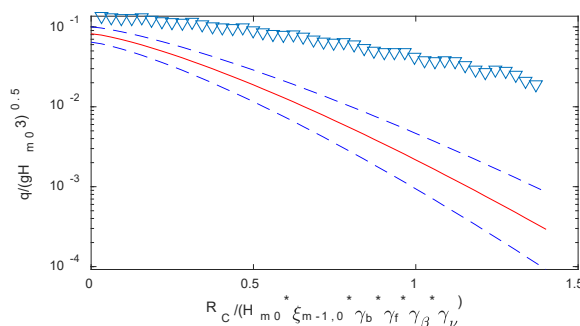


**Figure 3.12.** Comparison to Altomare (2016) (red solid line: prediction using mean value approach of Altomare; dashed line:  $\pm 1.64\sigma$ ; and triangle: SWASH values).

From the Figure 3.11, it is obvious that SWASH gave reliable dimensionless overtopping discharge corresponding to Van Gent's general formulae when the relative freeboard was more than 0.05. For low values of the dimensionless freeboard, the empirical formulae were overestimated.

However, compared with Altomare's formulae, the SWASH-based values seem to be much higher, especially for high relative freeboards. It is striking that the overtopping discharge hardly seems to decrease with increasing freeboard.

### 3.3.8. Wave overtopping discharge for a high sandy foreshore

A high sandy foreshore with the sea dike can be predicted with wave parameters of  $H_{m0,0} = 3$  m and  $T_{m-1,0,0} = 11$  s, and water depth at the toe  $h_{toe} = 1.5$  m. It was classified as a very shallow water where  $0.3 < \frac{h_{toe}}{H_{m0,0}} < 1$  for infinite slope, and for a real dike (as above description). The foreshore slope was roughly 1:500, whereas the seaward dike slope was  $\tan\alpha = 1:4$ , and the crest freeboard was 2.5 m.

Additionally, an infinite slope was applied, the storm duration was 8 h also. Roughly 20% of the waves, the mean overtopping discharge during the event was 330 l/s/m. It is striking that even though the water depth was half that of the previous case, and the wave height was also half that of the previous case, the overtopping discharge only decreased by less than 10%. This was probably due to the large increase in LF wave energy.

Now we compare the existing approaches. The more general formulae from Van Gent (1999) was used and compared with SWASH-based values. The Figure 3.13 was valid for low values of  $R_C/H_{m0}(0.33 + 0.022\xi_{m-1,0})$ , but for higher values of the relative freeboard (more than 0.09), Van Gent's formulae underestimated the mean overtopping rate for this kind of very gently sloping foreshore.

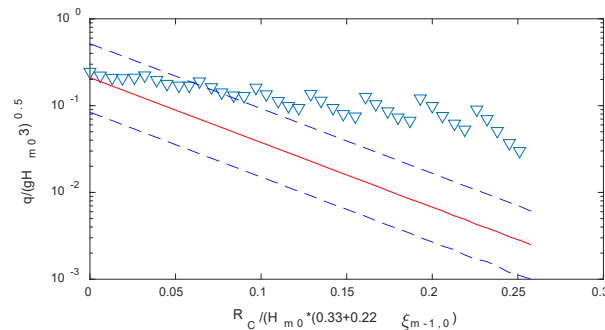


**Figure 3.13.** Comparison to Van Gent [4] (red solid line: prediction using mean value approach of Van Gent; dashed line: 5% under- and upper-exceedance limits; and triangle: SWASH values).

In general, the logarithm of the overtopping rate constantly went down with the increase of the dimensionless freeboard; the plot shows the underestimation of Van Gent's formulae, compared with numerical results. With small values of the freeboard, Van Gent and SWASH-calculated values were relatively appropriate. When the freeboard increased, the Van Gent's formulae lay far from the SWASH-based overtopping discharge.

Further comparison in case of Altomare (2016) will be given as follows. It is obvious that the water depth at the toe  $h_{toe} = 1.5$  m was larger than  $1.5H_{m0,0}$  ( $H_{m0,0} = 0.8$  m; see the significant wave height of Figure 3.6). According to his study, it leads to the calculated Iribarren number  $\xi_{m-1,0} = 9.1$  applying the dike slope only; therefore, the equivalent slope  $\delta$  in (very) shallow foreshore was not applied in this case. For the above reason, the Altomare's formulae turned into Van Gent's general formulae (Figure 3.13).

## 3.4. Discussion

### 3.4.1. Incident spectral wave periods on gently sloping foreshores

In order to predict wave overtopping over a dike, incident wave parameters at the toe such as  $H_{m0,o}$ ,  $T_{m-1,o}$  play an important role. Hofland et al. (2017), based on data from measurements and calculations for smooth linear foreshores and normal waves, found the evolution of spectral wave period near the toe. The ratio of wave period between offshore condition and extremely shallow waters could rapidly increase, up to about eight times. The bed slope was limited until  $\cot\theta = 250$ . For very gently and straight linear sloping foreshore, such as 1:500, 1:700, 1:800, 1:900, and 1:1000, associated with Table 3.5, this evolution of short-crested wave period of Hofland (2017) seems to be underestimated in the calculated cases for very shallow water (Figure 3.14).

Table 3.5. A comparison of various approaches in the shallow water case ( $h_{toe}/H_{m0,o} = 1$ ).

| Parameters        | Van Gent (1999) | SWASH and Altomare (2016) | Hofland (2017) and Altomare (2016) | SWASH (infinite slope) | SWASH (real dike) |
|-------------------|-----------------|---------------------------|------------------------------------|------------------------|-------------------|
| $H_{m0,o}$ [m]    | 3               | 3                         | 3                                  | 3                      | 3                 |
| $T_{m-1,o,o}$ [s] | 11              | 11                        | 11                                 | 11                     | 11                |
| $T_{m-1,o,t}$ [s] | 20.5            | 20.5                      | 14                                 | 20.5                   | 20.5              |
| $\xi_{m-1,0}$     | 4.38            | 0.73                      | 0.37                               | -                      | -                 |
| $\cot\delta$      | 0.25            | 0.04                      | 0.03                               | -                      | -                 |
| [degrees]         |                 |                           |                                    |                        |                   |
| $q$ [l/s/m]       | 192             | 7                         | ~0                                 | 400                    | 360               |

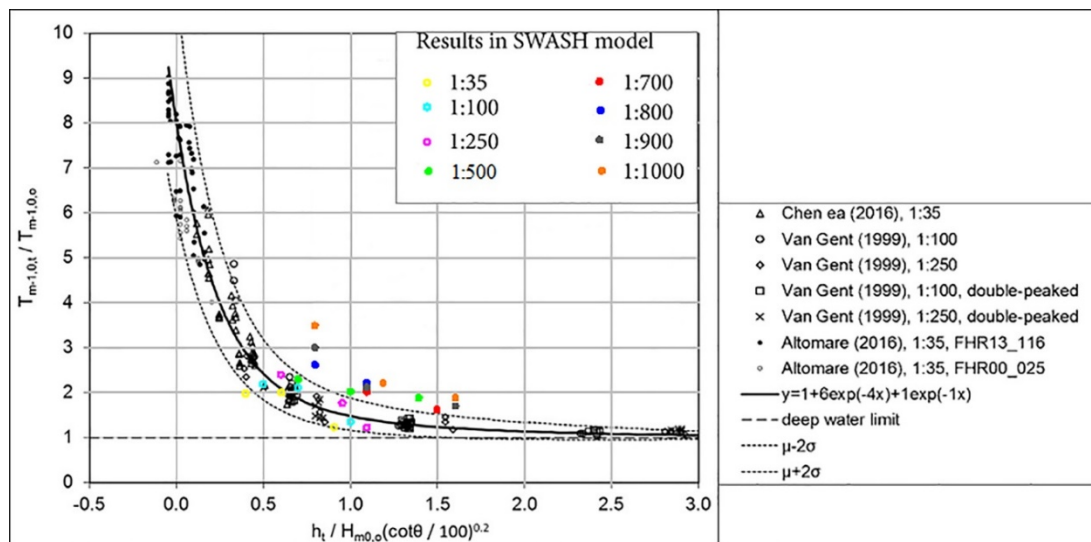


Figure 3.14. Compare SWASH results for very gently sloping foreshore and evolution of wave period of Hofland (2017).

For very gentle and straight linear sloping foreshores as Vietnamese typical bathymetry with slopes more gentle than 1:500, the spectral wave period near the toe of the structures increases more rapidly than for normally gentle slopes.

### 3.4.2. Wave overtopping discharge formulae for very gentle slopes

As shown in Table 3.5, it is clear that the mean wave overtopping discharge is more or less the same for the infinite slope and the real dike in very shallow water depths.

In order to predict overtopping discharge over sea-dikes, it is common practice that wave properties at the toe of structures are considered as a key factor. However, according to Altomare (2016), in cases where the toe of sea-dikes is located at very shallow water, waves do not actually break on dike slope but on its foreshore. Then the foreshore is considered as “a part” of the sea-dike; therefore, based on this study, wave parameters at the foreshore are precisely crucial instead of those

at the toe. An “equivalent slope” concept has been proposed to estimate wave overtopping discharges for shallow and very shallow foreshore. This application is valid for dikes with steep and gentle slopes,  $\cot\theta$ , less than 250. However, when the foreshores are gentler, like Vietnamese coastlines, “equivalent slope” become smaller and it also makes breaker parameter,  $\xi_{m-1,0}$ , much smaller than seven. Therefore, [Altomare’s](#) empirical formulae are no longer appropriate for these slopes. As shown in Figure 3.12, [Altomare’s](#) formulae tend to underestimate the wave overtopping discharge, compared with SWASH-computed values. This new approach is inaccurate for more gently sloping foreshores. More accurate formulae should be derived for this kind of very gentle slopes.

For the formulae of [Van Gent \(1999\)](#), the breaker parameter is larger since only the dike slope is included. This prediction seems to be better than the above approach, although, in comparison with SWASH-based values, it also underestimates the overtopping discharge at very shallow water. It needs to have more appropriate formulae for this kind of very mildly sloping and very shallow foreshores. However, the experiments reached their limits in this case due to scale effects for these very gentle slopes, so a numerical approach is the better option.

### 3.5. Conclusions

Vietnamese guidelines ([TCVN 9901:2014, 2014](#)) for dike design mainly apply [Van Gent \(1999\)](#) to calculate wave overtopping for (very) shallow foreshores, but actually this formula is derived for steep to mild slopes up to slopes of 1:250. Meanwhile, Vietnamese coastlines are characterized by very gently sloping foreshores with slopes up to 1:1000 or even more. The process of wave overtopping over the dikes with very gentle slope and shallow foreshore is far from being understood.

This study aims to give a new insight on the wave overtopping over a very gently sloping and shallow foreshore. First, the combination of SWAN (wind influence and no infra-gravity waves) and SWASH (no-wind but infra-gravity waves) proves to be a sufficient model combination for computing wave transformation over this very wide shelf. It is confirmed that shallow water associated with very gently sloping foreshore can cause significant changes of wave spectral shape from offshore to the toes of the dikes. The waves that reach the toe and overtop the dike crest are dominated by LF waves, even more than for less gently sloping beds.

The spectral wave period has been appropriately accepted to predict wave overtopping. [Hofland \(2017\)](#), also gives the relationship of spectral wave periods between offshore and the (extremely) shallow water. It is recommended to use within the range of foreshore slope from 20 to 250. For very gently sloping foreshores this spectral wave period near the toe is underestimated, as deduced from numerical model results for various foreshores that are gentler than previous study. The spectral wave period  $T_{m-1,0}$  for very gentle slopes seems to be approximately two times higher than according to [Hofland \(2017\)](#) for very mildly sloping foreshores ( $\cot\theta > 250$ ).

Some further conclusions can be made regarding wave overtopping. It is shown that the infinite slope approach seems to give reasonable overtopping discharges in an efficient manner. At very gentle (and very shallow) foreshores, existing formulae for shallow foreshore overtopping discharge underestimate the wave overtopping discharges  $q$ .

A better-founded wave overtopping formula with a shallow and very gently sloping foreshore should be established in physical scale models for more accurate prediction of wave overtopping. This chapter is limited to normally incident and long-crested waves, further research is recommended for oblique and/or short-crested waves.

---

## References

- Bosboom, J.; Stive, M.J.F. Coastal Dynamics I: Lecture Notes CT4305; [Delft Academic Press, Delft, the Netherlands, 2015](#).
- EurOtop. Manual on Wave Overtopping of Sea Defences and Related Structures—An Overtopping Manual Largely Based on European Research, but for Worldwide Application, 2nd ed.; 2018. <http://www.overtopping-manual.com/eurotop/downloads/>
- Zijlema, M.; Stelling, G.S.; Smit, P.B. SWASH: An operational public domain code for simulating wave fields and rapidly varied flows in coastal waters. [Coast. Eng. 2011, 58, 992–1012](#).
- Van Gent, M.R.A. Physical Model Investigations on Coastal Structures with Shallow Foreshores: 2D Model Tests with Single and Double-Peaked Wave Energy Spectra; [Delft Hydraulics/Waterbouwkundig Laboratorium: Delft, the Netherlands, 1999](#).
- Altomare, C.; Suzuki, T.; Chen, X.; Verwaest, T.; Kortenhaus, A. Wave overtopping of sea dikes with very shallow foreshores. [Coast. Eng. 2016, 116, 236–257, ISSN 0378-3839](#).
- Van Gent, M.R.A. Wave run-up on dikes with shallow foreshores, ASCE, [Journal of Waterway, Port, Coastal and Ocean Engineering, Vol. 127, No.5, Sep/ Oct 2001, 254-262](#).
- Van Gent, M.R.A. Numerical model simulations of wave propagations and wave run-up on dikes with shallow foreshores. [ASCE J. Waterw. Port. Coast. Ocean. Eng. 2001, 127, 2001](#).
- Munk, W.H. Surf beat. [Eos Trans AGU 1949, 30, 349–854](#).
- Tucker, M.J. Surf beats: Sea waves of 1 to 5 min. period. [Proc. R. Soc. A 1950, 202, 565–573](#).
- European Overtopping Manual for the Assessment of Wave Overtopping; EurOtop: 2007. <http://www.overtopping-manual.com/eurotop/downloads/>.
- Hofland, B.; Chen, X.; Altomare, C.; Oosterlo, P. Prediction formula for the spectral wave period  $T_{m-1,0}$  on mildly sloping shallow foreshores. [Coast. Eng. 2017, 123, 21–28](#).
- TAW. Technical Report on Wave Run-Up and Wave Overtopping at Dikes; [Technical Advisory Committee on Flood Defence: Delft, the Netherlands, 2002](#).
- Hoan, L.X.; Hanson, H.; Larson, M.; Donnelly, C.; Nam, P.T. Modeling shoreline evolution at Hai Hau beach, Vietnam. [J. Coast. Res. 2010, 26, 31–43](#).
- Phan Khanh, L. Wave Attenuation in Coastal Mangroves: Mangrove Squeeze in the Mekong Delta. [Ph.D. Thesis, Delft University of Technology, Delft, the Netherlands, 2019](#).
- Tas, S. Coastal Protection in the Mekong Delta: Wave Load and Overtopping of Sea Dikes as Function of Their Location in the Cross-Section, for Different Foreshore Geometries. [Master's Thesis, Delft University of Technology, Delft, The Netherlands, 2016; pp. 17–18](#).
- US Army Corps of Engineers. Shore Protection Manual; [US Army Corps of Engineers: Washington, DC, USA, 1984; Volume 1](#).
- Metoocean Criteria for the Thaibinh Development Blocks 102 & 106, Offshore Vietnam; [Petronas Carigali Vietnam Limited: Ho Chi Minh City, Vietnam, 2011](#).
- Stelling, G.; Zijlema, M. An accurate and efficient finite-difference algorithm for non-hydrostatic free-surface flow with application to wave propagation. [Int. J. Numer. Methods Fluids 2003, 43, 1–23](#).
- SWASH User Manual: SWASH Version 3.14A; the SWASH Team: [Delft, the Netherlands, 2016](#).
- Suzuki, T.; Altomare, C.; Veale, W.; Verwaest, T.; Trouw, K.; Troch, P.; Zijlema, M. Efficient and robust wave overtopping estimation for impermeable coastal structures in shallow foreshores using SWASH. [Coast. Eng. 2017, 122, 108–123](#).

---

Chen, X.; Hofland, B.; Altomare, C.; Suzuki, T.; Uijttewaal, W. Forces on a vertical wall on a dike crest due to overtopping flow. *Coast. Eng.* 2015, 95, 94–104, ISSN 0378-3839.

Chen, X. Impacts of Overtopping Waves on Buildings on Coastal Dikes. *Ph.D. Thesis, Delft University of Technology, Delft, the Netherlands, 2016.*

Hofland, B.; Diamantidou, E.; van Steeg, P.; Meys, P. Runup and overtopping measurements with a laser scanner. *Coast. Eng.* 2015, 106, 20–29.

TCVN 9901:2014 Hydraulic Structures-Requirements for Seadike Design, Vietnamese Version, 2014. TCVN 9901:2014 Công trình thủy lợi-Yêu cầu thiết kế đê biển, Hà Nội 2014; *Thuyloi University: Hanoi, Vietnam, 2014.*

## 4

## Wave Overtopping Volumes at Very Mild Shallow Foreshores

In Vietnam many sea dikes are situated at the coastline where the sea bed shows a very gentle slope, with slope angles as gentle as 1:1000. It is unknown how the wave attack on the inner dike slopes due to overtopping should be quantified for this case. In order to apply the cumulative overload method which can be used to evaluate the (grass) strength of the inner dike slopes, the distribution of the volumes of the overtopping waves should be known. In this chapter these distributions are determined for low-crested dikes with shallow, very gentle foreshores. To this end first a dataset of overtopping volumes is generated using the SWASH model. Prior to the calculations with very gentle foreshores, SWASH is validated with existing data with gentle slopes, albeit less gentle than the very gentle slopes of interest. Next, the single overtopping volumes are obtained for foreshore slopes of 1:500 to 1:1000, shallow water ( $h_t/H_{m0,t} \approx 1$ ), and relative low crest freeboards ( $R_c/H_{m0,t} \approx 0.3 - 1$ ). For the obtained sets of volumes, Weibull distributions are fitted. Lastly, empirical equations are obtained for the scale and shape parameter of a general Weibull distribution using a least squares procedure. The overtopping discharge that can be determined from the values of  $a$  and  $b$  as given by these empirical Weibull formulas resembles the simulated discharge well.

### 4.1. Introduction

Overtopping is one of the most important failure mechanisms of sea dikes, as it causes water to attack the rear-side of the dike, which is typically less protected than the seaward front side. It was the cause of many dike damaged in large storms like the 1953 Dutch flood, the 2005 Typhoon Damrey in Vietnam, and the 2006 Hurricane Katrina flood in New Orleans.

Whereas in old days the dike height was directly related to a wave height, later the mean overtopping discharge was taken as the parameter to describe the damage to inner dike slopes. However, it appears that the same mean overtopping discharge can lead more damage if the wave height at the toe is larger. Particularly, in the case where the wave height at the toe is large, but the overtopping discharge is the same, fewer but larger overtopping volumes will reach the inner slope, which will cause more damage than a larger number of smaller volumes. Therefore, attention is turning towards a description of the wave overtopping volume distribution.

In Vietnam the foreshores are very gentle, up to 1:1000. This alters the type of wave motion reaching the sea dikes, and the mean overtopping discharge (Nguyen et al., 2020). It is unclear however what the influence on the extreme overtopping volume is. The wave overtopping volume  $V$  is described by the amount of water that comes over the crest of the coastal structure in cubic meter per meter width (EurOtop Manual, 2018) for each single overtopping wave. An average overtopping discharge gives no indication of how many waves overtop or how much water is overtopped by individual waves, while the (maximum) amount of water that overtops in a single wave is usually linked to the maximum load on the (inner) slope of the dike.



On shallow foreshores where intense wave breaking occurs, long-period infragravity waves are generated. On the crests of these longer waves (with a larger water depth) the primary waves group together (Altomare et al., 2015, 2020, Suzuki et al., 2017, 2020). Here it can happen that many primary waves overtop the structure during one large infragravity wave at small interval, or even overlapping. This means that the usual way to describe single overtopping waves cannot be applied in a straightforward technique. This effect is altered even more when the foreshore is (very) gentle. In this chapter this effect is studied and quantified using a large set of calculations by the SWASH computer model.

This chapter is structured as follows. In the remaining part of this section important literature on overtopping volumes is given. Next, in Section 4.2, the applied methods will be introduced. Following, the procedure to obtain the Weibull parameters, a description of the physical modelling data and the numerical models used, and some further data analysis procedures are investigated. After that results will be presented, including results for deep water and shallow water, for steep and very gentle foreshore slopes. Finally, a discussion on the results and general conclusions are briefly presented.

#### 4.1.1. State-of-the-art in probability of wave overtopping for coastal structures

The probability of wave overtopping during a storm can be approximated by the ratio between the quantity of individual overtopping waves  $N_{ow}$  and the quantity of incoming waves  $N_w$  in a storm event:

$$P_{ov} = \frac{N_{ow}}{N_w} \quad (4.1)$$

Wave overtopping at sea dike slopes depends crucially on wave run-up because of the fact that the number of waves that overtop the crest of sea-dikes is roughly equal to the amount of wave run-ups which exceed that level of the dike crest. With the assumption that the run-up heights of the coastal structures are Rayleigh distributed, Van der Meer and Janssen (1994) (for typical dike slope angles) and Franco et al. (1999) (for vertical seawalls) proposed the following Rayleigh distribution for overtopping probability:

$$P_{ov} = \exp\left(-\left(\frac{1}{\chi} \frac{R_c}{H_{m0}}\right)^2\right) \quad (4.2)$$

The parameter  $\chi$  can be estimated by using the dimensionless 2% run-up height  $R_{u2\%}/H_{m0}$ . Based on a slightly difference for wave run-up formula  $R_{u2\%}$  in TAW (2002) and also given in EurOtop (2018), the following formula can be applied for relatively gentle slopes of smooth sloping coastal structures:

$$\frac{R_{u2\%}}{H_{m0}} = 1.65 \xi_{m-1,0} \quad (4.3)$$

Compared with former expression, Van der Meer et al. (2010) indicated the expression for the overtopping probability as below:

$$P_{ov} = \exp\left[-\left(\sqrt{-\ln 0.02} R_c / R_{u2\%}\right)^2\right] \quad (4.4)$$

The above empirical formula (4.3) of run-up level was found based on the fitting of run-up that was measured at a location on a straight slope, but overtopping discharge values were often measured near the landward side of the crest (EurOtop, 2018), therefore, this guideline gives notice that the number of overtopping waves  $N_{ow}$  has been overestimated in this formulation.

In an investigation of steep low-crested slopes of coastal structures in relatively deep water, Victor (2012) recommended another equation to predict the probability of overtopping, depending on the slope angle of the structure,  $\alpha$ , and significant wave height at the toe instead of using 2% run-up level  $R_{u2\%}$ :

$$P_{ov} = \exp \left[ - \left( (1.4 - 0.3 \cot \alpha) \frac{R_c}{H_{m0}} \right)^2 \right] \quad (4.5)$$

#### 4.1.2. State-of-the-art in deriving the maximum individual wave volume

The distribution of individual wave volumes for deep water cases can be described as a probability density function. Van der Meer and Janssen (1994) proposed the Weibull distribution to describe the overtopping volumes of individual waves. The exceedance distribution describes the percentage of wave volumes  $P_V$  exceeding a specified volume  $V$  for all waves that lead to overtopping:

$$P_V = P[V_i \geq V] = \exp \left[ - \left( \frac{V}{a} \right)^b \right] \quad (4.6)$$

in which scale factor  $a$  and non-dimensional shape factor  $b$  define the scale of the scale of the volume and the extreme tail of the distribution.

The expected maximum individual wave volume in the Weibull distribution in a certain number of overtopped waves,  $N_{ow}$  as the following expression (Van der Meer and Janssen, 1994) can be obtained from the equation (4.6):

$$V_{max} = a [\ln(N_{ow})]^{1/b} \quad (4.7)$$

Several relationships for the Weibull shape factor  $b$  and scale factor  $a$  are given in table 4.1. These are valid for smooth and impermeable structures like dikes. As the sum of all overtopped waves for a certain duration leads to the mean overtopping discharge  $q$ , and the waves reach the structure at a mean time interval of  $T_m$ , these parameters are incorporated in the equations for  $a$ .

**Table 4.1.** Weibull scale factor  $a$  and shape factor  $b$  in various studies

| Authors<br>(application)                                   | $a$ [m <sup>3</sup> /m]                           | $b$ [-]  |
|--|---|--|
| Van der Meer and Janssen, 1994<br>(dike slopes deep water) | $0.84(q T_m / P_{ov})$                            | 0.75   |
| Van der Meer et al., 2010<br>(dike slopes deep water)      | $[0.84 + 1.2(N_w P_{ov})^{-0.8}](q T_m / P_{ov})$ | 0.75   |
| Victor, 2012<br>(steep slopes deep water)                  | $1.13 \tanh(1.32b)(q T_m / P_{ov})$               | $\exp\left(-2.0 \frac{R_c}{H_{m0}}\right) + (0.56 + 0.15 \cot \alpha)$ |
| Hughes et al., 2012<br>(dike slopes deep water)            | $[0.84 + 1.2(N_w P_{ov})^{-0.8}](q T_m / P_{ov})$ | $\left[\exp\left(-0.6 \frac{R_c}{H_{m0}}\right)\right]^{1.8} + 0.64$   |
| Zanutigh et al., 2013<br>(including rubble mound slopes)   | $[0.84 + 1.2(N_w P_{ov})^{-0.8}](q T_m / P_{ov})$ | $0.73 + 55 \left(\frac{q}{g H_{m0} T_{m-1.0}}\right)^{0.8}$            |

Van der Meer and Janssen (1994) started with a constant  $b$  in overtopping measurements acquired for mild seaward slopes (1:3 to 1:4) and  $0.99 < R_c/H_{m0} < 3.16$ , however a variety of experimental data indicated a dependency of  $b$  on relative crest freeboard  $R_c/H_{m0}$  and slope angle  $\alpha$  (Victor, 2012). Hughes et al., 2012 adjusted the dimensionless ratio and removed the slope dependency. However, the adjustment of Victor (2012) is recommended for steep seaward slopes

(1:0.36 to 1:2.75) and low relative freeboard ( $0.11 < R_c/H_{m0} < 1.69$ ). The scale factor  $a$ , in all studies, are related to wave overtopping discharge  $q$ . In their study, [Zanuttigh et al, 2013](#), proposed a new relationship between shape factor  $b$  and the dimensionless mean overtopping discharge  $q/(gH_{m0}T_{m-1,0})$ . This formula was based on experimental results that included rubble mound structures.

A fast overtopping flow can lead to damage to the inner slope of the dike, especially if a grass cover is used as protection material. When the first erosion happens, the damage can spread out to material layer underneath, and as a result, dike breaching likely occurs ([Tega and Kobayashi, 1996](#); [Hughes, 2008](#)). The original cumulative over-load method presented by [Van der Meer et al., 2010](#), is used to evaluate the strength of the grass-turf cover in terms of peak flow velocities. The method supposes that dike erosion happens due to accumulative hydraulic loading originated mainly by the influence of each overtopping flow leading edge, approximately the first 1s to 3s of the wave. Only larger waves with local velocity larger than the critical velocity ( $u > u_c$ ) are taken into account since the smaller ones are considered to stimulate insignificant hazard. That method is enveloped through a variety of dike slope-related research in e.g. the Netherlands ([Van der Meer et al., 2010](#)), USA ([Hughes, 2011](#)) and Singapore ([Van der Meer., 2020](#)). Based on the investigation of [Van der Meer., 2015](#), the strength of lawn cover is presented by a critical velocity  $u_c$  and relying on the strength of grass, each landward slope is represented by a certain  $u_c$ . The cumulative overload method confirms that a small number of large waves leads to a cumulated overload which is comparable to the great number of small waves. Importantly, the local flow velocities are determined based on the wave overtopping volumes ([Hughes et al., 2012](#)).

Single overtopping volumes are related more directly to damage to rear slopes of dikes than the average overtopping discharge. For deeper foreshores the distribution has been described and researched well. For gentle to very gentle shallow foreshores, this distribution is not understood well yet. Therefore, in this chapter we will describe the overtopping volume distribution for these types of foreshores. Weibull parameters  $a$  and  $b$  from physical models are used to validate numerical model in steep and gentle slopes, e.g. slopes of 1/35, 1/50, 1/100, 1/250. Due to the fact that the gentle bed slopes along Vietnamese coastlines lead to a long distance between the near-shore and deep water, wave growth caused by wind can play a significant role. [Nguyen et al., 2020](#) (also given in Chapter 3), used the wave model SWAN (where the wind growth is included, but infragravity waves are not modelled) to estimate the wave transformation for the largest part of the domain from the offshore boundary to the coast. The obtained wave conditions correspond to a significant wave of height 3 m and a peak period of 11 s. In that chapter, these conditions were subsequently imposed at relatively deep water in the non-hydrostatic SWASH model (that does model the infragravity waves, but does not include wind growth), to determine the wave transformation from the relatively deep water to the coastline (dike).

In addition, based on previous research, infragravity waves, generated by wind-induced wave groups are of importance in the surf zone and for overtopping events ([Van Gent, 1999](#); [Suzuki et al., 2012](#); [Oosterlo et al., 2018](#); [Nguyen et al., 2020](#); [Lashley et al., 2020a, b](#)). Improvement of generation by [Rijnndorp \(2014\)](#) regarding infragravity waves in SWASH is triggered by second lower-order waves that the wave groups release after the primary waves break in the shallow waters. Moreover, [Suzuki et al. \(2011, 2017\)](#) confirmed that the depth-integrated wave transformation SWASH model generates satisfactory results about both wave evolution and overtopping for one dimensional calculation of shallow water ([Lashley et al., 2020a](#)). In particular, a good resemblance between physical and SWASH models is observed if the wave overtopping rate is more than 1 l/s/m ([Suzuki et al., 2017](#)). Based on the numerical model SWASH in association with the experimental data, [Suzuki et al., 2020](#), on the other hand, indicated that overtopping risk not only depends on wave overtopping rate  $q$  or individual volume  $V$  but also relies strongly on the time-dependent values of flow depth and velocity ( $d, v$ ). When using SWASH, the time dependent  $d$  and  $v$  can be completely obtained in

time series at all cross-shore locations, meanwhile these values are quite difficult to measure in experiments.

Furthermore, due to such very gently sloping foreshores in combination with a very wide cross-shore shelf, especially for the extremely mild slopes (in the order 1:1000), it is almost impossible to build up in scale laboratories in terms of wave overtopping prediction. Therefore, the near-shore time domain wave model SWASH based on NLSW equations is chosen in this chapter. It will translate waves in the deep water to the near-shore and model the required hydrodynamics near-shore region. The exceedance probability and the Weibull parameters between numerical result and previous studies will be compared. After that, a new prediction formula is proposed for the shape factor  $b$  in terms of very gently sloping foreshores.

## 4.2. Methods

### 4.2.1. Description of physical model data

This section describes the physical model data considered in the chapter. Existing data of overtopping on shallow and gentle foreshores is used to validate the SWASH model. The setup in which these data were obtained is briefly described here.

First of all, data is used from tests on two specific cases that have been carried out at Flanders Hydraulics Research (Antwerp, Belgium) by [Altomare et al., 2016](#). The wave flume was 70 m long, 4 m wide and 1.5 m high with a smooth, impermeable dike. Two types of steep foreshore slopes applied were 1/35 and 1/50 with a structure slope of 1:3 and 1:2, respectively. 1. Experiments were carried out with Iribarren number  $\xi_{op} < 0.5$  for these steep foreshore slopes (so not for the dike slope) corresponding to 0.047 for slope 1/35 and 0.007 for slope 1/50. Hence the wave breaking on the foreshore can be characterized as irregular spilling waves in both cases. The model scale compared to the Belgian prototype was order 1/25.

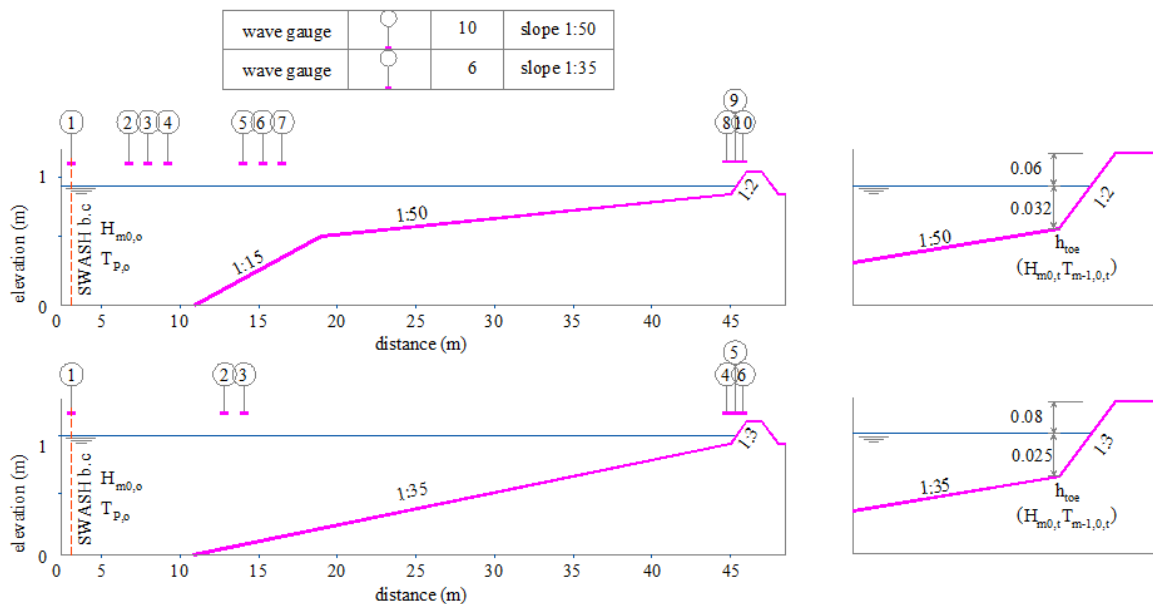


Figure 4.1: Physical and numerical model domain for foreshore 1:50 with a 1:2 dike slope (upper figure) and foreshore 1:35 with a 1:3 dike slope (lower figure), as applied by [Altomare et al., 2016](#). Right panels show close up of sea-dike location.

The water surface elevation was measured by using 10 wave gauges with a sample frequency of 50 Hz for the slope 1/50 and 6 wave gauges with the corresponding sample frequency of 20 Hz for the steeper foreshore slope. The gauges 8 to 10 in the former case and gauges 4 to 6 in the latter case correspond to the near-shore zone. The installed positions of wave gauges are illustrated in figure

4.1. Test conditions for both slopes are described in Table 4.2. A flume wave generator with piston motion with a 0.5 m stroke length is used for water wave formation.

**Table 4.2.** Test conditions for 2 slopes

| Slope | $H_{m0,o}$ [m] | $T_{p,o}$ [s] | cot m | $h_t$ [m] | cot $\alpha$ | $R_c$ [m] |
|-------|----------------|---------------|-------|-----------|--------------|-----------|
| 1/50  | 0.06           | 2.29          | 50    | 0.032     | 2            | 0.06      |
| 1/35  | 0.21           | 1.7           | 35    | 0.025     | 3            | 0.08      |

The average overtopping rate was determined from the entire volume of overtopped water. This volume was collected in an overtopping container placed right behind the landward slope of the dike. The volume is divided by the total test duration.

## 4.2.2. Numerical modelling setup

### 4.2.2.1 Description of numerical model SWASH

The numerical model SWASH (Simulating WAVes till SHore) is used in this chapter since this hydrodynamic model is capable for simulating non-hydrostatic flow which is based on non-linear shallow water (NLSW) equations with a pressure correction. It can be applied to compute the wave evolution in surf zone, non-linear interactions, triad wave wave interaction, wave breaking and wave run-up in shallow water.

The NLSW equations (Garette, 1967) derived from incompressible Navier Stokes equations express mass and momentum conservation as follows:

$$\frac{\partial \eta}{\partial t} + \frac{\partial hu}{\partial x} = 0 \quad (4.8)$$

$$\underbrace{\frac{\partial u}{\partial t}}_{\text{rate of change in time}} + \underbrace{u \frac{\partial u}{\partial x}}_{\text{advection}} + \underbrace{g \frac{\partial \eta}{\partial x}}_{\text{hydrostatic pressure}} + \underbrace{\frac{1}{h} \int_{-d}^{\eta} \frac{\partial q}{\partial x} dz}_{\text{non-hydrostatic pressure}} + \underbrace{c_f \frac{u|u|}{h}}_{\text{bottom friction}} = 0 \quad (4.9)$$

Whereas  $\eta$  is surface elevation estimated from still water depth  $d$  so total depth  $h = \eta + d$ ;  $u$  is depth-averaged water velocity in horizontal coordinate  $x$  (situated at still water depth  $d$  and positive  $z$ -axis direction is upward);  $q$  is non-hydrostatic pressure term;  $c_f$  is dimensionless bottom friction parameter, depending on the Manning's roughness coefficient  $n_m$  as given by the following equation (4.10):

$$c_f = \frac{n_m^2 g}{h^{1/3}} \quad (4.10)$$

### 4.2.2.2 Use of SWAN and SWASH models

SWAN calculations were performed to obtain the spectral wave shape with the effect of wind growth at the offshore boundary conditions.

In the SWASH calculations (dd and ds cases) incoming wave height and period  $H_{m0,o} = 3$  m,  $T_{p,o} = 11$  s are used in "offshore" boundary condition in all cases of very mild slopes of 1:500 and gentler, as described in table 4.3. Meanwhile, for steeper slope (1:100) the corresponding wave parameters are 3 m and 9 s, respectively (typical of wind-caused wave condition). The "offshore" location is considered to be located at relatively deep water where its water depth considered more than 4 times the corresponding wave height, as indicated in Hofland et al. (2017). The above SWASH boundary condition has been determined in Nguyen et al. (2020) (Chapter 3) and can be summarized as follows:

- Owing to very mildly sloping beach associated with a very wide sea shelf the wind effect must be taken into consideration. Therefore, the SWAN and SWASH models have been combined to accurately calculate the wave transformation over very long distance and reliably predict wave overtopping over the dikes.

- The deep-water hydraulic boundary used in the SWAN model is 4.5 m wave height, 11 s peak period and 12 m/s wind speed applied for a return period of 10 years based on Vietnam sea condition at 180 km distance from landward boundary correspond to 70 m water depth. This seaward boundary condition is the maximum condition in figure 3-23 (Shore Protection Manual, 1984) for fully developed sea due to the very wide sea shelf.

According to the [Shore Protection Manual, Volume 1\(1984\)](#), the wind velocity can be estimated based on the Wave forecasting nomograms in Figure 3-23, with significant wave height  $H_s = 4.5$  m and wave period  $T_p = 11$  s, we can find wind speed factor  $U_A = 15$  m/s.

The relationship between the wind speed factor and wind speed at 10 m elevation:

$$U_A = 0.71U_{10}^{1.23} \quad (4.11)$$

So we can determine  $U_{10} = 12$  m/s as mentioned above.

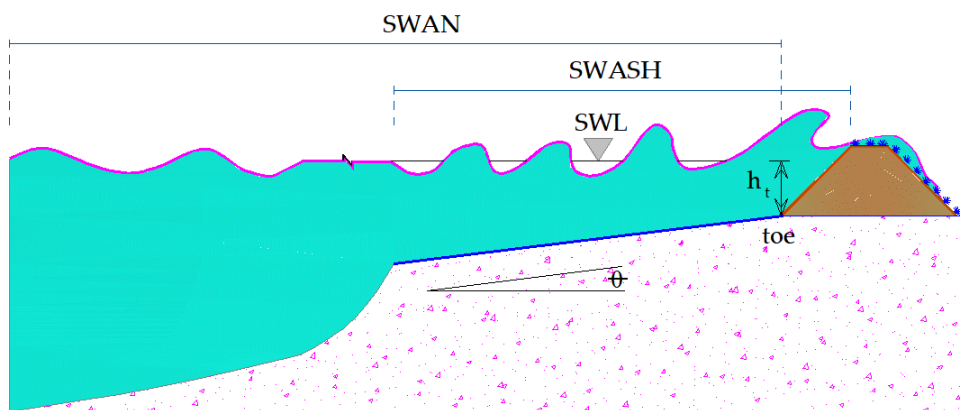


Figure 4.2: a sketch of SWAN and SWASH application.

- The SWAN-based wave parameters at relatively deep water depth were used as SWASH boundary condition at the same depth ( $h_0 = 3$  m), corresponding to  $H_{m0,o} = 3$  m,  $T_p = 11$  s as described above. The total spectrum from SWAN is used in the calculation.

A standard JONSWAP shape wave spectrum is imposed for the seaward boundary condition in the SWASH model. For the very mildly sloping foreshores, wave reflection is relatively small. The duration for a calculation of one simulation is 5 hours. The grid size is 0.5 m, time interval is 0.05 s and one vertical layer is used in cases of the shallow water since the dimensionless depth  $k_{op}h_0$  (where  $k_{op}$  is the wave number that is based on the peak wave period) is smaller than 0.5.

Initially, to determine the incoming wave parameters at the toe of the dike, the above input wave height and period have been included at the hydraulic boundary condition. In these simulations, at the landward boundary a sponge layer with a length of 1000 m is applied, which is approximately 3 to 5 times the wave length at the open boundary ([the SWASH team, 2016](#)), only used for obtaining  $T_{m-1,0}$ .

The overtopping volumes and discharge are obtained from the SWASH calculations with a setup equal to the above described model setups that were used to derive the incoming wave parameters

at the toe. Only the sponge layer is replaced with a high dike slope. The procedure for obtaining  $q$  and  $V$  is described in section 4.2.3.

#### 4.2.2.3 Test programme

The test programme is given in Table 4.3. In cases dc (indicated in the first column), the first computation has been made to replicate the physical tests of [Altomare et al. \(2016\)](#). Next, in cases dd-01 to dd-04 deep-water conditions have been simulated, that should give comparable results to the empirical calculations that were made for these deep-water configurations. Here the wave overtopping process for a foreshore slope of 1:100 with deep water at the structure toe ( $h_t/H_{m0,o} \geq 4$ ) will be estimated. Next, the same foreshore slope will be investigated with shallow water conditions at the toe ( $h_t/H_{m0,o} < 4$ ). After that this chapter will consider the wave overtopping risks for very gentle slopes at shallow water zone.

Finally, many new cases have been simulated for shallow water and very gentle configurations. The basic variables are based on the Vietnamese typical foreshore as explained in the previous section. The main variables that are varied are the slope angle of the bed (cot  $m$ ), the crest freeboard of the dike, and the distance to the toe. 8 cases of freeboards for steeper slope 1:100, 49 cases in total for very gentle slopes 1:500, 1:600, 1:700, 1:800 and 1:1000 are used in order to predict the wave overtopping risks (as table 4.3). As many dikes in Vietnam have low crest heights, a range of low crests have been simulated.

**Table 4.3.** Cases calculated in this study

| Calculation id.      | classification             | $H_{m0,o}$ [m] | $T_p$ [s] | $h_t$ [m] | distance to the toe $x$ [m] | Virtual crest freeboard $R_c$ [m] | 1: cot $m$ |
|----------------------|----------------------------|----------------|-----------|-----------|-----------------------------|-----------------------------------|------------|
| dc-1                 | Shallow water, calibration | 0.06           | 2.29      | 0.032     | 45                          | 0.06                              | 1:50       |
| dc-2                 | Shallow water, calibration | 0.21           | 1.7       | 0.025     | 45                          | 0.08                              | 1:35       |
| dd-01 ... .. dd-04   | Deep water                 | 3.5            | 9         | 14        | 600                         | 3.6, 3.8, 4, 4.3                  | 1:100      |
| ds-001 ... .. ds-004 | Shallow water              | 3.5            | 9         | 3         | 1100                        | 1, 1.5, 2, 2.5                    | 1:100      |
| ds-005 ... .. ds-009 | Shallow water              | 3              | 11        | 3         | 5000                        | 0.5, 0.8, 1, 1.3, 1.5             | 1:500      |
| ds-010 ... .. ds-014 | Shallow water              | 3              | 11        | 3         | 6000                        | 0.5, 0.8, 1, 1.3, 1.5             | 1:600      |
| ds-015 ... .. ds-019 | Shallow water              | 3              | 11        | 3         | 7000                        | 0.5, 0.8, 1, 1.3, 1.5             | 1:700      |
| ds-020 ... .. ds-024 | Shallow water              | 3              | 11        | 3         | 8000                        | 0.5, 0.8, 1, 1.3, 1.5             | 1:800      |
| ds-025 ... .. ds-029 | Shallow water              | 3              | 11        | 3         | 10000                       | 0.5, 0.8, 1, 1.3, 1.5             | 1:1000     |
| ds-030 ... .. ds-032 | Shallow water              | 3              | 11        | 3.8       | 6000                        | 1.5, 1.8, 2                       | 1:600      |
| ds-033 ... .. ds-035 | Shallow water              | 3              | 11        | 3.8       | 8000                        | 1.5, 1.8, 2                       | 1:800      |
| ds-036 ... .. ds-038 | Shallow water              | 3              | 11        | 3.8       | 10000                       | 1.5, 1.8, 2                       | 1:1000     |
| ds-039... .. ds-043  | Shallow water              | 3              | 11        | 4.5       | 6000                        | 1, 1.3, 1.5, 1.8, 2               | 1:600      |

|                      |               |   |    |     |       |                     |        |
|----------------------|---------------|---|----|-----|-------|---------------------|--------|
| ds-044 ... .. ds-048 | Shallow water | 3 | 11 | 4.5 | 8000  | 1, 1.3, 1.5, 1.8, 2 | 1:800  |
| ds-049 ... .. ds-053 | Shallow water | 3 | 11 | 4.5 | 10000 | 1, 1.3, 1.5, 1.8, 2 | 1:1000 |

### 4.2.3. Data analysis

SWASH calculations were made for all offshore boundary conditions. The water depths and bed slopes were mentioned in table 4.3 with such a high dike slope that no overtopping occurred, in order to find “virtual” overtopping discharges for different freeboard, as previously described and validated by [Nguyen et al. \(2020\)](#). Hereby the (virtual) overtopping discharge for any virtual crest level on that slope is determined through integration of the flow layer thickness and velocity at that elevation on the high slope.

Moreover, in order to quantify the amount of infragravity wave energy at the dike toe, the significant infragravity wave height at that location is estimated by integrating the energy density spectra of incoming signal (from the simulations without the dike) over the low-frequencies range as mentioned in equation (4.12):

$$H_{m0,IG} = 4 \int_{0.005}^{0.05} E(f)df \quad (4.12)$$

Furthermore, the individual wave overtopping volumes can be obtained by integrating the instantaneous wave overtopping rate per wave:

$$V_i = \int_{D_i} q_i t_i \quad (4.13)$$

The duration  $D_i$  over which the volume is determined is taken between two clear local minimums of discharge  $q$ . The discharge does not become zero between the overtopping events that are caused by primary waves, which is probably related to the presence of infragravity waves. Therefore, in this manner, the volume is estimated over a single primary wave, and not over an infragravity wave. Notably, the maximum overtopping volume is assumed as a fixed exceedance percentage  $V_{0.1\%}$  or the overtopping volume exceeded by 1 in 1000 waves:

$$V_{0.1\%} = V(P_{0.1\%}) \quad (4.14)$$

As mentioned above, the proportion of overtopping waves is one of the key factors to determine scale factor  $a$ , therefore the number of single- and double-peaked waves will be accurately considered. A characteristic sample of the instantaneous discharge rate is shown in figure 4.3. Note that the prototype values are shown. The instantaneous overtopping discharge  $q(t)$  will be eliminated if its volume is smaller than  $0.0001 \text{ m}^3/\text{m}$  in order to avoid influence from noise.



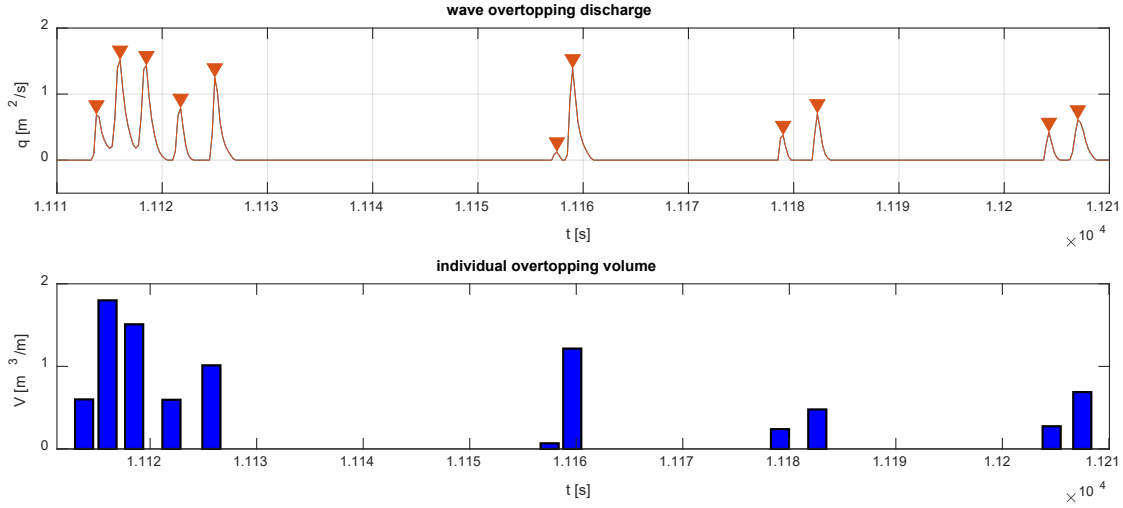


Figure 4.3: Identification of the individual overtopping volumes corresponding to the wave overtopping discharge for simulation ds-007 with  $H_{m0,o}/h_t = 1$ . Top: signal of discharge at the (virtual) crest, with peak discharge per separate overtopping wave indicated by a triangle. Bottom: corresponding integrated volume per overtopping wave.

As seen in figure 4.3, the wave corresponding to the first three peaks are considered to be part of a multiple peak (infragravity) wave. The remaining waves in the figure are single-peak. The sixth overtopping peak in this example is still accounted for in this calculation as single-peak waves because its wave overtopping volume is  $0.069 \text{ m}^3/\text{m}$ .

In addition, the two-parameter Weibull distribution in eq. (4.6) as given in previous studies is mentioned in literature review. Meanwhile, factors  $a$  and  $b$  obtained from SWASH are determined (in the following section) in order to compare the empirical formulae and validate the physical data for the steeper slopes. Finally, the maximum wave overtopping volume can be solved.

#### 4.2.4. Analysis of the $a$ - and $b$ -values from individual wave overtopping volumes

The mean overtopping discharge is the total volume of all overtopped waves ( $V_{tot}$ ), divided by the total duration that all waves take ( $N_w T_m$ ). As not all waves lead to overtopping, the overtopped volume is equal to the number of overtopping waves (the total number of waves times the probability of an overtopping  $P_{ov}$ , times the mean overtopping volume per overtopping wave  $\bar{V}$ ). This leads to the following relation:

$$q = \frac{V_{tot}}{N_w T_m} = \frac{\bar{V} N_w P_{ov}}{N_w T_m} = \frac{\bar{V} P_{ov}}{T_m} \quad (4.15)$$

The theoretical expected value of the overtopping volume is obtained from the Weibull distribution as:

$$\bar{V} = E[V]_{Weibull} = a \Gamma\left(1 + \frac{1}{b}\right) \quad (4.16)$$

in which  $\Gamma$  stands for the gamma function.

Substitution the equation (4.16) into the equation (4.15) leads to:

$$a = \frac{1}{\Gamma\left(1 + \frac{1}{b}\right)} \frac{q T_m}{P_{ov}} \quad (4.17)$$

For  $b = 0.75$  the above equation leads to:

$$a = 0.8399 \frac{qT_m}{P_{ov}} \quad (4.18)$$

The  $a$  and  $b$  values are consistent with [Van der Meer and Janssen \(1994\)](#) that are mentioned in Table 4.1.

In the remaining part of the section, a brief approach is given to determine the Weibull parameters  $a$  and  $b$  from the SWASH-based individual overtopping volumes.

The variance of the Weibull distribution is given as:

$$\sigma^2(V) = a^2 \left[ \Gamma\left(1 + \frac{2}{b}\right) - \left(\Gamma\left(1 + \frac{1}{b}\right)\right)^2 \right] \quad (4.19)$$

On the other hand, based on the individual wave overtopping volumes  $V_i$  during time series with  $N$  waves, the mean value and variance can be defined by:

$$\bar{V} = \frac{\sum_{i=0}^N V_i}{N} \quad (4.20)$$

$$\sigma^2(V) = \frac{\sum_{i=0}^N (V_i - \bar{V})^2}{N - 1} \quad (4.21)$$

According to the above equations, the shape factor  $b$  can be estimated in accordance with following iterative equation:

$$\sigma^2(V) = \left( \frac{\bar{V}}{\Gamma\left(1 + \frac{1}{b}\right)} \right)^2 \left[ \Gamma\left(1 + \frac{2}{b}\right) - \left(\Gamma\left(1 + \frac{1}{b}\right)\right)^2 \right] \quad (4.22)$$

Based on equation (4.16), the scale factor  $a$  then can be defined as:

$$a = \frac{\bar{V}}{\Gamma\left(1 + \frac{1}{b}\right)} \quad (4.23)$$

According to the equation (4.22), it is difficult to solve the gamma function if we substitute the variance and average of the volume  $\bar{V}$ , so it would be better if the shape factor  $b$  can be obtained based on iterative analysis. The iterative procedure for determining  $a$  and  $b$  is as follows:

1. The first shape factor  $b_1$  can be estimated as 1.0.

2. With this shape factor value, associated with the SWASH-based individual wave overtopping volume  $\bar{V}$ , we substitute these values into the right hand of equation (4.22), therefore, the first value of  $\sigma^2(V)$  can be determined, called  $\sigma_1^2(V)$ .

If  $\sigma_1^2(V)$  is equal to the original  $\sigma^2(V)$ , then the iterative procedure is done, the shape factor  $b_1$  is a proper value of the equation (4.22).

If  $\sigma_1^2(V)$  is different from  $\sigma^2(V)$ , then we choose another value of the shape factor, named  $b_2$ .

3. According to  $b_2$  and  $\bar{V}$ , the similar procedure is performed as the second step. This step must be iterated until the value for  $b_i$  starts to converge: the difference of 2 consecutive values is less than 1%.

4. Substitute the final shape factor  $b = b_i$  into equation (4.23), we can determine the scale factor  $a$ .

### 4.3. Results

#### 4.3.1. Validation of wave spectra for steep slopes between the experiment and numerical models

The data obtained from the physical wave flume are first used to validate the SWASH model for shallow water. Figure 4.1 illustrates cross sections of the laboratory flume used for validation. The cross-shore distance from the offshore boundary to the sea dike used for both cases is roughly 46 m. The x-directional grid size applied in the numerical model was 0.02 m. The numerical durations applied were 40 minutes and 21 minutes corresponding to the bed slope 1:35 and slope 1:50, similar to the laboratory model, which resulted in at least 1000 incoming primary waves. The corresponding output time steps were 0.05 s and 0.02 s for the slope 1:35 and slope 1:50, respectively. The Manning coefficient applied was  $0.012 \text{ sm}^{-1/3}$ . Power spectrum algorithms (Welch, 1967) have been imposed to convert a signal from time series into frequency domain.

Figure 4.4 and 4.5 show a comparison of the wave energy density spectra of the laboratory and numerical water level fluctuation (total wave signal) for several locations. There are two “offshore” positions of wave gauge 4 and 7 (corresponding to the distance  $x$  equal to 9 m and 15.6 m) for slope 1:50, of wave gauge 1 and 3 (corresponding to the distance  $x$  equal to 3.4 m and 14 m) for slope 1:35; and two “near shore” positions of gauge 8 and 10 ( $x = 45.6$  m and 46 m, respectively) for slope 1:50, of wave gauge 4 and 6 ( $x = 44.6$  m and 45 m, respectively) for slope 1:35.

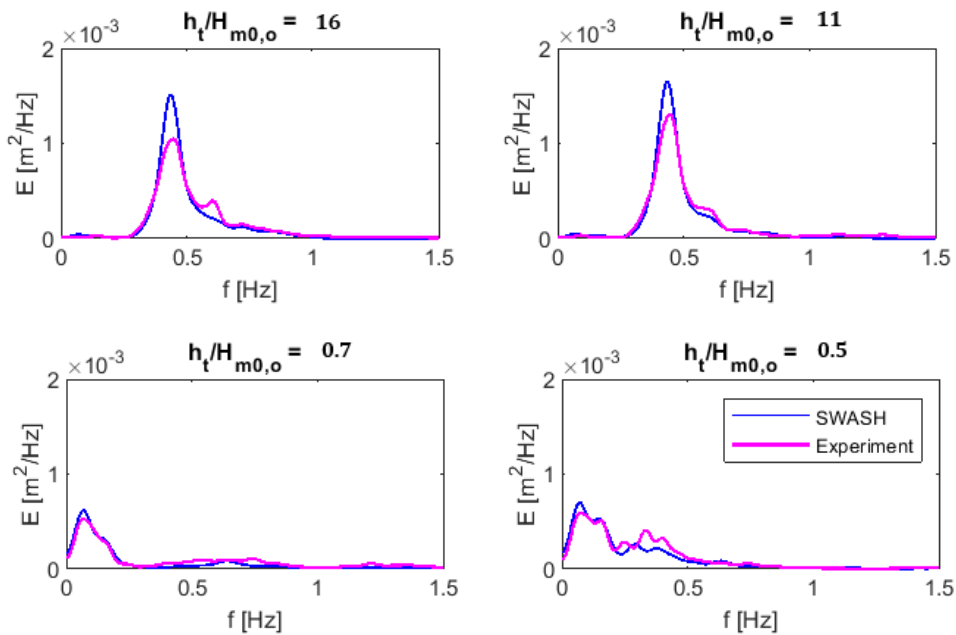


Figure 4.4: wave spectra validation between numerical and physical models for slope 1:50 (equivalent to the wave gauge of 4, 7, 8 and 10), corresponding to test dc-01.

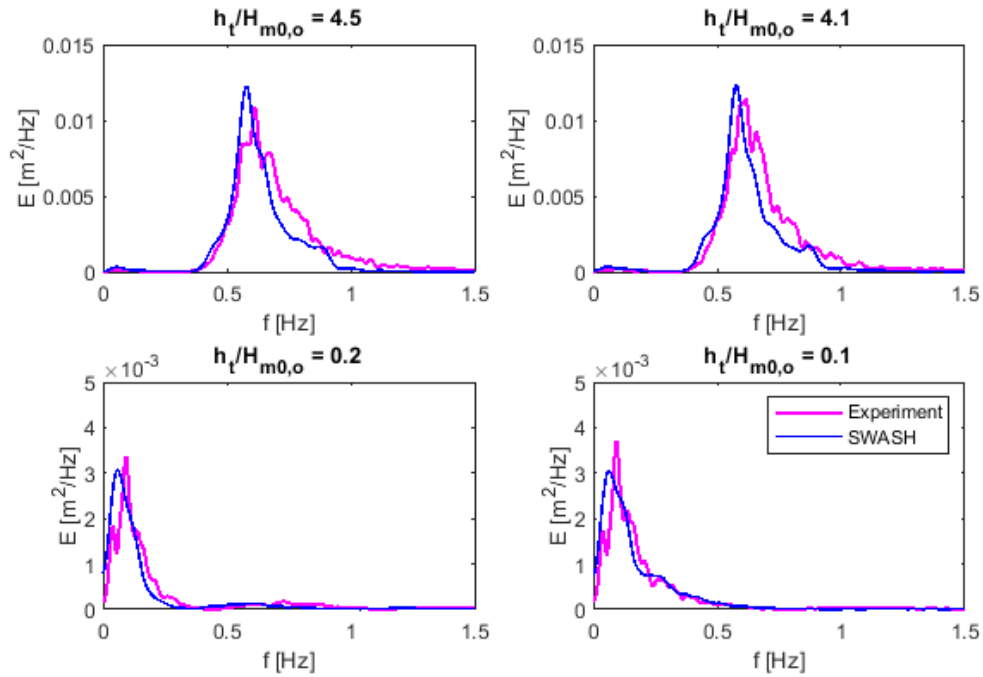


Figure 4.5: wave spectra validation between numerical and physical models for slope 1:35. Positions corresponding to locations of wave gauges 1, 3, 4 and 6 in test dc-02.

As shown in figure 4.4 the wave energy density spectra calculated are very comparable with the measured data, although in offshore the wave spectra seem to be a little bit larger for the slope 1:50. At wave gauge 1 and 3 in figure 4.5, the energy density spectra in the simulated model seems to be slightly overestimated in comparison to measured data in the laboratory. In shallow water (wave gauge 8 and 10 for the slope 1:50 and wave gauge 4 and 6 for the slope 1:35) the infragravity waves are dominant compared with high-frequency waves due to wave-wave interaction and breaking. The wave spectral shape is flattened at that water region, which has been confirmed in previous studies (Altomare et al., 2016, Suzuki et al., 2017).

In addition, figure 4.6 below shows the cumulative wave overtopping volume and the overtopping layer thickness and velocity from which it is derived, for the slope 1:35. The cumulative wave overtopping volume is originated from integration of wave overtopping discharge  $q(t) = v(t) \cdot d(t)$  from the SWASH model.

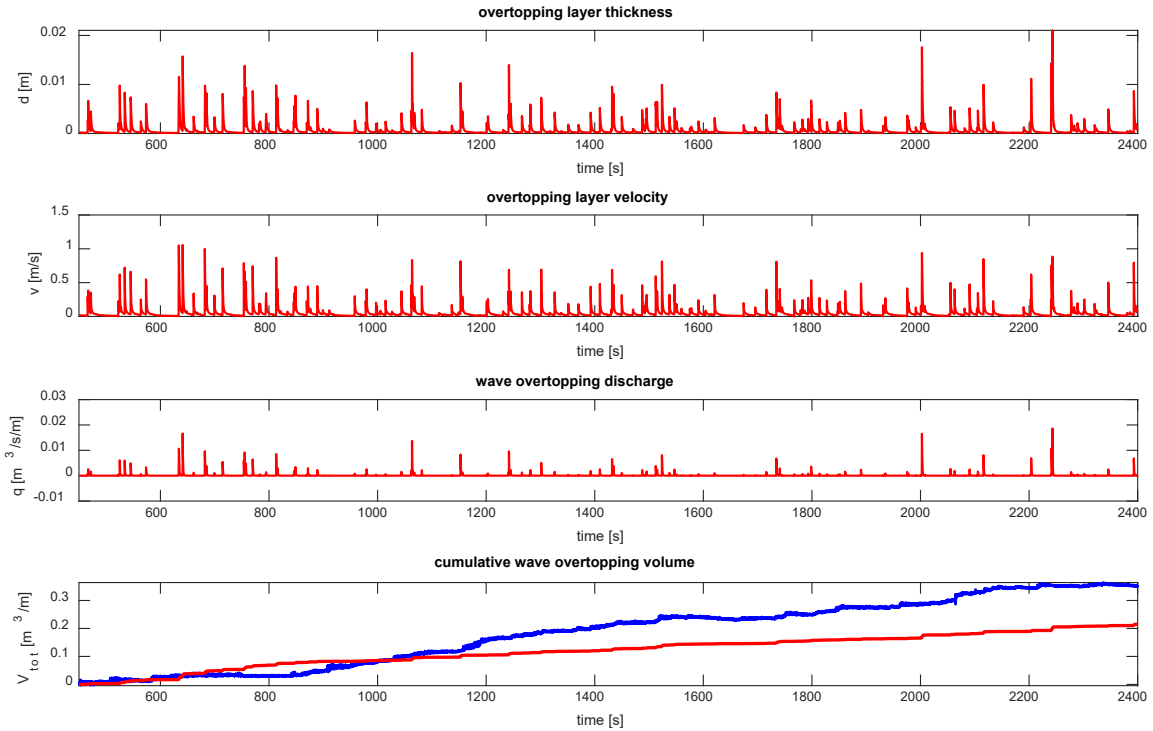


Figure 4.6: simulated overtopping layer thickness, velocity, wave overtopping rate and cumulative overtopping volume (red line) associated with measured cumulative overtopping volume (blue line) for the slope 1:35

In spite of showing a quite closely match in energy density spectra for slope 1:35, figure 4.6 demonstrates the difference between computed cumulative wave overtopping (red line) and measured value (blue line). The observed cumulative overtopping volume reaches nearly double the value from the model as mentioned in a bottom figure. This is in line with the somewhat larger offshore wave height in the simulations, and could partly be due to the natural variability of the overtopping discharge (the calculated mean overtopping discharge over the first one-third of the plot does follow the measured value).

### 4.3.2. Normally gentle foreshore slope 1:100

#### 4.3.2.1 In deep water

Next the computed overtopping for deep water conditions is compared to literature, cases dd-01 through dd-04. As mentioned above, the wave overtopping parameters are calculated for a foreshore slope of 1:100 with deep water at the toe of the dike with a depth of  $h_t = 14$  m and a mild sea-dike slope (1:3). At the offshore hydraulic boundary, the wave height and period imposed are  $H_{m0,o} = 3.5$  m,  $T_p = 9$  s; four (virtual) freeboards  $R_C$  are considered, whose dimensionless values are  $0.99 < R_C/H_{m0} < 3.16$ .

The mean squared method is used to compare the numerical SWASH results with the existing formulae in terms of wave overtopping.

In particular, the root mean square error ( $RMSE = \sqrt{\frac{\sum_1^N (Predicted_i - Actual_i)^2}{N}}$ ),

relative bias ( $RE = \frac{\sum_1^N (Predicted_i - Actual_i)}{\sum_1^N Actual_i} \cdot 100\%$ )

and correlation coefficient ( $R^2 = \frac{\sum[(x-x_m)(y-y_m)]}{\sqrt{[\sum(x-x_m)^2 \sum(y-y_m)^2]}}$ ) are evaluated,

whereas  $x_m$ ,  $y_m$  are mean of data set  $x$  and  $y$ , respectively. “Predicted” and “Actual” terms indicate the SWASH value and the literature value, respectively.

Scale factor  $a$  and shape factor  $b$  calculated from the numerical model are compared with the values from previous studies. The calculated results of Weibull parameters are shown in figure 4.7.

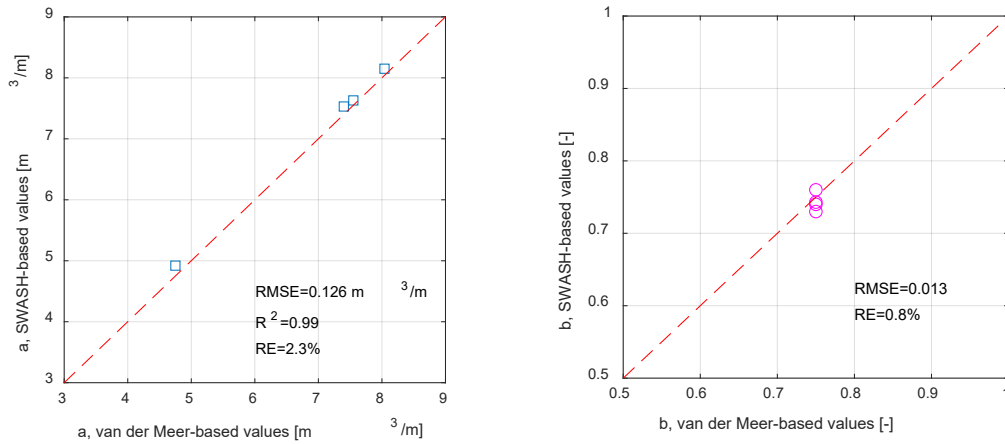


Figure 4.7: comparison of  $a$  (left figure) and  $b$  (right figure) from SWASH and Van der Meer et al. (2010).

According to figure 4.7, small values of RMSE and CE associated with strong correlation coefficient  $R^2$  show a good correspondence between the simulated results and Van der Meer’s research in deep water. The good correspondence of scale factor  $a$  means that the mean overtopping discharge corresponds well too.

#### 4.3.2.2 In shallow water

Several cases (ds-001 to ds-004) with a foreshore slope 1:100, but with a shallow foreshore are investigated in this section. Lower freeboards are applied as the wave height at the toe is lower due to depth-induced breaking. According to 4 different crest freeboards for the slope 1:100, wave spectra at some locations are shown in figure 4.8. The variation of wave height and period is investigated in figure 4.9.

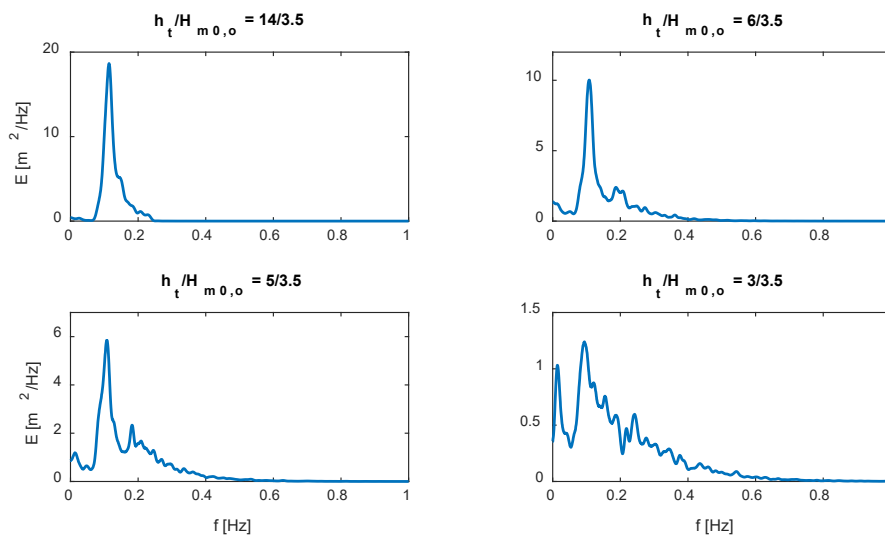


Figure 4.8: wave spectra estimated for a slope 1:100 at some locations for case ds-001

It should be noted that short waves start to break at distance 300 m from the toe, shown in the upper right of figure 4.8 also, but the height of the infragravity waves seems to stay more or less constant in this nearshore area with shallow water (the upper figure). At the same time, the lower graph in figure 4.9 indicates a constant rise of wave spectral wave period  $T_{m-1,0}$  especially after breaking, from 9 s in offshore to 13.6 s at the toe of structure ( $h_t/H_{m0,0} = 0.857$ ).

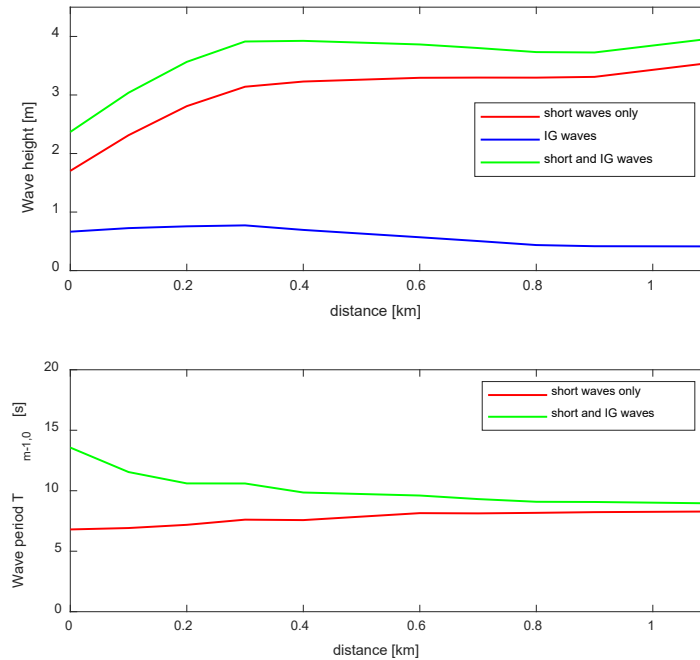


Figure 4.9: the evolution of wave height (upper figure) and period (lower figure) for case ds-001, where '0' indicates dike toe

Apart from this, several overtopping-related parameters for the foreshore slope of 1:100 (ds-001 – ds-004) are compared to existing empirical relations in table 4.4. Here the  $P_{ov}$  formula is estimated from Van der Meer et al., 2010 and overtopping rate  $q$  based on Van Gent of EurOtop, 2018.

Table 4.4. Parameters for the slope 1:100

| $R_c$<br>[m] | $T_{m-1,0,t}$<br>[s] | $P_{ov}$ [-]<br>Van der Meer, 2010 | $P_{ov}$ [-]<br>SWASH | $q$ [m <sup>3</sup> /s/m]<br>EurOtop, 2018 | $q$ [m <sup>3</sup> /s/m]<br>SWASH |
|--------------|----------------------|------------------------------------|-----------------------|--|------------------------------------|
| 1            | 13.57                | 0.93                               | 0.93                  | 0.363                                      | 0.344                              |
| 1.5          | 13.57                | 0.89                               | 0.90                  | 0.185                                      | 0.197                              |
| 2            | 13.57                | 0.75                               | 0.76                  | 0.072                                      | 0.076                              |
| 2.5          | 13.57                | 0.61                               | 0.59                  | 0.041                                      | 0.045                              |

According to the result in table 4.4, the percentage of wave overtopping and overtopping rate show a satisfactory fit between the existing formulae and the SWASH model. It can be concluded that the SWASH model was set up to correctly calculate overtopping for shallow foreshores.

### 4.3.3. Very gentle slopes in shallow water

#### 4.3.3.1 Wave parameters at the toe

As mentioned in section 2.3, the same wave parameters  $H_{m0} = 3m$  and  $T_p = 11s$  are imposed at the deep-water boundary for the computations with very gentle foreshores. At the toe of the structure, the wave height decreases compared with the offshore value. The wave height for more gentle slopes decreases more because the waves travel for a longer distance over the shallow

foreshore (see table 4.5). Conversely, the spectral energy wave period increases. Low-frequency energy is created in the shallow water due to triad wave-wave interaction, as confirmed by previous studies (Altomare et al., 2016; Hofland et al., 2017; Suzuki et al., 2017). Note that the incoming wave conditions at the toe are reported.

**Table 4.5.** Some relevant parameters at the toe in shallow water

| 1:cot m | $h_t$ [m] | $H_{m0,t}$ [m] | $\frac{R_c}{H_{m0,t}}$ [-]   | $\frac{T_{m-1,0,o}}{T_{m-1,0,t}}$ [-] | $N_w$ at toe [-] |
|---------|-----------|----------------|------------------------------|---------------------------------------|------------------|
| 1:500   | 3         | 1.90           | 0.26, 0.42, 0.53, 0.68, 0.79 | 1.59                                  | 1722             |
| 1:600   | 3         | 1.67           | 0.30, 0.48, 0.60, 0.78, 0.90 | 1.53                                  | 1808             |
| 1:700   | 3         | 1.58           | 0.32, 0.51, 0.63, 0.82, 0.95 | 1.52                                  | 1763             |
| 1:800   | 3         | 1.54           | 0.32, 0.52, 0.65, 0.84, 0.97 | 1.60                                  | 1736             |
| 1:1000  | 3         | 1.40           | 0.36, 0.57, 0.71, 0.93, 1.07 | 1.65                                  | 1700             |
| 1:600   | 3.8       | 2.54           | 0.59, 0.71, 0.79             | 1.30                                  | 1930             |
| 1:800   | 3.8       | 2.10           | 0.71, 0.86, 0.95             | 1.30                                  | 1854             |
| 1:1000  | 3.8       | 1.96           | 0.77, 0.92, 1.02             | 1.37                                  | 1798             |
| 1:600   | 4.5       | 2.95           | 0.34, 0.44, 0.51, 0.61, 0.68 | 1.23                                  | 1920             |
| 1:800   | 4.5       | 2.60           | 0.38, 0.50, 0.58, 0.69, 0.77 | 1.25                                  | 1870             |
| 1:1000  | 4.5       | 2.11           | 0.47, 0.62, 0.71, 0.85, 0.95 | 1.18                                  | 1685             |

#### 4.3.3.2 Wave overtopping parameters

Next, we present one typical case with a foreshore slope 1:600 and a crest freeboard of  $R_c = 1.5$  m, corresponding to the case ds-014. In this case the number of the multiple-peaked waves is 30 with over total 1097 overtopping waves, occupying only 2.7% of all  $N_w$  waves. The number of multiple-peaked waves even reach roughly 6.2 % for low crest freeboard ( $R_c = 0.5$  m) for slope 1:500. Similarly, in other very gentle slopes the percentage of multiple peak waves at the lowest crest freeboard can only occupy up to 6.5%. These percentages are relatively small compared with the total number of overtopping waves.

Figure 4.10 shows the time series of overtopping layer thickness, velocity and discharge for the case with a foreshore slope of 1:600. Calculations of wave overtopping for many simulations indicated that time-varying overtopping layer thickness and velocity have a resemblance to saw-tooth shapes. From the beginning these values increase from zero to maximum in very short time, then continuously decline from maximum in a relatively longer time than the initial increase period. It is noticeable that there are multiple peak waves encountering over the water layer thickness.



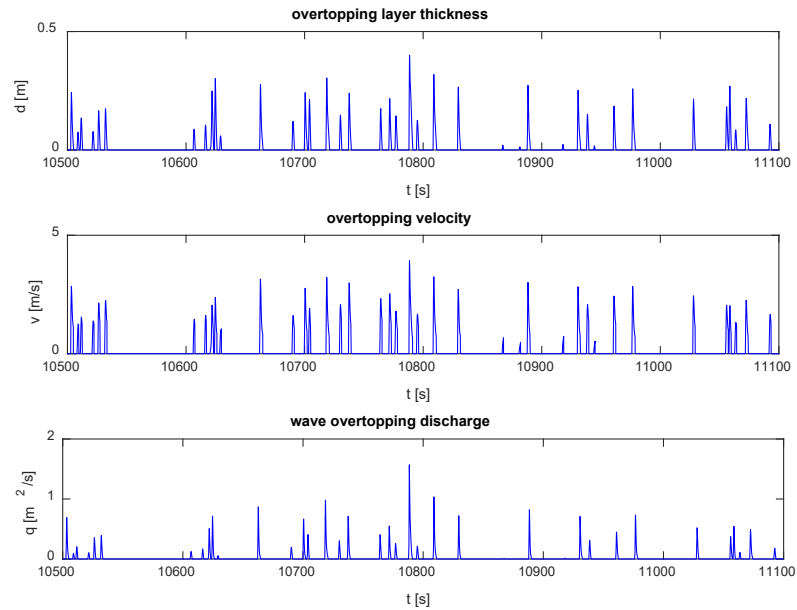


Figure 4.10: Water layer thickness, velocity and wave overtopping discharge against certain time series for slope 1:600 and  $R_C = 1.5\text{m}$  (ds-014).

A time history of the individual wave volumes is illustrated on a bar graph as figure 4.11 for the full simulation duration. Six of the overtopping wave volumes can reach as high as roughly  $30\text{ m}^3/\text{m}$  but almost water volumes have not exceeded  $3.5\text{ m}^3$ . In this particular simulation 1097 waves overtop from the 1808 incoming waves during the 5-hr duration of the storm duration, having a probability of wave overtopping  $P_{ov} = 0.60$ . The overtopping rate is  $q = 54\text{ l/s/m}$ . Individual overtopping duration ranges from 1 to 3 sec.

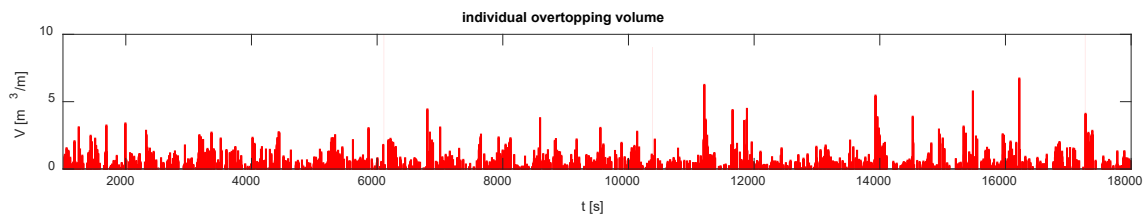


Figure 4.11: wave by wave overtopping volumes for a simulation of slope 1:600 and  $R_C = 1.5\text{m}$  (ds-014).

The rank-ordered distribution of individual overtopping volume against number of overtopped waves for this simulation is given in figure 4.12.

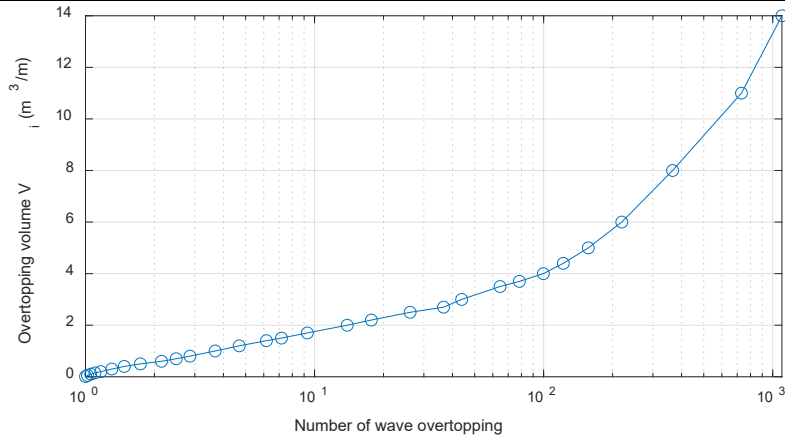


Figure 4.12: number of overtopped waves for slope 1:600 and  $R_C = 1.5\text{m}$  (ds-014).

Figure 4.13 compares some previous research versus Weibull distribution against probability of exceedance for simulation ds-014. For relatively small exceedance probabilities (small volumes) the difference between studies seems not be significant, but for the lower exceedance probabilities (large volumes), there is some difference in the wave overtopping volume.

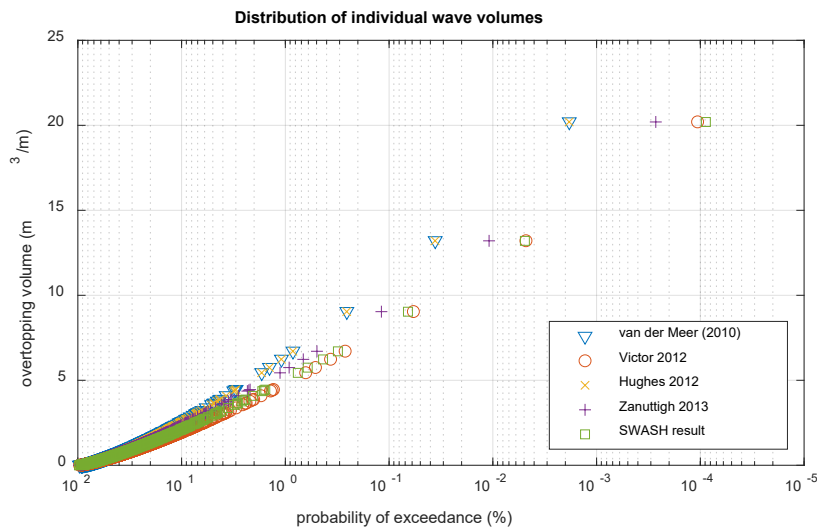


Figure 4.13: comparison of empirical and numerical estimate of individual overtopping volume against exceedance probability for slope 1:600 and freeboard 1.5 m (ds-014).

The Weibull distribution can be determined based on two Weibull parameters  $a$  and  $b$  as empirical equation (4.12). The shape factor  $b$  was estimated according to a specified individual wave overtopping volume  $V_i$  in accordance with the iterative equation (4.15). After that we can define the scale factor  $a$  through the equation (4.16) based on the mathematical Gamma function.

The SWASH results resemble those of Victor most, while the other distributions somewhat overestimate the larger overtopping volumes. The linear trend of the highest volumes in their study clearly deviates from the theoretical Weibull distribution.

#### 4.3.3.3 Weibull parameters for very gentle slopes in shallow water

First of all, the comparison between the shape factor  $b$  and previous studies is given in figure 4.14. It can be clearly seen that the SWASH results for  $b$  appear to exhibit a large scatter compared to other authors' values, from about 0.7 to roughly 1.8 whereas this factor from Van der Meer et al., 2010 is purely 0.75 and Victor, 2012 also shows underestimated values, ranging from 0.7 to nearly 1.2. It can be explained that all previous researchers assigned the shape factor based on an investigation of sea defenses in relatively deep water. Therefore, in section 4.3.4 we will introduce a new equation of

the shape factor for very gentle and shallow foreshores. As mentioned in the literature review, according to the equation (4.16), when the factor  $b$  and wave overtopping rate  $q$  are given, the scale factor  $a$  can easily be determined.

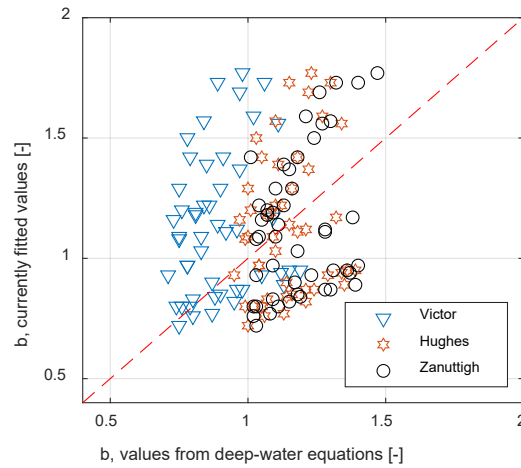


Figure 4.14: comparison of shape factor  $b$  between the SWASH and previous studies.

Following, we investigate the proportion of overtopping waves in the SWASH model and previous existing equations (according to [Van der Meer et al., 2010](#) and [Victor, 2012](#)) in Figure 4.15. Regarding percentage of overtopping waves, the gentle foreshore values are totally underestimated comparing these data and the empirical formula from [Victor, 2012](#). Particularly, for the higher crest freeboards there is more deviation between them. However, the  $P_{ov}$  originated from [Van der Meer et al., 2010](#) shows a good agreement with the numerical model results, especially for higher crest freeboards. Apparently, the empirical equation based on [Van der Meer et al., 2010](#) fits well the values from the SWASH model regarding the proportion of overtopping waves for very gentle slopes.

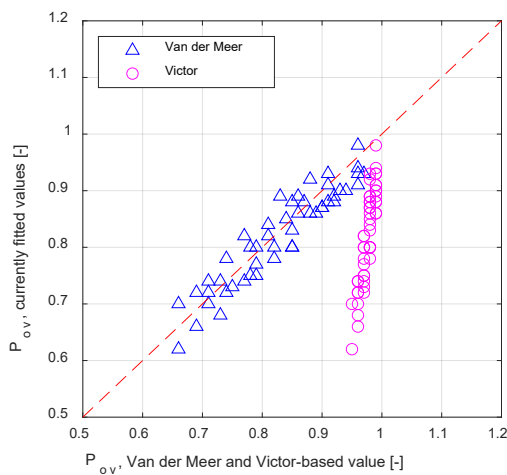


Figure 4.15: comparison of percentage of overtopping waves from SWASH and literature

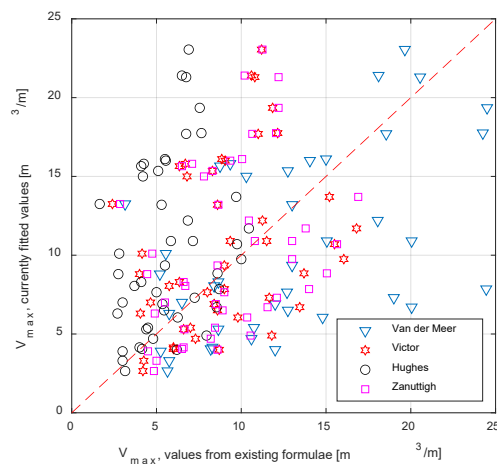


Figure 4.16: comparison of maximum overtopping wave volumes from SWASH and literature

Alternatively, the maximum overtopping volumes are compared in figure 4.16. The overtopping volumes of [Hughes et al., 2012](#) and [Zanuttigh et al., 2013](#) seem to mostly underestimate the results from the SWASH model, especially for lower freeboards (larger values of  $V_{max}$ ). A similar trend also occurs in case of Victor's empirical formula. In contrast to the equation of [Van der Meer et al., 2010](#), for which almost all values overestimate the data from the SWASH even for lower relative freeboards

but the trend seems better. Obviously, a big gap between the numerical model and literature studies in term of proportion of overtopping waves proves an inappropriate application for the present case with very gentle slopes in shallow water.

A reason could be that the presence of double-peak waves in numerical model might cause the lower percentage of overtopping waves. Furthermore, the influence of very gentle bed slopes in shallow water may be one of the main reason for this deviation between numerical model and the existing studies. More importantly, the previous researchers investigated just focus on the sea defense structures in the relatively deep water.

#### 4.3.3.4 The impact of relative crest freeboard, foreshore slope and relative spectral wave period on the shape factor $b$

Firstly, the influence of the dimensionless crest freeboard on the scale and shape parameters for very gentle and shallow foreshores with Weibull-distributed wave heights is investigated in figure 4.17 and figure 4.18.

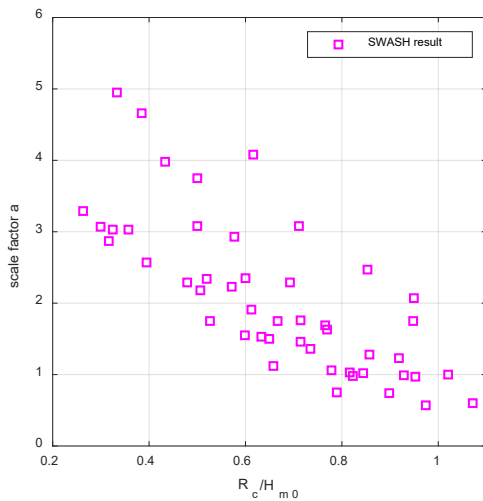


Figure 4.17: influence of relative freeboard on the scale factor  $a$

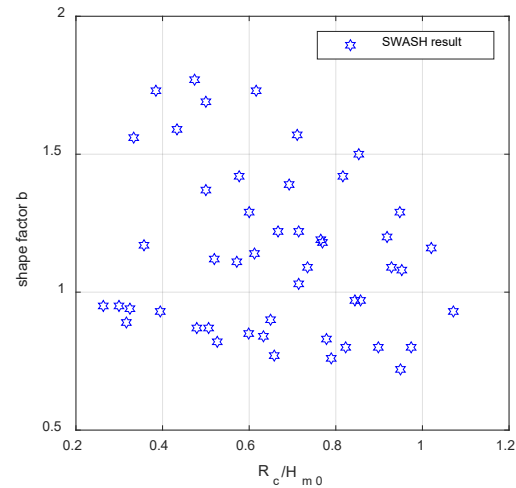


Figure 4.18: influence of relative freeboard on the shape factor  $b$

Generally, the scale factor  $a$  appears to gradually increase with the decreasing relative freeboards  $\frac{R_c}{H_{m0}}$  while the trend of the same relation in the shape factor is not clear at all. In figure 4.17, the data approximately conform to a negative trend line for values of the dimensionless crest free boards. It can be clearly seen that this factor is inversely proportion to the relative crest freeboard.

In addition, the impact of foreshore slope and relative spectral wave period on the shape factor  $b$  is also observed in figure 4.19 and 4.20.

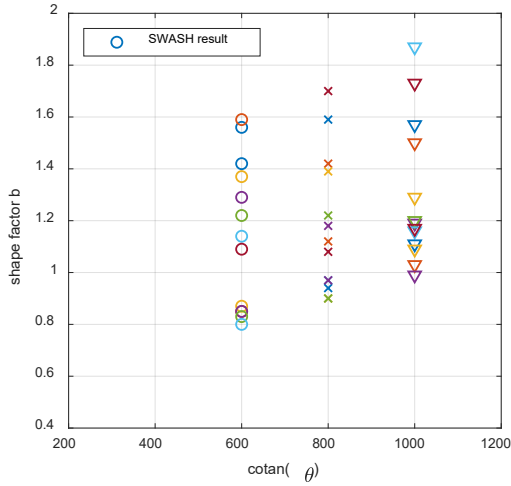


Figure 4.19: influence of cotangent of the foreshore slope  $\cot(\theta)$  on the shape factor

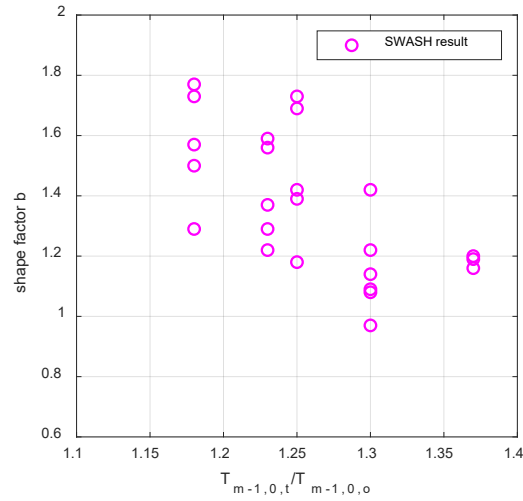


Figure 4.20: influence of the relative spectral wave period  $T_{m-1,0,t}/T_{m-1,0,o}$  on the shape factor

Interestingly, based on the graphs, it appears that the dependency of the shape factor on the cotangent of the foreshore slope in general conforms to a linear trend line, increasing for increasing of  $\cot(\theta)$ . In contrast to that relation, figure 4.20 indicates the downward linear trend of the shape factor for increasing the relative spectral wave period  $T_{m-1,0,t}/T_{m-1,0,o}$ .

To summarize, the shape factor  $b$  of the two-parameter Weibull distribution of the individual wave overtopping volumes for very gentle and shallow foreshores appears to not only be a function of the relative crest freeboard, as described by previous authors, but also to be proportional to the cotangent of the foreshore slope and inversely proportion to the relative spectral wave period  $T_{m-1,0,t}/T_{m-1,0,o}$ . Notably, the influence of the infragravity waves at the toe of the sea defense structures with these gentle foreshore slopes leads to increased spectral wave periods at the toe, which can reach 2 times those in the offshore area (Nguyen et al., 2020).

#### 4.3.4. A new equation of the shape parameter $b$ for very gentle and shallow foreshores.

In the previous studies, the shape factor  $b$  has been formulated for deep and flat foreshores. It means the effects of foreshore slope and the variation of spectral wave period at the toe have not been taken into account. Therefore, to create a new equation of shape factor for very gentle and shallow foreshores, the foreshore slope and relative spectra wave period  $T_{m-1,0,t}/T_{m-1,0,o}$  are included.

A predicted equation of shape factor, depending on dimensionless freeboard  $R_c/H_{m0}$ , foreshore slope  $\cot(\theta)$  and the ratio  $T_{m-1,0,t}/T_{m-1,0,o}$ , can be described as below:

$$b = x_0 \left( \frac{R_c}{H_{m0,t}} \right)^\alpha [\cot(\theta)]^\beta \left( \frac{T_{m-1,0,t}}{T_{m-1,0,o}} \right)^\gamma \quad (4.24)$$

We take the logarithm of both sides of the above function, and we obtain:

$$\ln(b) = \alpha \ln \left( \frac{R_c}{H_{m0}} \right) + \beta \ln(\cot(\theta)) + \gamma \ln \left( \frac{T_{m-1,0,t}}{T_{m-1,0,o}} \right) \quad (4.25)$$

Based on the sequences of  $b$ ,  $R_c$ ,  $H_{m0}$ ,  $\theta$  and  $T_{m-1,0}$  estimated from the SWASH model, we carry out regression analysis in order to find out  $\alpha, \beta, \gamma$  using the Method of Least Squares (Aldrich, 1998).

Letting  $\ln(b) = B$ ,

$$\ln(R_c/H_{m0}) = X_1, \quad (4.26)$$

$$\ln[\cot(\theta)] = X_2,$$

$$\ln(T_{m-1,0,t}/T_{m-1,0,o}) = X_3,$$

we could have the relation between  $B$  and  $X_1, X_2, X_3$  as below:

$$B = a_o + \alpha X_1 + \beta X_2 + \gamma X_3 \quad (4.27)$$

The random error between a set of data  $B_i$  and  $B_i^{sw}$  originated from SWASH is:

$$\varepsilon_i = B_i - B_i^{sw} \quad (4.28)$$

We define the associated error as:

$$S = \sum_{i=1}^m \varepsilon_i^2 = \sum_{i=1}^m (B_i - B_i^{sw})^2 \quad (4.29)$$

The goal is to find values of  $\alpha, \beta, \gamma$  and  $a_o$  that minimize the error  $S$ . In multivariable calculus we know that this requires us to find the above values such that:

$$\frac{\partial S}{\partial a_o} = 0; \quad \frac{\partial S}{\partial \alpha} = 0; \quad \frac{\partial S}{\partial \beta} = 0; \quad \frac{\partial S}{\partial \gamma} = 0 \quad (4.30)$$

We have obtained that the values of  $\alpha, \beta, \gamma$  and  $a_o$  which minimize the error satisfy a following matrix problem:

$$\begin{pmatrix} \sum_{i=1}^m B_i \\ \sum_{i=1}^m B_i X_{1i} \\ \sum_{i=1}^m B_i X_{2i} \\ \sum_{i=1}^m B_i X_{3i} \end{pmatrix} = \begin{pmatrix} a_o \\ \alpha \\ \beta \\ \gamma \end{pmatrix} \begin{pmatrix} m & \sum_{i=1}^m X_{1i} & \sum_{i=1}^m X_{2i} & \sum_{i=1}^m X_{3i} \\ \sum_{i=1}^m X_{1i} & \sum_{i=1}^m X_{1i}^2 & \sum_{i=1}^m X_{1i} X_{2i} & \sum_{i=1}^m X_{1i} X_{3i} \\ \sum_{i=1}^m X_{2i} & \sum_{i=1}^m X_{2i} X_{1i} & \sum_{i=1}^m X_{2i}^2 & \sum_{i=1}^m X_{2i} X_{3i} \\ \sum_{i=1}^m X_{3i} & \sum_{i=1}^m X_{3i} X_{1i} & \sum_{i=1}^m X_{3i} X_{2i} & \sum_{i=1}^m X_{3i}^2 \end{pmatrix} \quad (4.31)$$

Then numerical techniques for linear algebra with 4 variables yield that the best fit is obtained with  $a_o = -2.495$ ,  $\alpha = -0.22$ ,  $\beta = 0.46$  and  $\gamma = -1.64$ . We find the equation of the shape factor, in the range of  $R_c/H_{m0,t}$  from 0.26 to 1.07 and  $T_{m-1,0,t}/T_{m-1,0,o}$  from 1.18 to 1.59, as below:

$$b = \frac{1}{12.117} \left( \frac{R_c}{H_{m0,t}} \right)^{-0.22} [\cot(\theta)]^{0.46} \left( \frac{T_{m-1,0,t}}{T_{m-1,0,o}} \right)^{-1.64} \quad (4.32)$$

#### 4.3.5. A new equation of the wave overtopping discharge for very gentle bed foreshores

The new average wave overtopping discharge  $q$  for very gentle and shallow bed foreshores is formulated later on. Initially, the relation between the dimensionless mean overtopping rate versus the relative crest freeboard for all 49 cases is investigated in figure 4.21. As seen, the higher values of relative crest freeboard  $R_c/H_{m0}$  lead to lower values of dimensionless average discharge  $q/\sqrt{gH_{m0}^3}$ .

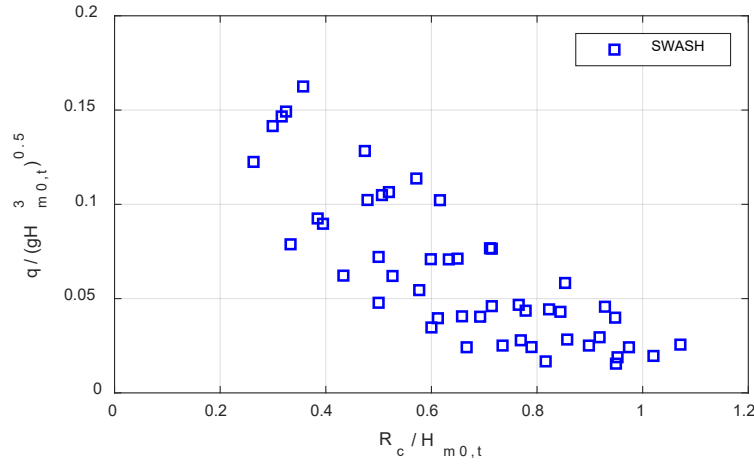


Figure 4.21: Dimensionless average overtopping discharge versus crest freeboard

Based on the previous studies, the dimensionless average wave overtopping discharge relies mainly on the wave height and period at the toe ( $H_{m0,t}, T_{m-1,0}$ ) and the exponential of the relative freeboard  $R_c/H_{m0,t}$  and  $1/\xi_{m-1,0}$ . Due to the fact that the wave height has decreased due to wave breaking, and the wave period has increased the surf-similarity parameter  $\xi_{m-1,0}$  becomes rather large and waves will be surging. Hence the influence of the dike slope is expected to be limited. Therefore the influence of dike slope is omitted, and  $\xi_{m-1,0}$  effectively becomes wave steepness  $S_{m-1,0}$ .

Therefore, the shape of wave overtopping discharge  $q$  can be predicted as:

$$\frac{q}{\sqrt{gH_{m0,t}^3}} = A \cdot T_{m-1,0}^\alpha H_{m0,t}^\beta \exp\left(\gamma \frac{T_{m-1,0} R_c}{H_{m0,t}^{3/2}}\right) \quad (4.33)$$

Taking the logarithm both sides of the above function, and we can obtain:

$$\ln\left(\frac{q}{\sqrt{gH_{m0,t}^3}}\right) = \ln(A) + \alpha \ln T_{m-1,0} + \beta \ln H_{m0,t} + \gamma \frac{T_{m-1,0} \cdot R_c}{H_{m0,t}^{3/2}} \quad (4.34)$$

Based on the sets of values of  $q, R_c, H_{m0}$  and  $T_{m-1,0}$  as obtained from the SWASH model, the regression analysis is also performed according to Least Squares fitting, similar to the previous section.

Finally, a new predicted equation of the average wave overtopping discharge, in the range of  $R_c/H_{m0,t}$  from 0.26 to 1.07 and  $T_{m-1,0,t}/T_{m-1,0,o}$  from 1.18 to 1.59, can be gained as below:

$$\frac{q}{\sqrt{gH_{m0,t}^3}} = 13.329 T_{m-1,0}^{-1.131} H_{m0,t}^{-2.964} \exp\left(-0.247 \frac{T_{m-1,0} R_c}{H_{m0,t}^{3/2}}\right) \quad (4.35)$$

A comparison of the new equation to numerical model results is illustrated in figure 4.22. It can be seen clearly the figure confirms a good agreement for the SWASH model. However, the higher values of mean overtopping rate  $q > 0.15 \text{ m}^3/\text{s}/\text{m}$  show a little bit more deviation with numerical values.

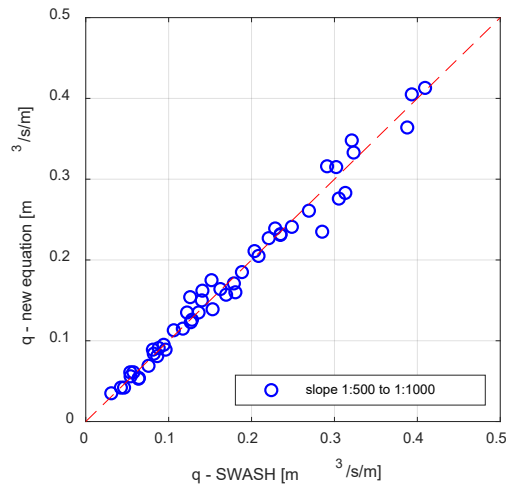


Figure 4.22: Comparison of the average discharge between the SWASH model and the new formula.

#### 4.3.6. The scale parameter and wave overtopping volume for very gentle bed foreshores

As mentioned in previous section, when the shape factor  $b$  and the average discharge  $q$  are determined then the scale factor can be completely solved according the equation (4.10) through Gamma function ( $a = \frac{1}{\Gamma(1+\frac{1}{b})} \frac{qT_m}{P_{ov}}$ ). The scale parameter  $a$  estimated is compared with that in the numerical data in figure 4.23. As seen, the comparison of this factor between the SWASH model and the new equation shows quite well agreement.

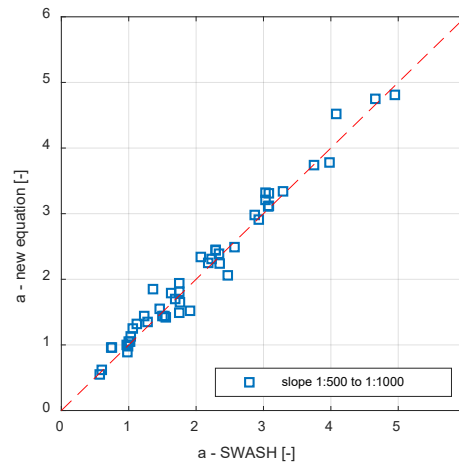


Figure 4.23: Comparison of the scale factor between the SWASH model and the new formula.

Eventually, the expected maximum individual wave volume in the Weibull distribution in a certain number of overtopped waves can be determined based on the equation (4.23) through the exceedance distribution.

## 4.4. Discussion

### 4.4.1. Accuracy of SWASH in wave overtopping

SWASH has been validated for its use to simulate wave overtopping in deep water and shallow water regions. Since an aim of this chapter is to validate the numerical SWASH model with laboratory data and literature studies, the boundary conditions and parameters are set similar for all the simulated cases. Previous authors (Lashley et al., 2020a; Suzuki et al., 2017; Gruwez et al., 2020)



also confirmed that this numerical simulation demonstrated promising results for wave overtopping in steep and mild sloping foreshores.

SWASH calculations have been made of shallow foreshores with  $h_t/H_{m0,o} = 1$  to 1.5 and bed slopes ranging from relatively steep (1:35) to very gentle (1:1000), corresponding to 55 test cases. Regarding the validation between the laboratory experiments and predicted model, the slope 1:50 shows more accuracy than the calculations in the slope 1:35 in relation to the wave spectra. On the other hand, for the slope 1:50 the wave overtopping rate in the laboratory reaches only more than a half compared with that in the SWASH model, approximately 0.1 l/s/m at 1/25 scale or less than 1 l/s/m in prototype when translating by Froude number similarity. Causes can be statistical scatter or the representation of roughness and friction in the developing boundary layer of the overtopping flows. However, this is a typical error in terms of overtopping discharge. As can be seen in TAW (2003), the standard deviation of the scatter around the empirical overtopping equation at  $q = 1$  l/s/m also roughly corresponds to a factor of 2. It is also stated in the findings of Suzuki et al., 2017 and Lashley et al., 2020 that the error in  $q$  depends on the magnitude of the overtopping discharge. They indicated that SWASH more accurately predicted the higher wave overtopping discharge that were larger than 1 l/s/m in prototype scale. More importantly, it is seen that SWASH effectively works for shallow foreshores in terms of wave transformation from offshore to toe and wave overtopping rate over the sea dikes with foreshores from steep to mild slopes.

The simulation results of wave spectra on steep slopes (1:35 and 1:50) are consistent with those in the physical model. Figure 4.4 and figure 4.5 confirm that the shallow foreshore flattens the wave spectra shape and shifts energy of wave spectra shifted from high frequencies at offshore water to low-frequencies due to wave breaking and triad wave-wave interaction. It also confirms that the SWASH model captures the wave transformation from offshore to the toe of the sea-dike well since wave properties ( $H_{m0}, T_{m-1,0}$ ) at the dike toe are key factors to determine wave overtopping. For more gentle slopes no data exist to validate the model, as these slopes do not fit in laboratory flumes which have a limited length.

#### 4.4.2. New equations of the shape parameter and the average overtopping discharge for sea dikes with shallow and very gentle foreshores

The SWASH model has been set up to calculate the wave overtopping process against four main scenarios, including steep foreshores and very gentle foreshores, from deep water to shallow water. The deep water and less steep cases were used to compare the present SWASH setup with previous studies. In deep water for steeper bed slopes both two Weibull parameters seem to be fit well with Van der Meer et al., 2010. For these kind of slopes in shallow water, it can be clearly seen that the SWASH model effectively works with existing formulae in terms of the percentage of wave overtopping and the overtopping rate. In shallow water, for very gentle slopes (gentler than 1:500) the two Weibull parameters are no longer consistent with literature studies. It makes sense since the previous researchers mainly focused on deep water with flat foreshores. Interestingly, the percentage of wave overtopping established by Van der Meer et al., 2010 seems to quite closely match for very gently sloping foreshores. So apparently the Rayleigh distribution for run-up levels still holds.

Importantly, the scale factor  $a$  is considered as a function of the average overtopping discharge, mean wave period and probability of overtopping. As a result, when the mean overtopping rate  $q$  and the shape factor  $b$  are defined, then the scale factor  $a$  is completely solved. Therefore, in this chapter we mainly focus on the shape factor  $b$  and the average overtopping discharge  $q$ .

As mentioned above the effect of the foreshore slope is quantified by Weibull factors  $a, b$  and  $P_{ov}, T_{m-1,0}$ . The percentage of wave overtopping  $P_{ov}$  seems to fit quite well with the formula given by Van der Meer et al., 2010 even for this very mild foreshore. Conversely, the shape parameter established by previous studies demonstrates a big gap with predicted results. The effects of the dimensionless crest freeboard, foreshore slope and relative spectral wave period on the shape factor

are also investigated in this chapter. It turns out this factor is not only a function of relative crest freeboard, but also proportional to cotangent of foreshore slope and inversely proportional to relative spectral wave period which are not yet mentioned before in literature review. A new equation of the shape factor  $b$  is introduced as (4.32).

Obviously, the infragravity wave is taken account of in this new equation since this low-frequency wave energy is becoming more dominant in the surf zone after breaking (see figure 4.9).

Regarding average wave overtopping discharge, a new formula for very gentle and shallow bed foreshores is also proposed as equation (4.35). These above equations are applied based on numerical results conducted for low crest freeboards in the range of  $R_c/H_{m0,t}$  from 0.26 to 1.07 and with infragravity wave energy generated on the very gentle foreshores, such that the spectral wave period increases with a factor of  $T_{m-1,0,t}/T_{m-1,0,o}$  from 1.18 to 1.59. More importantly, this equation is valid only the values of the wave height and period filled in with the units of m and s, respectively, and could not be applied outside the absolute values that they were made for.

## 4.5. Conclusions

Under attack of extreme wave conditions, the inner slope of dikes covered by grass can become more vulnerable and be eroded over time. In this failure mechanism the overtopping waves constitute the hydraulic load that leads to damage of the sea dike. The cumulative overload method proposed by [Van der Meer et al., 2015](#), can be applied to evaluate the strength of grass cover. The local flow velocity is also used in this method to determine the damage of the grass cover. This local flow velocity is calculated from the individual wave overtopping volumes per wave. Therefore, to determine the damage of the dike under wave overtopping flows, the wave volumes need to be properly quantified, which is the aim of this chapter.

Wave overtopping is one of the key factor to design the sea defense structures, however, the process of overtopping rate on sea dikes with very gently sloping and shallow foreshores is proved not to closely match with the existing approaches ([Nguyen et al., 2020](#)) and wave overtopping risks on the sea dikes are not yet fully understood. For these above reasons, this chapter focus mainly on two issues. First, wave transformation from the deep-water until the shallow area and a cumulative wave overtopping volume is validated between numerical model and experiment laboratory for steep sloping foreshores (1:35 and 1:50). Second, new formulae for the shape parameter and average wave overtopping rate are established for very gently sloping foreshores with shallow water and low crest heights. Hereby, the exceedance distribution and wave overtopping volume can be described with a two-parameter Weibull distribution. These equations are established based on a set of data obtained by the SWASH model for very gentle sloping and shallow foreshores, ranging from the slopes of 1:500 to 1:1000, since the laboratory experiments come to their limitation owing to scale effects of wave flume for this kind of very gentle slopes; moreover the costs for a relevant experiment (if being carried out) would be extremely high since the foreshore of these types of slopes would need to be very long. The formulae were based on shallowness of the foreshore of  $h_t/H_{m0,o} \approx 1$  to 1.5 and a low-crested freeboard of the dike  $R_c/H_{m0,t} \approx 0.25$  to 1. Regarding the wave overtopping discharge, the new equation can be improved by changing the absolute values of the wave height  $H_{m0,t}$  and the wave period  $T_{m-1,0}$  by dimensionless terms such as the wave steepness or the relative wave period. This chapter is also limited to long-crested normally incoming waves, hence physical model tests of short-crested incident waves are recommended for further studies.

## Bibliography

Aldrich, J., 1998. Doing Least Squares: Perspectives from Gauss and Yule. *International Statistical Review*. 66 (1): 61–81. doi:10.1111/j.1751-5823.1998.tb00406.x

Altomare, C.; Crespo, A.J.C.; Domínguez, J.M.; Gómez-Gesteira, M.; Suzuki, T.; Verwaest, T. Applicability of Smoothed Particle Hydrodynamics for estimation of sea wave impact on coastal structures. *Coast. Eng.* 2015, 96, 1–12.

Altomare, C.; Suzuki, T.; Verwaest, T. Influence of directional spreading on wave overtopping of sea dikes with gentle and shallow foreshores. *Coast. Eng.* 2020, 157, 103654.

Altomare, C.; Suzuki, T.; Chen, X.; Verwaest, T.; Kortenhaus, A., 2016. Wave overtopping of sea dikes with very shallow foreshores. *Coast. Eng.*, 116, 236–257, ISSN 0378-3839.

Bosboom, J.; Stive, M.J.F., 2015. Coastal Dynamics I: Lecture Notes CT4305; *Delft Academic Press, Delft, the Netherlands*.

EurOtop, 2018. Manual on Wave Overtopping of Sea Defences and Related Structures—An Overtopping Manual Largely Based on European Research, but for Worldwide Application, 2nd ed.; <http://www.overtopping-manual.com/eurotop/downloads/>

Franco, C. and Franco, L., 1999. Overtopping formulas for caisson breakwaters with nonbreaking 3D waves. *Journal of waterway port coastal and ocean engineering - ASCE*, 125(2): pp. 98-108.

Garrett, C. J. R. (1967). Discussion: the adiabatic invariant for wave propagation in a non-uniform moving medium. In *Proceedings of the Royal Society of London A: Mathematical, Physical and Engineering Sciences*, volume 299, pages 26–27. The Royal Society.

Gruwez, V., Altomare, C., Suzuki, T., Streicher, M., Cappietti, L., Kortenhaus, A. and Troch, P., 2020. An inter-model comparison for wave interactions with sea dikes on shallow foreshores. *J. Mar. Sci. Eng.* 2020, 8, 985; doi:10.3390/jmse8120985.

Hughes, S. (2008). Combined wave and surge overtopping of levees: flow hydrodynamics and articulated concrete mat stability. *Technical Report ERDC/CHL TR-08-10, Coastal and Hydraulics Laboratory, U.S. Army Engineer Research and Development Center, United States*.

Hughes, S.A., 2011. Adaptation of the levee erosional equivalence method for the hurricane storm damage risk reduction system (HSDRRS). *Coastal and Hydraulics lab, US Army Engineer Research and Development Center*.

Hughes, S.A., Thornton, C.I., Van der Meer, J.W., and Scholl, B.N., 2012. Improvements in describing wave overtopping processes. *Coastal Engineering Proceedings*, 1(33):35.

Hofland, B.; Chen, X.; Altomare, C.; Oosterlo, P., 2017. Prediction formula for the spectral wave period  $T_{m-1,0}$  on mildly sloping shallow foreshores. *Coast. Eng.*, 123, 21–28.

Hofland, B.; Diamantidou, E.; van Steeg, P.; Meys, P., 2015. Runup and overtopping measurements with a laser scanner. *Coast. Eng.*, 106, 20–29.

Lashley, C.H; Zanuttigh, B.; Bricker, J.D.; van der Meer, J.; Altomare, C.; Suzuki, T.; Roeber, V.; Oosterlo, P., 2020a. Benchmarking of numerical models for wave overtopping at dikes with shallow mildly sloping foreshores: Accuracy versus speed. *Env. Model. and Software* 130 (2020) 104740.

Lashley, C.H; Zanuttigh, B.; Bricker, J.D.; van der Meer, J.; Altomare, C. and Suzuki, T., 2020b. Relative magnitude of infragravity waves at coastal dikes with shallow foreshores: A prediction tool. *American Society of Civil Engineers*. DOI: 10.1061/(ASCE)WW.1943-5460.0000576

Nguyen, T.-H; Hofland, B.; Chinh, V.D. Stive, M.J.F., 2020. Wave overtopping discharge for very gently sloping foreshores. *Water* 12(6): 1695. DOI: 10.3390/w12061695

---

Oosterlo, P.; Mc Call, R.T.; Vuik, V.; Hofland, B.; Van der Meer, J.W. and Jonkman, S.N., 2018. Probabilistic Assessment of Overtopping of Sea Dikes with Foreshores including Infragravity Waves and Morphological Changes: Westkapelle Case Study. *Journal of Marine Science and Engineering* 2018, 6, 48. DOI:10.3390/jmse6020048.

Rijnsdorp, D.; Smit, P. B. and Zijlema, M., 2014. Non-hydrostatic modelling of infragravity waves under laboratory conditions. *Coast. Eng.*, 85, 30-42

Suzuki, T.; Altomare, C.; Veale, W.; Verwaest, T.; Trouw, K.; Troch, P.; Zijlema, M., 2017. Efficient and robust wave overtopping estimation for impermeable coastal structures in shallow foreshores using SWASH. *Coast. Eng.*, 122, 108–123.

Suzuki, T.; Altomare, C.; Yasuda, T.; Verwaest, T., 2020. Characterization of Overtopping Waves on Sea Dikes with Gentle and Shallow Foreshores. *Journal of Marine Science and Engineering*, 2020, 8, 752; doi: 10.3390/jmse8100752.

Suzuki, T.; Verwaest, T.; Hassan, W., Veale, W.; Reyns, J., Trouw, K.; Troch, P. and Zijlema, M., 2012. The applicability of SWASH for modelling wave transformation and wave overtopping: A case study for the Flemish coast. *Proceedings in ACOMEN 2011*.

Suzuki, T.; Verwaest, T.; Veale, W.; Trouw, K.; Zijlema, M., 2012. A numerical study on the effect of beach nourishment on wave overtopping in shallow foreshores. *Coast. Eng. Proceeding* 1(33).

SWASH User Manual: SWASH Version 3.14A; the SWASH Team: Delft, the Netherlands, 2016.

Tega, Y. and Kobayashi, N. (1996). Wave overwash of sub-aerial dunes. In *ASCE, Proc. 25th ICCE*, pages 4148–4161, Orlando, United States.

Trung, L.H., 2014. Overtopping on grass covered dikes - Resistance and failure of the inner slopes, *PhD thesis, Delft University of Technology, the Netherlands, 2014*.

US Army Corps of Engineers. Shore Protection Manual; *US Army Corps of Engineers: Washington, DC, USA, 1984; Volume 1*.

Van der Meer, J. and Janssen, W., 1994. Wave run-up and wave overtopping at dikes. In: Kabayashi, Demirbilek, Wave forces on inclined and vertical wall structures. *American Society of Civil Engineers*, pages 1-27.

Van der Meer, J. W., Hardeman, B., Steendam, G. J., Schuttrumpf, H., and Verheij, H., 2010. Flow depths and velocities at crest and landward slope of a dike, in theory and with the wave overtopping simulator. *Coastal Engineering Proceedings*, 1 (32):10.

Van der Meer, J. W., Thornton, C., and Hughes, S., 2011. Design and operation of the US wave overtopping simulator. [http://www.vandermeerconsulting.nl/downloads/stability\\_a/2011\\_vandermeer\\_design\\_operation.pdf](http://www.vandermeerconsulting.nl/downloads/stability_a/2011_vandermeer_design_operation.pdf)

Van der Meer, J.W., Steendam, G.J. and Van Hoven, A., 2015. Validation of cumulative overload method based on tests by the new wave run-up simulator. [http://www.vandermeerconsulting.nl/downloads/stability\\_a/2015\\_vandermeer.pdf](http://www.vandermeerconsulting.nl/downloads/stability_a/2015_vandermeer.pdf)

Van der Meer, J.W., Steendam, G.J. and Van Hoven, A., 2015. Validation of cumulative overload method based on tests by the new wave run-up simulator. [http://www.vandermeerconsulting.nl/downloads/stability\\_a/2015\\_vandermeer.pdf](http://www.vandermeerconsulting.nl/downloads/stability_a/2015_vandermeer.pdf)

Van der Meer, J.W., Steendam, G.J., Mosca, C.A., Bolatti Guzzo, L., Takata, K., Cheong, N.S., Eng, C.K., Ang, L., Ling, G.P., Siang, C.W., Seng, C.W., Karthikeyan, M., Yap, F., Govindasamy, V., 2020. Wave overtopping tests to determine tropical grass species and topsoils for polder dikes in a tropical country. *ASCE, Proc. VICCE 2020*.

Victor, L., 2012. Optimization of the hydrodynamic performance of overtopping wave energy converters: experimental study of optimal geometry and probability distribution of overtopping volumes. [PhD thesis, Ghent University](#).

Welch, P. D. (1967). The use of fast-Fourier-transform for the estimation of power spectra: A method based on time averaging over short, modified periodograms. [IEEE Transactions on audio and electro-acoustics](#), 15(2):70–73

Zanuttigh, B., Van der Meer, J.W., Bruce, T. and Hughes, S., 2013. Statistical Characterisation of Extreme Overtopping Wave Volumes. [Proc. ICE, Coasts, Marine Structures and Breakwaters 2013, Edinburge, UK](#).

# 5

## Practical Implications for Dike Design in Vietnam

Sea dikes have been constructed with the intention to protect the inland from extreme wave conditions for decades to come. This chapter first introduces the situation of the existing dike systems in Vietnam. Followed by a case study in a typical area, investigating and comparing the existing methods with the new equations of wave overtopping rates and the Weibull parameters, as proposed in the previous chapter. Then, the results will be discussed and conclusions are formulated in the last section

### 5.1. Introduction

Positioned on the Eastern margin of Indochinese peninsula, Vietnam is bordered by the Gulf of Tonkin, the Gulf of Thailand, the South China Sea (Bien Dong in Vietnamese), and by the countries of China, Cambodia and Laos. Vietnam has a land area of about 320,000  $km^2$  with a coastline of more than 3,250 km long, even excluding the about 3,000 islands dispersed along the entire length (figure 5.1). The coastal areas of the country have a population of roughly 18 million people; approximately a quarter of the national population, although these districts occupy only 16 percent of the total land area. The northwestern and central regions are mainly characterized by a series of mountains and hills, while the central and eastern coastal areas are basically formed by low plains. The plains in the central zone are mainly narrow, lying along the coastal areas. The Red River Delta in the North and the Mekong Delta in the South are the largest low-level plains in the country (Nguyen et al., 2019, Thao et al., 2013).

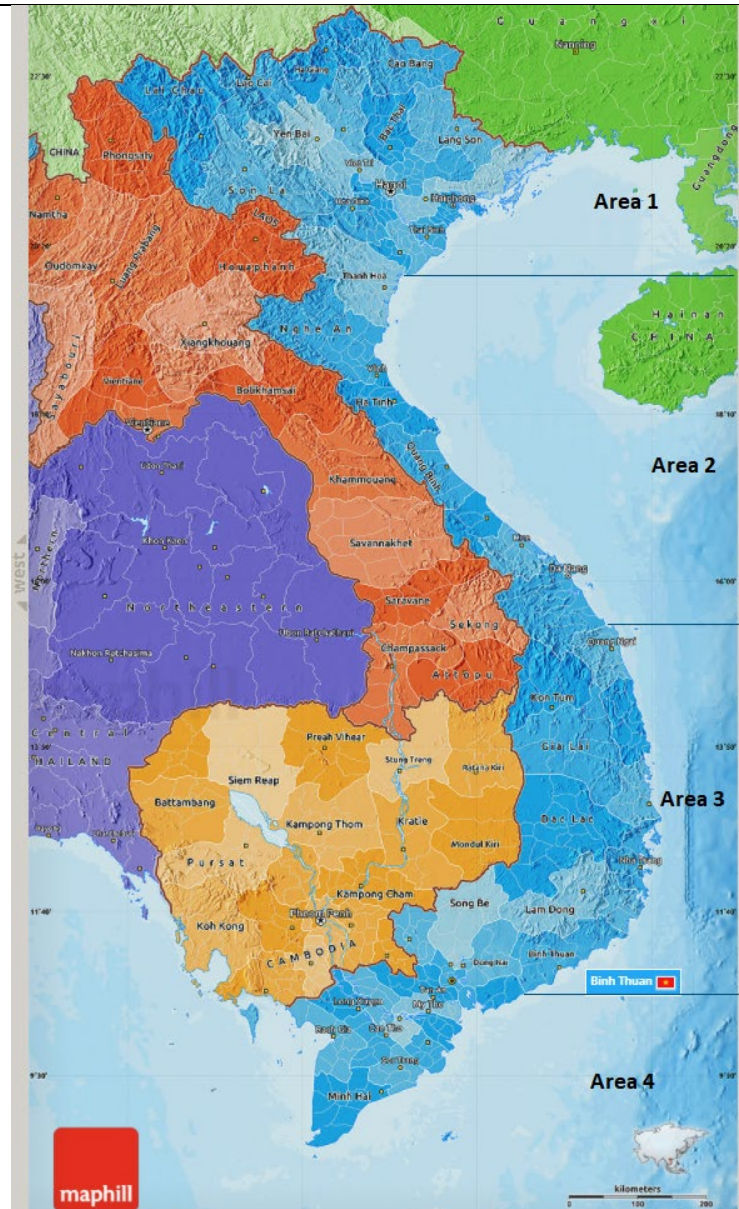


Figure 5.1: Map of the entire Vietnam (Maphill, 2021)

Based on its geographical features, the Vietnamese coastal areas can be typically classified by 4 type of environments:

- Area 1: From the North to Ninhbinh Province, the coastal area varies from cliffs and rocky coasts to a deltaic depositional environment. A small amount of sediment discharge is carried by short rivers, including sand and gravel. A deltaic seaward accretion occurs in the Red River Delta in several areas, but extreme erosion also occurs in the estuaries (Thao et al., 2013).
- Area 2: From Thanhhoa to Quangnam Province, the coastal region is typically flat, smooth and depositional. Coastal sand and bay beaches can be popularly seen and associated with rocky coasts and cliffs.
- Area 3: From Quangngai to Binhthuan Province, the coast contains eroding areas and low cliffs, dunes, estuaries and gulfs. Erosion can be found in the roughly 10 coastal lagoons that are presented here, spreading from the north to the east of Vietnam.

- Area 4: From Baria-Vungtau Province to the most southern coastal part, including the Mekong Delta, the coast is typically formed by low-land plains with mangroves forestation growing quite popular. An enormous long-term sediment supply was deposited during the Holocene, but the Mekong Delta has seriously eroded at up to 70% of the total 160 km shoreline in length in the period from 1973 to 2014 (Besset et al., 2016).

Dikes have been used as a coastal defense to protect the hinterland from damages and flooding for the past decades. The low-lying areas in the Red River Delta and the Mekong River Delta both have substantial systems of sea-dikes. The dike systems in these deltas are shown in figure 5.2. In the Central area, short dike systems are built for low-land areas around the coasts. The total length of the sea-dikes is roughly more than 2 659 km in order to prevent serious flooding of houses and to protect lives (Ledden et al., 2020). This is for example much more than the 430 km of primary sea-dikes in the Netherlands.

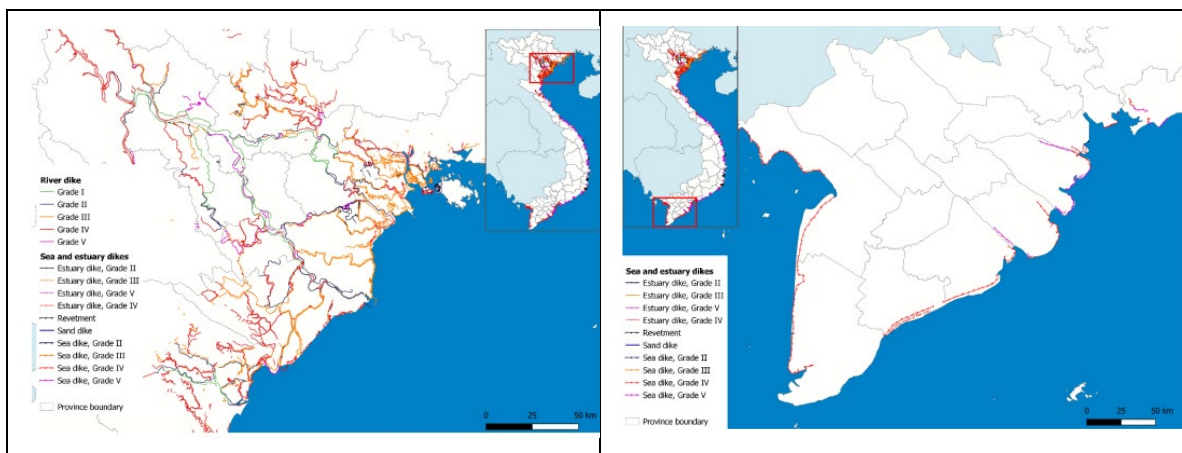


Figure 5.2: Dike systems in the Red River Delta (upper figure) and the Mekong River Delta (lower figure). Source: data from Vietnam disaster management authority.

## 5.2. Case study: Sea-dike design in Binhthuan province

In this section, the analysis of the SWAN and SWASH model combination is used to demonstrate and evaluate the applicability of the new and existing equations (e.g. Van Gent, 1999). There are no data available from the measurements to compare with the outcome of numerical data, therefore, the numerical results will be compared with the new equations proposed in the previous chapter.

Data related to water levels, waves and other parameters in Vietnam are limited (since measurement campaigns are expensive and often owned by companies or institutes), therefore, in this chapter, some of the sparsely available data are used as hydraulic boundary conditions. In this calculation, we will use a part of a project in the Central coast system. The purpose of this project is to construct two new sea-dike systems in Binhthuan Province, after typhoon Damrey (November 2017) destroyed a part of the existing dike. The 1<sup>st</sup> dike system is built far from the densely populated town and the 2<sup>nd</sup> dike system is close to the residential area.

Firstly, the case study is modelled in the Central coast (Binhthuan Province) of Vietnam, where erosion rapidly occurred, see figures 5.3a and 5.3b. Then, the Binhthuan situation is estimated in detail through wave energy spectrum and dissipation terms of the wave energy balance. Furthermore, wave parameters at the toe of a sea-dike are also calculated with the presence of the IG wave. Following, the wave overtopping risk of this area is investigated and the Weibull-parameter distribution is given, based on new equations introduced for low-crested dikes at typical very gentle and shallow foreshores, such as exist in Vietnam.



Next, the used model approach is presented. SWAN will be adopted to translate waves from offshore waves to near-shore waves, and a SWAN-based wave spectrum is subsequently applied in SWASH as input boundary, in order to simulate the wave attenuation up to the dike toe. The main reason behind this combination is, that running SWAN can reduce the computational time for the entire domain up to 50 km or even more from offshore to near-shore. In addition, in this model the wind effect is taken into consideration. Due to the very gently sloping bottom of the near-shore in Vietnam, the foreshore is very long and, as a result, the wind-induced wave growth plays a significant role. In contrast, wind generation is not included in the SWASH model, thus this model is only used in the near-shore.

The case study in Binhthuan Province is described and investigated in the following sections.

### 5.2.1. Natural and hydraulic characteristics

#### Topography

The location of our case study is located near an estuary and coastal region belonging to Lienhuong town. This town is quite densely populated on the Northern side of the coastal area. The coastline is quite flat with an elevation change from +2.5 m to +3.2 m above MSL. The highest terrain is a dune with the elevation from +7.0m to +10.0m above MSL. The bathymetry slope changes from 0.1% to 0.3% seaward; the gradient increases from the estuary to the dune. A natural elevation is -5.0m above MSL; where the distance from the current coastline is changing from 150 m to 350 m.

#### Wave and wind climate

Wave data at the offshore are collected based on long-term observations at Bachho Station (Table 5.1). This station is located roughly 60 km away from this case study's area in the North direction at the water depth of 50 m.

Table 5.1. Wave height and period observed at Bachho Station

| Direction | 100 years | 50 years | 20 years | 10 years | 1 years |
|-----------|-----------|----------|----------|----------|---------|
| NE        | 7.2m      | 6.4m     | 5.5m     | 4.5m     | 3.5m    |
|           | 9.7s      | 9.5s     | 9.2s     | 8.7s     | 8.1s    |
| E         | 6.2m      | 5.4m     | 5.0m     | 3.8m     | 3.0m    |
|           | 9.4s      | 9.1s     | 8.9s     | 8.5s     | 7.9s    |
| SE        | 5.2m      | 4.1m     | 3.3m     | 2.8m     | 2.3m    |
|           | 7.8s      | 7.5s     | 7.2s     | 6.9s     | 6.2s    |
| S         | 3.3m      | 3.1m     | 2.9m     | 2.5m     | 1.8m    |
|           | 7.3s      | 7.1s     | 7.0s     | 6.7s     | 5.6s    |
| SW        | 5.5m      | 4.8m     | 4.4m     | 4.1m     | 3.0m    |
|           | 8.7s      | 8.6s     | 8.5s     | 8.1s     | 7.9s    |

Based on the data collection at Bachho Station, the significant height with a return period of 100 years is 7.2m and the peak period is 9.7s.

There are two kinds of wind climate in this region: The South-West monsoon dominant from May to October (rainy season), and the North-East monsoon from November to April (dry season). In the dry season, the average velocity of the prevailing wind is around 1.6 to 2.8 m/s, while in the rainy season this value is 1.8 to 4.5 m/s. The wind velocity observed in this direction with a return period 100 years is approximately 30 m/s.

#### Storm history

According to the observations during 84 years, from 1910 to 1994, approximately 20% of the total years witnessed extreme storms involving the province of Binhthuan. Recently, the number of storms increased with more serious damages as a consequence. The storms and typhoons mostly occur from October to December.

### Tidal characteristics

Based on the data provided by the Southern Institute of Water Resources Research (SIWRR, Vietnam), a diurnal tidal regime is dominant here, as there is one trough and one peak daily during 18 to 22 days per month. The remaining days are semi-diurnal but the average amplitude is quite small. The tidal amplitude can vary from 1.5m to 2.0m at spring tide.

### Climatic condition

Located in a typical tropical monsoon region, this area is hot and dry year-round, dominated by dry heat, little rain and strong wind. The average yearly temperature is around  $26.5^{\circ} - 27.5^{\circ}$ , the maximum yearly temperature can reach  $30^{\circ} - 32^{\circ}$ .

The rain season concentrates mainly from May to October, occupying 85 % of the total amount of rainfall over a year.

### Coastal situation

Along the coastline, belonging to Lienhuong town, a dike is located next to the estuary extending to the dune. This coastline has the shape of a concave curve, which has been rapidly eroding for years. The authorities have already invested in building a temporary revetment of 600m long to protect the hinterland from landslides. At spring tide, the water nearly reaches the residential area. The coastal length, where people's lives are threatened, is almost 1 km along the coastline, due to frequent landslides. So far, since 2014 twenty-nine houses completely collapsed, hundreds of other houses are in danger, and nearly a hundred families have already moved out.

According to satellite broadcasting from 2010 to 2018, the coastline already retreated from 50 m to 80 m over a length of 1 km. At the moment, the coastline is close to a crowded residential area, and the current erosion situation is threatening about 2000 households.

Images related to post-storm erosion in this area are shown below (figure 5.3). After the storm, the populated area had to be moved much further landward, roughly half of a kilometer compared with the former location. Furthermore, the grass-covered sea-dike system was largely destroyed, especially the grass cover was entirely disappeared as mentioned in figure 5.3c.



a. Houses are damaged by erosion.



b. Protection after damage and sliding.



c. A dike near the estuary

d, A concave coastline is eroded

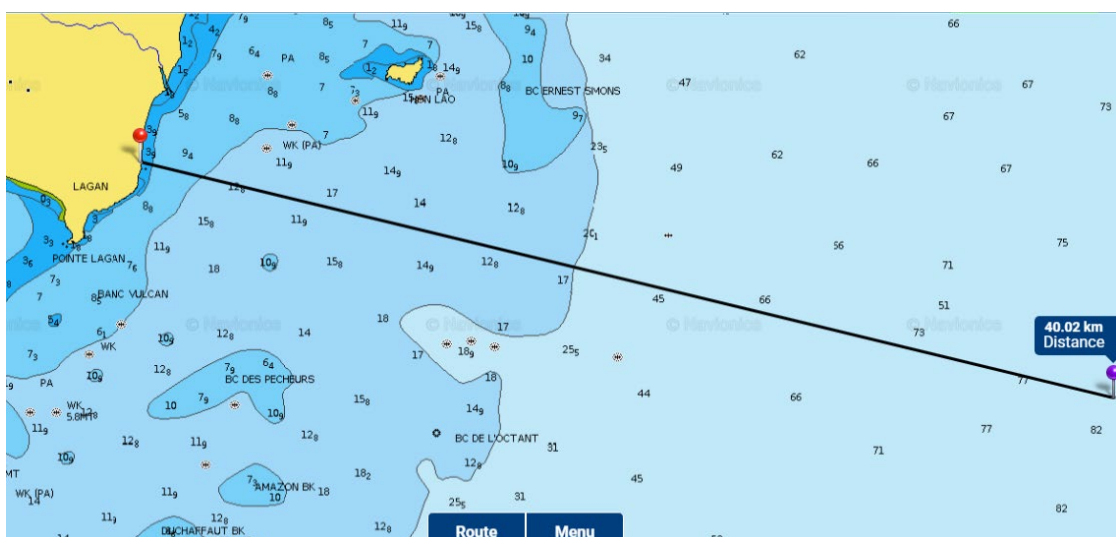
Figure 5.3: Eroded situation in Binhthuan Province after Damrey storm (November 2017).

Pictures a and b are taken at Street 13 (Lienhuong Town), by [Icoffshore \(HUCE\)](#).

### 5.2.2. SWAN hydraulic boundary condition

This subsection describes the setup of the SWAN Cycle III ([the SWAN team, 2021](#)). As a transect is taken that is rather perpendicular to the coastline and depth contours, see figure 5.4, a 1D calculation seems to be valid. In order to run a numerical model, boundary conditions need to be provided. According to the data in the previous section, the offshore wave boundary conditions can be selected as below:

- The wave height and period are  $H_{m0} = 7.2 \text{ m}$  and  $T_p = 9.7 \text{ s}$ , respectively with a return period of 100 years.
- The wind speed at 10 m elevation of  $U_{10} = 30 \text{ m/s}$ .
- The water level in extreme conditions is a combination of a spring tide and a storm surge. A storm surge contains the following components: water set up, wind-induced set up, barometric pressure influence and the influence of coastal shape. The extreme water level estimated is 3.8 m MSL, including the spring tide of 1.8 m and the storm surge level of 2 m ([Icoffshore, 2018](#)).



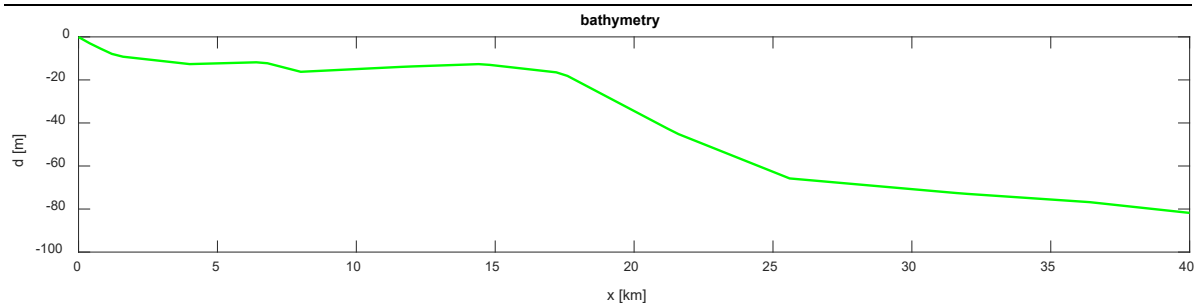


Figure 5.4: Case study in Binhthuan Province (upper picture) and corresponding bathymetry (lower picture) where 0 indicates the landward.

We make the slightly conservation assumption that the wind and waves have the same direction, perpendicular to the coastline. The cross-shore bathymetry along this direction is used up to 40 km seaward, at the water depth 82 m, see figure 5.4. The computational domain in SWAN includes the full cross-shore distance of this transect.

SWAN is used in one dimension, corresponding to a cross-shore bathymetry which is perpendicular to the coastline. The length of the computational domain is 40 km where the offshore sea bed is at the elevation of -82m. The Cartesian convention system is adopted with a grid cell size of 40m for a regular grid. At the same time, a JONSWAP-shape spectrum is applied in a boundary condition and a closed boundary is imposed at the shoreward boundary.

Moreover, SWAN is a third-generation wave model. It calculates the generation and transformation of the wave energy (spectra) including wind effect, quadruplet wave-wave interaction, triad wave-wave interaction and white capping. Due to the very gentle slope with a wide continental shelf, the wind generation cannot be ignored and, as a result, a constant wind with a speed of 30 m/s is imposed with an assumption that the wind direction is shoreward.

### 5.2.3. SWASH model

Calculations in the SWASH model include two different cases: evaluation of wave parameters at the near-shore region and of the wave overtopping process over the dike with the same input in the SWASH offshore boundary condition. The SWASH boundary conditions are spectrum which is obtained from the SWAN model. The former case is performed without the sea dike, in order to estimate wave height and wave period at the toe of the structure (to prevent the reflected wave over the dike) for the duration of 1 hour. In this case, at the landward boundary, the wave is weakly reflected by a sponge layer in order to reduce the wave reflection. In the latter case, the wave overtopping process is investigated in a short-term sea state of about a 5-hour duration.

A cross-shore distance of 8 km from the offshore to the toe of the structure is applied in the SWASH model in both calculations. Although the computational grid here is smaller than in SWAN, because the resolution is much higher, and wave motion is phase-resolved, the running time is lower than in the SWAN model. The grid cell size used is 0.4 m for the overtopping process and 5 m for the wave parameters. The sea bottom elevation at the offshore boundary is -20.2 m MSL, while the toe elevation is -3.8 m MSL. The bathymetry is applied on a regular grid, being interpolated from the bathymetry corresponding to the water depth in the SWAN model. A SWAN-derived wave spectrum is used at a seaward boundary condition.

A cross section of a Vietnamese typical sea-dike system is designed as in figure 5.5, where  $h_c$  is the height of the sea-dikes. Grass is covered on the surface of crest and landward side. For the wave overtopping calculation, the seaward slope of the dike is 1:4, the crest freeboard and the crest height of the dike is given in Table 5.2.

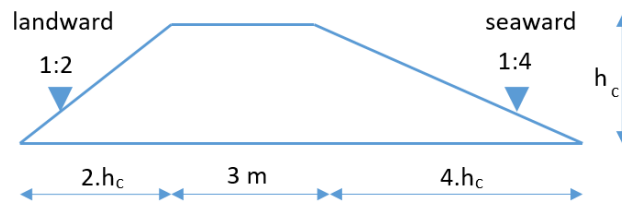


Figure 5.5: a cross-section of a typical dike design based on Vietnamese guidelines

Table 5.2. The crest freeboard and dike height of the sea-dikes

|        | $R_c$ [m] | $h_c$ [m] | $R_c/H_{m0}$ | Allowable $q$<br>[l/m/s] | Allowable $V_{max}$<br>[m <sup>3</sup> /m] |
|--------|-----------|-----------|--------------|--------------------------|--|
| Dike 1 | 3.5       | 9.5       | 0.95         | 5                        | 2 - 3                                      |
| Dike 2 | 5.7       | 7.3       | 1.54         | 5                        | 2 - 3                                      |

In both cases, Manning's coefficient is imposed for bottom friction with a default value applied that is  $0.019 \text{ m}^{-1/3}\text{s}$ . Moreover, wave breaking is activated, the non-hydrostatic pressure is applied in a shallow water equation. Explicit time integration is imposed whereas the Courant number ranges from 0.1 to 0.5, appropriate for non-linear analysis.

### 5.3. Results

#### 5.3.1. Wave dissipation over very gentle slope foreshore

Due to the wind effects, the significant wave height in the SWAN calculation is gradually increasing for roughly 19 km in distance until the wave height reaches the maximum value of 8.2 m. Following, this value rapidly decreases due to a sudden decrease of the water depth from -66 m at 25 km from the shore to the water depth -13 m at a distance of 18 km from the shore. At the same time, the first peak of wave breaking can be observed at the 15 km distance landward, since the wave "feels" the bottom at that location (see the red line in the first plot of figure 5.6).

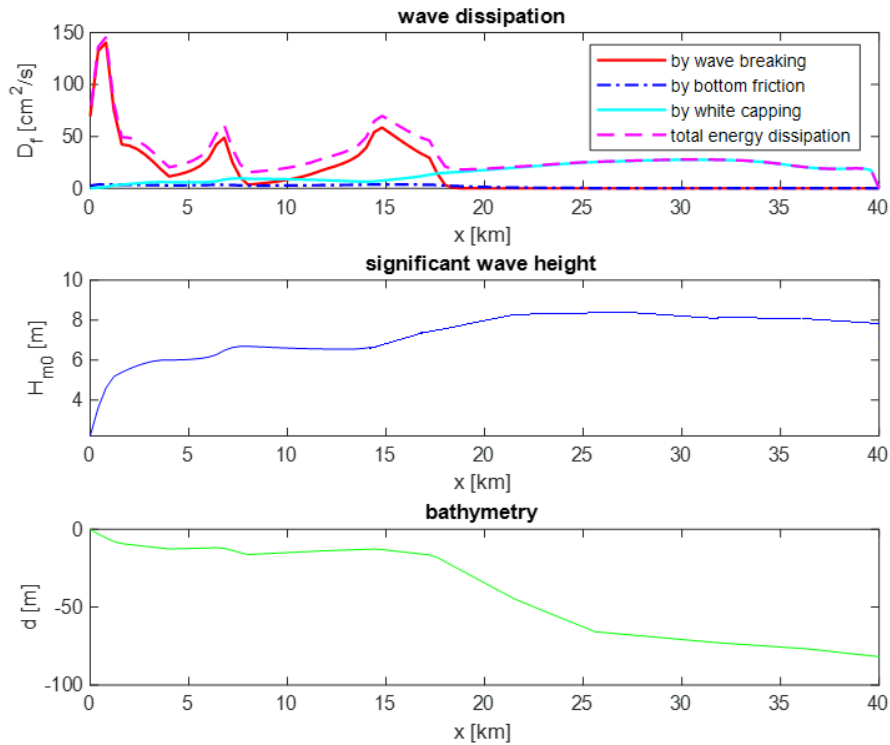


Figure 5.6: The change of wave dissipations in SWAN model where 0 indicates the landward.

The wave height is more or less the same in roughly 8 km before decreasing at the distance 7 km from the shoreline because of a sudden change in bottom profile. Meanwhile, the second peak of wave breaking can be clearly seen at that position. The “real” wave breaking happens at the distance less than 2 km from the coast, corresponding to the third highest peak of the red line in the first plot of figure 5.6.

### 5.3.2. Wave spectra and wave parameters at the toe

To evaluate the variation of wave energy, a SWAN-derived wave spectrum is imposed in an offshore boundary condition. The water energy is measured at 6 locations along the sea bed bathymetry. From figure 5.7, it can be seen that when a wave propagates towards the shoreline, the shape of the variance density spectrum is also changed. In this plot, the horizontal axis represents the frequency range and the vertical axis indicates the water energy density.

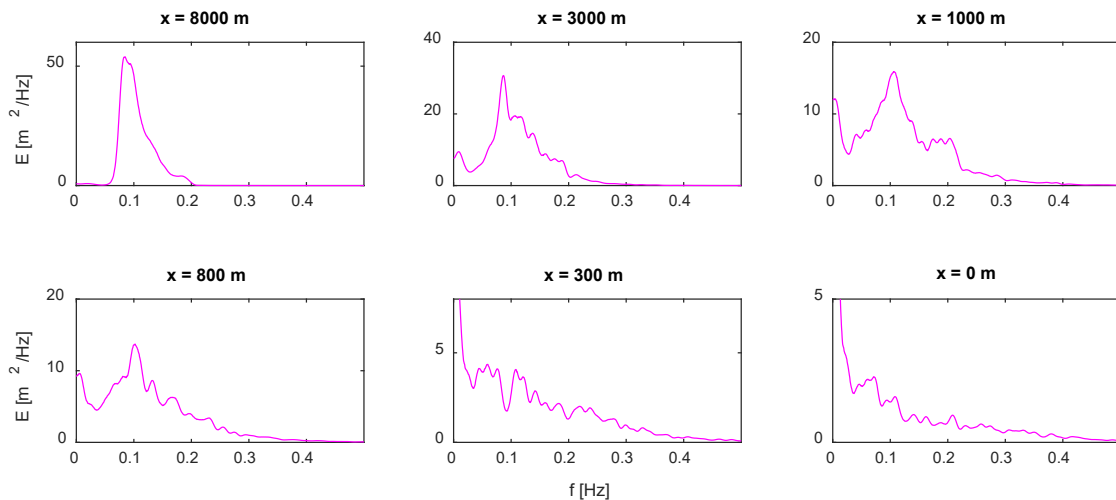


Figure 5.7: Wave spectra at several locations in SWASH model

The alteration of the wave energy shape can be derived from the two following phenomena: energy dissipation caused by wave breaking (in the near-shore) and white capping (in the offshore), and energy transfer caused by wave interactions. At the offshore boundary, corresponding to the first plot at a distance  $x=8000$  m from the coast, the shape of the water spectrum is still asymmetric around the peak, steeper on the low-frequencies domain and the extended tail on the high-frequencies domain as JONSWAP spectrum shape.

At the distance of 3000 m from the near-shore, a clear difference in the wave spectral shape can be seen. On the low-frequencies, a peak can be observed which presents a low frequency wave at the intermediate water zone. At the same time, another striking encounter is the presence of a secondary peak on the high-frequencies side, which is a result of an energy shift caused by non-linear wave interactions. The mechanism of this energy transfer is caused by resonance among the waves. The wave breaks at the distance of 1000 m where multiple peaks can be encountered on the higher-frequencies side and the IG wave increases as well. Reaching the coast, the water energy transfers from the higher-frequencies to the lower-frequencies domain and the shape of the variance density spectra turns into a flattened shape (as shown in two last plots in figure 5.7). As a result, IG waves become dominant in shallow water.

The wave height and wave period at the toe are investigated in figure 5.8.

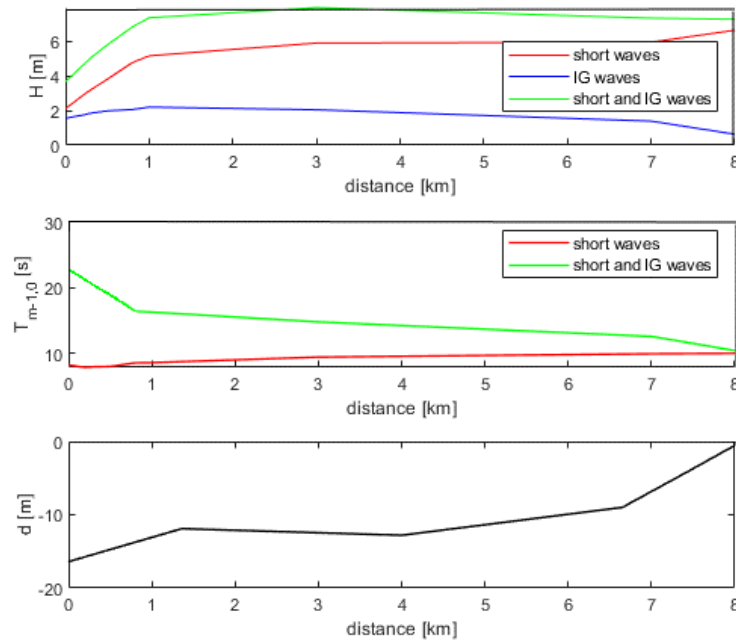


Figure 5.8. The change of wave heights (an upper plot), wave periods (a middle plot) corresponding to the bathymetry (a lower plot) in the SWASH calculation.

The wave parameters at the toe can be defined based on figure 5.8:  $H_{m0} = 3.7$  m;  $T_{m-1,0} = 22.5$  s

The ratio  $\frac{T_{m-1,0,t}}{T_{m-1,0,0}}$  calculated from the numerical model for very gentle foreshores is overestimated given the measurement in figure 5.5 of Hofland et al. (2017). It can be explained by the fact that the research by Hofland et al. (2017) applied for straight linear sloping foreshores, moreover, the scope of this study is used for foreshore slopes in ranges of 1:35 to 1:250 and does not apply to the very gentle slopes, like the Vietnamese foreshores.

### 5.3.3. Wave overtopping discharge

The SWASH calculation for the average wave overtopping rate for dike 2, shown in figure 5.9, is related to the wave overtopping layer thickness, overtopping velocity, mean discharge and cumulative overtopping volume.

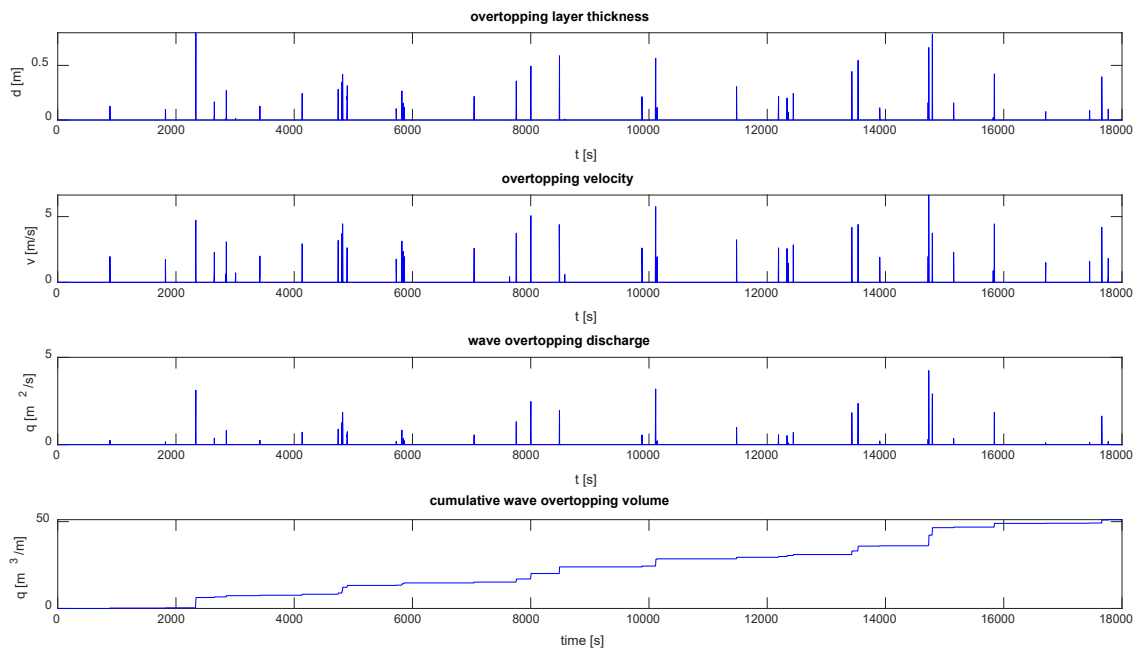


Figure 5.9. Overtopping layer thickness, velocity, average discharge and cumulative overtopping volume for  $R_c/H_{m0} = 1.54$  (dike 2)

A new equation of the average wave overtopping rate in chapter 4 for very gentle and shallow water foreshores can be described as:

$$\frac{q}{\sqrt{gH_{m0,t}^3}} = 13.329 T_{m-1,0}^{-1.131} H_{m0,t}^{-2.964} \exp\left(-0.247 \frac{T_{m-1,0} R_c}{H_{m0,t}^{3/2}}\right) \quad (5.1)$$

A comparison of the average discharge between the previous study of [Van Gent \(1999\)](#), the SWASH model and from the new equation can be listed in table 5.2 as follows.

Table 5.2. A comparison between several methods.

|        | <a href="#">Van Gent (1999)</a><br>[l/m/s] | SWASH result<br>[l/m/s] | The new equation by <a href="#">Nguyen et al. (2022)</a><br>[l/m/s] |
|--------|--|-------------------------|---|
| Dike 1 | 372  | 20.7                    | 11.8  |
| Dike 2 | 150  | 3.4                     | 2.1   |

Based on the figure 5.9 (in case of  $R_c/H_{m0} = 1.54$ ), the average wave overtopping discharge estimated from the SWASH model is  $q = 3.4$  l/ms, acceptable for [Van der Meer et al. \(2016\)](#) as well as for the allowable average discharge in Vietnamese guidelines based on [TCVN 9901:2014 \(2016\)](#). The cumulative wave overtopping volume over the sea-dike in 5 hours can reach roughly  $50$  m<sup>3</sup>/m. For dike 2 (in case of  $R_c/H_{m0} = 0.95$ ), the average rate does not exceed the Vietnamese guidelines for non-residential areas.

According to the table 5.2, it proves that the new equation of the wave overtopping discharge for very gentle and shallow foreshores, proposed from the previous chapter, shows a good agreement with that in the SWASH result, even for the case where  $R_c/H_{m0} = 1.54$ .



### 5.3.4. Wave overtopping volume

The wave-by-wave overtopping volume during 5 hours can be expressed in figure 5.10 for both dikes.

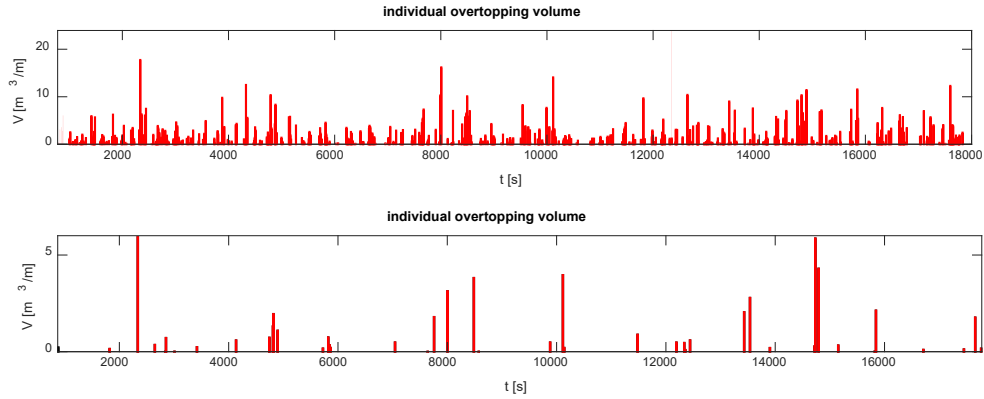


Figure 5.10. wave-by-wave overtopping volume for dike 1 with  $R_c/H_{m0} = 1.54$  (an upper plot) and for dike 2 with  $R_c/H_{m0} = 0.95$  (a lower plot).

Based on figure 5.10, the maximum wave overtopping volume during for the return period of 100 years is roughly  $V_{max} = 7 \text{ m}^3/\text{m}$  in case of dike 2. This value is still acceptable based on the EurOtop manual (Van der Meer et al., 2016) when the allowable wave volume is  $10 \text{ m}^3/\text{m}$ , which is allowable for a good grass cover. However, the maximum volume of dike 1 exceeds the allowable value. For an unprotected (sand) slope the limiting value of  $0.1 \text{ l/s/m}$  is given, which is clearly exceeded for both dikes.

Figure 5.11 expresses a comparison of the exceedance probability of the wave volume.

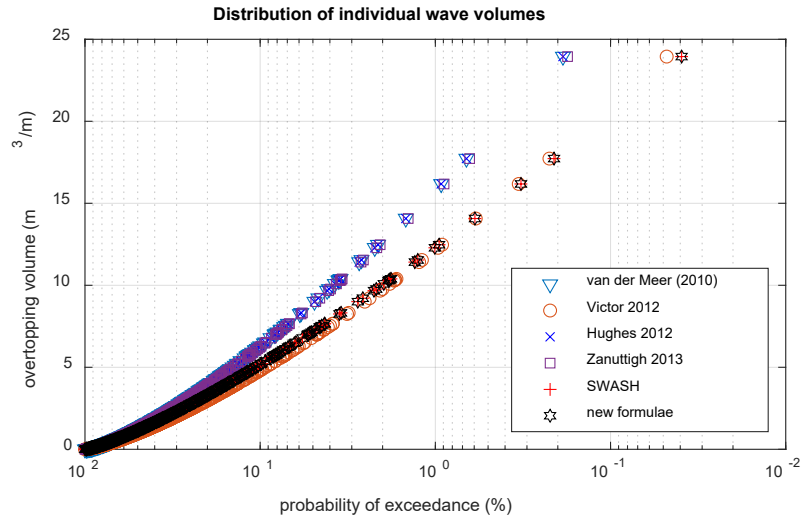


Figure 5.11. A comparison of individual overtopping volume against exceedance probability for dike 1 ( $R_c/H_{m0} = 0.95$ ).

A new equation of the shape factor given in chapter 4 is expressed as below:

$$b = \frac{1}{12.117} \left( \frac{R_c}{H_{m0,t}} \right)^{-0.22} [\cot(\theta)]^{0.46} \left( \frac{T_{m-1,0,t}}{T_{m-1,0,o}} \right)^{-1.64} \quad (5.2)$$

Substitute the above expression, we can determine:  $b = 0.82$

The scale factor can be determined based on the Gamma function, based on the SWASH-derived individual wave volumes and the shape factor  $b$  as equation (5.2). The individual wave overtopping volume in SWASH can be determined through the individual wave overtopping discharge as below:

$$a = \frac{\bar{V}}{\Gamma\left(1 + \frac{1}{b}\right)} \quad (5.3)$$

Substituting the values  $b$  and  $\bar{V}$ , the scale factor can be obtained:  $a = 1.85$ .

Compared with the SWASH-based Weibull parameters ( $a = 1.83$ ;  $b = 0.80$ ), these above values are comparable. Similar to dike 2, the results can be shown in table 5.3.

Table 5.3. A comparison of Weibull parameters between the numerical model and the new equation.

|        | $R_c/H_{m0}$ | $a$ [-]<br>SWASH | $a$ [-]<br>new formula | $b$ [-]<br>SWASH | $b$ [-]<br>new formula |
|--------|--------------|------------------|------------------------|------------------|------------------------|
| Dike 1 | 0.95         | 1.83             | 1.85                   | 0.80             | 0.82                   |
| Dike 2 | 1.54         | 4.7              | 4.1                    | 0.72             | 0.65                   |

Clearly, the new equation of the shape factor (and then the scale factor) is appropriate for this type of very gentle slopes in shallow water for a low-crested dike (or dike 1), corresponding to the ratio  $R_c/H_{m0} = 0.95$ . However, this formula is not satisfactory in case of a higher freeboard ( $R_c/H_{m0} = 1.54$ ).

#### 5.4. Conclusion

The standards for sea-dike design in Vietnam are mainly based on Western guidelines, however, the existing standard is limited in the average overtopping discharge (TCVN 9901:2014, 2016). The wave overtopping volume is not mentioned in these guidelines. The lack of the wave overtopping volume can cause a misunderstanding when investigating the damages of serious storms or typhoons over sea-dikes. Particularly, in the case of a fewer number of larger overtopping volumes, these are leading to more hazards than larger but smaller volumes. From figure 5.9, it can be clearly seen that only nearly 50 overtopped waves but more than one third of these values reach or exceed the allowable volumes for grass cover ( $2 - 3 \text{ m}^3/\text{m}$ ).

The new formulae of the average overtopping rate and the Weibull parameters used for these types of very gently sloping foreshores in the previous chapter seem to be well matched with the numerical model for the low-crested freeboard of the dike  $R_c/H_{m0,t} \approx 0.25$  to 1, although the ratio of spectral wave periods at the dike toe over that value at the offshore  $T_{m-1,0,t}/T_{m-1,0,o}$  overestimates the measurement in the research of Hofland et al. (2016) and Nguyen et al. (2020). However, it can be acceptable since the hypothesis of previous studies related to straight linear foreshores, confirm the results. Therefore, these new empirical equations for very mild slopes are more valid for the low-crested freeboards of the sea-dike rather than the higher-crested dikes.

With these empirical models available, designers can perform SWASH computations for a shorter duration with a coarser grid to obtain the wave conditions, and still obtain a statistically robust estimate of the extreme overtopping volume. Moreover, in future when better phase-averaged or empirical models become available to estimate the wave conditions at the toe, especially  $T_{m-1,0,t}$ , one will not need SWASH anymore to determine the maximum volume for a certain dike. However, these models will still have to be formulated.

---

Further study is recommended for field measurements of the wave developments and overtopping over the extremely gentle foreshores.

---

## References

- Besset, M., Anthony, E. J., Brunier, G., & Dusouillez, P. (2016). Shoreline change of the Mekong River delta along the southern part of the South China Sea coast using satellite image analysis (1973–2014). *Geomorphologie*, 22, 137–146.
- Hofland, B.; Chen, X.; Altomare, C.; Oosterlo, P., 2017. Prediction formula for the spectral wave period  $T_m-1,0$  on mildly sloping shallow foreshores. *Coast. Eng.*, 123, 21–28.
- Hughes, S.A., Thornton, C.I., Van der Meer, J.W., and Scholl, B.N., 2012. Improvements in describing wave overtopping processes. *Coastal Engineering Proceedings*, 1(33):35.
- Icoffshore, 2018. Report of a basic design for a sea-dike system in Lienhuong Town, Binhthuan Province. *Vietnamese version*.
- Ledden, V.M., Tung, T.T, Nguyen, H.D., Nguyen, L.T., 2020. Coastal development between opportunity and disaster risk: An assessment of the coastal protection system in Vietnam. <https://documents1.worldbank.org/curated/en/832061596654131528/pdf/Coastal-Development-between-Opportunity-and-Disaster-Risk-An-Assessment-of-the-Coastal-Protection-System-in-Vietnam.pdf>
- Nguyen, K.A.; Liou, Y.A., Terry, P.J., 2019. Vulnerability of Vietnam to typhoons: A spatial assessment based on hazards, exposure and adaptive capacity. *Science of the Total Environment* 682 (2019) 31-46.
- Nguyen, T.-H; Hofland, B.; Chinh, VD. Stive, M.J.F., 2020. Wave overtopping discharge for very gently sloping foreshores. *Water* 12(6): 1695. DOI: 10.3390/w12061695.
- SWAN User Manual: SWAN Cycle III version 41.31AB; The SWAN Team: *Delft, The Netherlands, 2021*.
- TCVN 9901:2014. Hydraulic Structures-Requirements for Seadike Design, Vietnamese Version, 2014. TCVN 9901:2014 Công trình thủy lợi-Yêu cầu thiết kế đê biển. Hà Nội 2014; *Thuyloi University: Hanoi, Vietnam, 2014*.
- Thao, N. V., Thanh, T. D., Saito, Y., & Gouramanis, C. (2013). Monitoring coastline change in the Red River Delta using remotely sensed data. *Journal of Marine Science and Technology – Vietnam* 13, 151–160.
- Van der Meer, J. W., Hardeman, B., Steendam, G. J., Schüttrumpf, H., and Verheij, H., 2010. Flow depths and velocities at crest and landward slope of a dike, in theory and with the wave overtopping simulator. *Coastal Engineering Proceedings*, 1 (32):10.
- Van der Meer, J. W., Allsop, N., Burce, T., De Rouck, J., Kortenhaus, A., Pullen, T., Schüttrumpf, H., Troch, P., and Zanuttigh, B. (2016). EurOtop Manual on wave overtopping of sea defences and related structures. An overtopping manual largely based on European research, but for worldwide application.
- Van Gent, M.R.A. Physical Model Investigations on Coastal Structures with Shallow Foreshores: 2D Model Tests with Single and Double-Peaked Wave Energy Spectra; *Delft Hydraulics/Waterbouwkundig Laboratorium: Delft, the Netherlands, 1999*.
- Victor, L., 2012. Optimization of the hydrodynamic performance of overtopping wave energy converters: experimental study of optimal geometry and probability distribution of overtopping volumes. *PhD thesis, Ghent University*.
- Zanuttigh, B., Van der Meer, J.W., Bruce, T. and Hughes, S., 2013. Statistical Characterisation of Extreme Overtopping Wave Volumes. *Proc. ICE, Coasts, Marine Structures and Breakwaters 2013, Edinburge, UK*.

# 6

## Conclusions and Recommendations

*“And God shall wipe away all tears from their eyes;  
and there shall be no more death,  
neither sorrow, nor crying,  
neither shall there be any more pain:  
for the former things are passed away.”*

- Revelation 21:4 KJV.

In the current work, predictive equations for the mean wave overtopping discharge and for the distribution of individual overtopping volumes have been developed for dikes with shallow and very gently sloping foreshores. Firstly, state-of-the-art studies and research of the wave overtopping process and its relevant parameters were investigated (Chapter 2). Secondly, the effect of infragravity (IG) waves over very gentle slopes was explored. Followed by an exploration of the average overtopping discharge and overtopping volumes, based on a series of numerical calculations using very mildly sloping and shallow foreshores up to 1:1000 (Chapter 3 and 4). Then, an application for a dike design in Vietnam is presented, where the new formulae are applied for these types of foreshore slopes (Chapter 5). In the present chapter, the main conclusions resulting from the previous chapters are given and combined with further recommendations for future studies.

## 6.1. Conclusions

The main target of this dissertation was to increase the knowledge on and understanding of the wave overtopping processes for sea dikes with very gently sloping foreshores where shallow waters have impact on the overtopping waves. The study provided new empirical formulae to assess the wave overtopping rate and the two-parameter Weibull distributed individual overtopping volumes for a sea dike under the attack of wave overtopping. In order to achieve this purpose, the dissertation subsequently provided answers to the underlying questions of this thesis, as articulated in Chapter 1.

### 6.1.1. The evolution of wave parameters at the toe of a sea-dike and the role of IG waves

Incoming wave parameters, such as the significant wave height  $H_{m0}$  and the spectral wave period  $T_{m-1,0}$ , have an important role in accurately predicting the average overtopping discharge over a sea-dike. Owing to very mild foreshores and associated with very wide continental shelves, the wind effect could not be ignored. During propagation of wind-induced waves over a long distance there is continuous energy input and dissipation and when approaching the foreshore transfer to other frequencies. In most widely applied numerical models either wind growth (phased-averaged, e.g. SWAN) or IG-wave generation (phase-resolved, e.g. SWASH) is modelled, such that a suitable location of the transition between the two model domains needs to be chosen. On the shallow foreshore, the IG waves become, compared to short waves, more dominant in the very mild slope area. At the toe of the dike, the shape of the wave spectra is flattened, due to the process of wave-wave interaction. This process was already observed in previous studies (Altomare et al., 2016, Suzuki et al., 2017) and, in particular, this flattened shape has also been validated for less gentle slopes (1:35 to 1:250) in physical models as well as numerical models, as mentioned in Chapter 4. It was observed that on very gentle foreshores the growth of IG waves is more pronounced than on less gentle foreshores. It is conjectured that, as on more gentle slopes the waves travel in shallow water for a longer distance before reaching a certain depth, more IG waves develop. Thereby this flattened shape seems to be reached already at a larger relative depth  $h_t/H_{m0,0}$ , than would be expected for a less gentle slope. This effect is also thought to cause the increased spectral wave period  $T_{m-1,0}$  that was found in this thesis. The wave period reached up to two times higher values for very mildly sloping foreshores than for less gentle slopes as found by Hofland et al. (2017).

### 6.1.2. Validation of wave spectra and average overtopping discharge for steep slopes

The wave spectra derived from SWASH simulations for steep foreshores (1:35 and 1:50) are well matched with the results measured in the laboratory at Flanders Hydraulics Research (Belgium) by Altomare et al. (2016). Moreover, it confirms that the SWASH model captures very well the wave propagation over the long distance to the toe of the dike as well as the physical transformation of the waves, such as triad wave-wave interaction and wave breaking in the surf zone. Nevertheless, the cumulative wave overtopping discharge for a slope of 1:35 expresses a slightly smaller value compared with the experimental result.

### 6.1.3. Average overtopping discharge for very mild foreshores

Numerical calculations have been made for very gently sloping foreshores, ranging from 1:500 to 1:1000, and proved that the existing formulae of the average wave overtopping discharge that were developed for less gentle slopes are not quantitatively accurate for this type of slope, including the research of Van Gent (1999) and Altomare et al. (2016). As a result, a more accurate equation should be established for this typical slope. Based on 49 test cases generated for low-crested dikes and bed slopes ranging up to 1:1000, and associated with a least squares method, a new formula of average discharge is suggested in the range of  $h_t/H_{m0,o}$  from 1.0 to 1.5 and the low-crested freeboard of the dike  $R_c/H_{m0,t} \approx 0.25$  to 1. This new formula of the average overtopping rate is described as follows:

$$\frac{q}{\sqrt{gH_{m0,t}^3}} = 13.329 T_{m-1,0}^{-1.131} H_{m0,t}^{-2.964} \exp\left(-0.247 \frac{T_{m-1,0} R_c}{H_{m0,t}^{3/2}}\right) \quad (6.1)$$

In this equation the wave height and period have the units of m and s, respectively. Moreover, this expression cannot be applied on other scale (e.g. laboratory scale) and only in the range of the applied wave heights and wave periods for which they have been developed (e.g.  $1.5 \text{ m} < H_{m0,t} < 3 \text{ m}$  and  $10 \text{ s} < T_{m-1,0,t} < 17 \text{ s}$ , etc).

### 6.1.4. The two-parameter Weibull distribution for very gentle and shallow foreshores

The inner grass-covered dike slopes are often destroyed due to overtopping waves in extreme storms. In order to evaluate the grass strength of this slope through the cumulative over-load method, the Weibull distribution of the overtopping waves should be determined.

Based on the previous studies (Van der Meer and Janssen, 1994; Van der Meer et al., 2010; Victor, 2012; Hughes et al., 2012; Zanuttigh et al., 2013), the shape parameter  $b$  of the two-parameter Weibull distribution is established for a deep and flat sea bed. In this dissertation, the foreshore slope  $\theta$  and the relative wave period  $T_{m-1,0,t}/T_{m-1,0,o}$  are taken into consideration. A new equation of the shape parameter is formulated for very mild foreshores as below:

$$b = \frac{1}{12.117} \left(\frac{R_c}{H_{m0,t}}\right)^{-0.22} [\cot(\theta)]^{0.46} \left(\frac{T_{m-1,0,t}}{T_{m-1,0,o}}\right)^{-1.64} \quad (6.2)$$

The empirical formula is valid in the range of shallow foreshores ( $h_t/H_{m0,o}$  from 1.0 to 1.5) and low-crested dikes ( $R_c/H_{m0,t} \approx 0.25$  to 1.0).

It can be clearly seen that the Weibull distribution is estimated based on the two parameters,  $a$  and  $b$ , based on the research of Van der Meer and Janssen (1994). When the shape factor  $b$  and the average overtopping discharge  $q$  are known, the scale parameter  $a$  can be readily derived:

$$a = \frac{1}{\Gamma\left(1 + \frac{1}{b}\right)} \frac{q T_m}{P_{ov}} \quad (6.3)$$

### 6.1.5. A case study in Vietnam

Vietnam has long coastlines, which are often threatened by extreme storms and/or typhoons originating from the East Sea. Like the Netherlands, Vietnam has vast areas with low-lying plains in the Red River Delta and the Mekong River Delta. Unlike in the Netherlands these areas are preferably protected by dike systems. However, dikes are mostly overtopped during extreme weather conditions and flooding can often occur after these storms. Hazards, caused by overtopping on the dike crests and the inner slopes, lead to a large number of damaged sea-dikes and failures for decades. A case study in Binhthuan Province is executed, where in 2017 the Damrey Typhoon destroyed almost the total length of the existing dike. A new dike system needed to be designed to replace the damaged structure.

With the use of the new empirical formula for the average overtopping discharge, a new dike design will perform better and will satisfy the safety requirements. Additionally, wave overtopping volumes are not (yet) mentioned in Vietnamese guidelines (TCVN 9901:2014, 2016), which leads to insufficient information for wave overtopping behavior over sea-dikes during extreme weather conditions. The parameters for the Weibull distribution quantifying the wave overtopping are investigated in this particular case and the comparison between the SWASH calculation and a new formula, as investigated and proposed in this thesis, is given. The results seem to be well matched in the numerical model compared with the new empirical equations and, thus, provide a promising addition for updated Vietnamese guidelines.

## 6.2. Recommendations and future research

The preceding sections provided the conclusions. In this section recommendations and options for further research will be examined.

### 6.2.1. Numerical calculations for very gentle and shallow foreshores

In Chapter 3, the SWASH model has been used to investigate the spectral wave period for very mildly sloping foreshores for a variety of slopes, ranging from 1:500 to 1:1000. The same wave parameters  $H_{m0}$ ,  $T_{m-1,0}$  were applied at a boundary condition in the SWAN model, whose output became the input data of the wave spectrum in SWASH. However, the parameter ranges for the input data are still limited. More comprehensive calculation series are needed to make the results more robust. Further research could extend the range of applicability by adding the effect of variations of the waves at the offshore hydraulic boundary of the model.

Regarding the average overtopping discharge in this chapter, broader boundary conditions need to be applied as well, and more detailed work is recommended for short-crested waves in the near future. Moreover, the effect of altered dike characteristics like a higher crest elevation, and the presence of aspects like roughness, berms, crest walls, and use of different slopes should be determined.

### 6.2.2. New formulae of average discharge and individual volumes for very mild and shallow foreshores

In Chapter 4, new empirical equations of the mean wave overtopping rate and the shape factor are introduced, based on 49 test cases for these types of slopes (up to the order of 1:1000), and have been applied for the crest freeboard of the dike  $R_c/H_{m0,t}$  from 0.25 to 1.0 and a shallowness of the foreshore  $h_t/H_{m0,o} \approx 1$  to 1.5. Moreover, the mean wave overtopping rate's equation is valid only the values of the wave height and period filled in with the units of m and s, respectively, and may not be applied outside the absolute values that they were made for.

Further studies may focus more extensively on short-crested waves. The costs for a relevant experiment would be extremely high since the foreshore of these (higher) slopes would need to be very long and wide. Therefore, a composite model, in which a numerical analysis and an experimental measurement are combined, may be used. In this case, the near-shore wave spectra can be computed with a (large domain) 2D SWASH calculation. The near-shore wave signal as obtained from this model will be input data for a wave maker of a short foreshore-dike system. Such a composite model may be more feasible. Moreover, a quick response team that could perform field measurements in a real typhoon situation could yield a final validation of the knowledge.



---

## References

- Altomare, C.; Suzuki, T.; Chen, X.; Verwaest, T.; Kortenhaus, A (2016). Wave overtopping of sea dikes with very shallow foreshores. *Coast. Eng.* 2016, 116, 236–257, ISSN 0378-3839.
- Hofland, B.; Chen, X.; Altomare, C.; Oosterlo, P., 2017. Prediction formula for the spectral wave period  $T_{m-1,0}$  on mildly sloping shallow foreshores. *Coast. Eng.* 2017, 123, 21–28.
- Suzuki, T.; Altomare, C.; Veale, W.; Verwaest, T.; Trouw, K.; Troch, P.; Zijlema, M., 2017. Efficient and robust wave overtopping estimation for impermeable coastal structures in shallow foreshores using SWASH. *Coast. Eng.* 2017, 122, 108–123.
- TCVN 9901:2014 Hydraulic Structures-Requirements for Seadike Design, Vietnamese Version, 2014. TCVN 9901:2014 Công trình thủy lợi-Yêu cầu thiết kế đê biển, Hà Nội 2014; [Thuyloi University: Hanoi, Vietnam, 2014.](#)
- Van der Meer, J. and Janssen, W., 1994. Wave run-up and wave overtopping at dikes. In: Kabayashi, Demirbilek, Wave forces on inclined and vertical wall structures. *American society of civil engineers*, pages 1-27.
- Van der Meer, J. W., Hardeman, B., Steendam, G. J., Schuttrumpf, H., and Verheij, H., 2010. Flow depths and velocities at crest and landward slope of a dike, in theory and with the wave overtopping simulator. *Coastal Engineering Proceedings*, 1 (32):10.
- Victor, L., 2012. Optimization of the hydrodynamic performance of overtopping wave energy converters: experimental study of optimal geometry and probability distribution of overtopping volumes. *PhD thesis, Ghent University.*
- Zanuttigh, B., Van der Meer, J.W., Bruce, T. and Hughes, S., 2013. Statistical Characterisation of Extreme Overtopping Wave Volumes. *Proc. ICE, Coasts, Marine Structures and Breakwaters 2013, Edinburge, UK.*

# Acknowledgements

I tended to forget those days, yet, one day all the memories came back to my mind. I arrived in the beautiful and ancient city of Delft on a gloomy and cold day of March, but in contrast to the boring weather, I was amazed at the friendly and lovely people here. Without them, I would not have been able to overcome the thousands of difficulties in my life. Even anonymous strangers comforted me on a bus after a “positive” day in hospital. Needless to say, the nearly 7 years of doing the thesis (exact working time is less than 5 years) had given me roller-coaster experiences, like having lived a life. In times of chronic and severe pain, I also experienced extreme happiness and the most fortunate thing that I had: to meet nice friends.

One of my best friends is Kim Anh. I learned a lot from her including to have courage in life. I still remember the cold and rainy February day in 2018, that Kim Anh helped me to move my private things to prepare for an important journey. The wind and rain in TU Delft was so strong and chilling that we fell off our bicycles countless times, but she kept moving forward. We were all as wet as drowned rats and I don't remember if my face was filled with rain or with tears.

Yen, Vu (Map) and your cute son, thank you for your nice house. Living there for nearly a month is an unforgettable memory for me, just feeling like it was my home. I hope I can return to Westervoort one day to visit your lovely family.

My Chinese roommate Rong and I, overcoming the cultural differences, also became close friends. She always tried to talk to me when I felt bored. No less than 100 times she asked me: How do you feel today? The unnamed stories we shared together usually ended at 10pm before saying goodbye to go home.

I am extremely grateful to my Prof. Marcel Stive. You were always there whenever I needed. You not only gave me moral support, but also provided much needed critical advice on my thesis as well as in my life. As a great friend you were always standing beside me in the most difficult moments in my life. Sometimes I felt broken down into pieces, but you always lifted me up. Knowing you, I learnt how a great person can be. Your name should be on this thesis as much as mine.

I am thankful to my co-promotor, Dr. Bas Hofland, for your patience, guidance and great support. I have greatly benefited from your meticulous editing. I am highly grateful that you continued to have faith in me over the years.

I would like to thank for the nice advice, Dr. Tomo Suzuki, who always made me feel remarkably excited about my work. I don't know how you did it, but you made me love the academic journey.

This thesis was carried out under the financial assistance of the Ministry of Education and Training (Vietnam), with great support from the Valorisation Centre (TU Delft, the Netherlands). Marjan and Veronique, I feel grateful for your kindness and overwhelming generosity to deal with my private financial problems. I also thank Stephan, Inge and other staff from the department of CITG, TU Delft, for providing me a comfortable and lovely office (3.65 and 3.83) and for giving me the opportunity to complete this work. I also would like to send my deep gratitude to Mariette – a very kind women who is always ready to correct the English language in my thesis, even during her precious travel to

her lovely daughters in her winter vacation. We also had a nice potluck party together with Asian guys and girls at her house.

I would like to thank a number of people for their help during the production of my thesis. Vu Ngan, Kim Anh do you remember our lunch cohort? Sometimes I hope we can return to those funny moments to joke and laugh. Ho Vinh, Martijn, Rijnsdorp and Lodewijk, I feel grateful for your kindness in correcting the Matlab transcripts and numerical models when I needed them. Linh, Son, Hung, Tung, Anh Duoc, Thang, Hoang Anh, Sanh, and so many Vietnamese guys living in Delft, you all made my life much more interesting with funny stories and barbecues.

Thank you to my parents, my dear departed Dad and my great Mom, for your endless love and support. Mom, Dad, thank you for fielding a ridiculous number of phone calls even in the early morning or midnight, for always reminding me of the end goal.

Thank you my dear sister, Thu Hien, for being there for me always and for telling me that I am cool even when I didn't feel that way.

Thank you to Ha Chi, my sweet Noel girl, for being my baby. Parents in this world all wish to have a lovely and awesome daughter like you.

Thank you to my "Donk\*y" or "Mam\*t" or "Chick\*n," or whatever you are, for constantly listening to me talk things out, for proofreading over and over, for cracking jokes when things became terrible and for the endless sacrifices you have made in order to encourage me to pursue the Ph.D. thesis as a friend, a colleague and as a member of my family.

Last but not least I would like to thank all of my friends, family members, colleagues and doctors and nurses in Reinier de Graaf and LUMC for encouraging me whenever I need them. Without you, I am nobody.

TU Delft, 2022

Thu-Ha NGUYEN

# Curriculum Vitae

Hà Thi Thu NGUYỄN

28-08-1982 Born in Thanhhoa, Vietnam.

## Education

1996-2000 Lam Son High School for the Gifted Students  
2001-2006 Bachelor in Offshore Engineering  
Hanoi University of Civil Engineering, Vietnam (HUCE)  
2007-2009 Master of Marine Engineering  
Hanoi University of Civil Engineering, Vietnam (HUCE)  
2015-2022 PhD Candidate  
Department of Hydraulic Engineering  
Delft University of Technology, the Netherlands (TU Delft)  
*Thesis:* Wave Overtopping Processes for Very Mild Sloping and  
Shallow Foreshores  
*Promotor:* Prof.dr.ir. M.J.F. Stive  
*Copromotor:* Dr. ir. B. Hofland

## Professional experience

2007-2008 State Research Project on Coastal Engineering, code B2007-03-29TD,  
2011-2012 State Research Project on Coastal Engineering, code DTB 11.4,  
2006-2009 National Research Project on Offshore Engineering, code KC.09.16  
2012 Making the manuscript of standards for breakwaters and revetments at Spratly  
Islands. Proceedings of the Scientific Conference on Coastal Engineering of the  
Spratly Islands, organized by the Ministry of Defence, Code DTB 11.4, Volume  
6.5, Hanoi (2012);  
2006 – 2015 Lecturer in Offshore and Coastal Engineering  
Hanoi University of Civil Engineering, Vietnam (HUCE).

## Awards

2002, 2003 The best student's award, sponsored by Vietsovpetro J.V  
2005 Certificate of Appreciation for the Donation of Children's Education and Health  
in Underprivileged Areas for Years, by Hanoi's Youth Organization.

# List of Publications

1. **Ha T.T. Nguyen;** M.J.F. Stive; H.J. Verhagen., 2016. A numerical study on the influence of low-frequency wave period on wave overtopping in a very gentle foreshore. The ECSA 56 Coastal Systems in Transition Conference, 4-7 September 2016, Bremen, Germany.
2. **Nguyen, T.-H;** Hofland, B.; Chinh, V.D. Stive, M.J.F., 2020. Wave overtopping discharge for very gently sloping foreshores. *Water* 12(6): 1695. DOI: 10.3390/w12061695.
3. **Nguyen, T.-H;** Hofland, B.; Chinh, V.D.; Lashley, C.H.; Stive, M.J.F., 2022. Wave overtopping volumes at very mild shallow foreshores. Prepare to submit.